The Central Atlantic Magmatic Province (CAMP) in Morocco

Andrea Marzoli, Hervé Bertrand, Nasrrddine Youbi, Sara Callegaro, Renaud Merle, Laurie Reisberg, Massimo Chiaradia, Sarah Brownlee, Fred Jourdan, Alberto Zanetti, et al.

JOURNAL OF PETROLOGY

Journal of Petrology, 2019, Vol. 60, No. 5, 945–996
doi: 10.1093/petrology/egz021
Advance Access Publication Date: 19 April 2019
Original Article

OXFORD

The Central Atlantic Magmatic Province (CAMP) in Morocco

Andrea Marzoli [1]*, Hervé Bertrand[2], Nasrrddine Youbi[3,4], Sara Callegaro [5], Renaud Merle[6], Laurie Reisberg[7], Massimo Chiaradia[8], Sarah I. Brownlee[9], Fred Jourdan[10], Alberto Zanetti[11], Joshua H.F.L. Davies[8]†, Tiberio Cuppone[1], Abdelkader Mahmoudi[12], Fida Medina[13], Paul R. Renne[14,15], Giuliano Bellieni[1], Stefano Crivellari[16], Hind El Hachimi[17], Mohamed Khalil Bensalah[3,4], Christine M. Meyzen[1] and Christian Tegner [18]

[1]Geoscience Department, Padova University and IGG-CNR, Padova, Italy; [2]Laboratoire de Géologie de Lyon, Ecole Normale Supérieure de Lyon, Université Lyon 1, CNRS UMR 5276, Université de Lyon, Lyon, France; [3]Department of Geology, Faculty of Sciences-Semlalia, Cadi Ayyad University, Marrakech, Morocco; [4]Instituto Dom Luiz, Faculdade de Ciências, Universidade de Lisboa, Lisboa, Portugal; [5]Centre for Earth Evolution and Dynamics (CEED), University of Oslo, Oslo, Norway; [6]Department of Geosciences, Swedish Museum of Natural History, Stockholm SE-104 05, Sweden; [7]Centre de Recherches Pétrographiques et Géochimiques, UMR 7358 CNRS-Universtité de Lorraine, France; [8]Department of Earth Sciences, University of Geneva, Genéve, Switzerland; [9]Department of Geology, Wayne State University, Detroit, USA; [10]Department of Applied Geology, Curtin University, Bentley, Australia; [11]IGG-CNR, Pavia, Italy; [12]Département de Géologie, Université Moulay-Ismail, Meknes, Morocco; [13]Moroccan Association of Geosciences, Rabat, Morocco; [14]Berkeley Geochronology Center, Berkeley, USA; [15]Department of Earth and Planetary Science, University of California, USA; [16]Instituto de Geociencias, University of São Paulo, São Paulo, Brazil; [17]Department of Geology, Faculty of Sciences, Chouaïb Doukkali University, El Jadida, Morocco; [18]Centre of Earth System Petrology (ESP), Department of Geoscience, Aarhus University, Denmark

*Corresponding author. E-mail: andrea.marzoli@unipd.it
†Present address: Département des sciences de la Terre et de l'atmosphère, Université du Québec à Montréal, 201, avenue du Président-Kennedy, Montréal, Québec, H2X 3Y7, Canada

Received June 5, 2018; Accepted April 1, 2019

ABSTRACT

The Central Atlantic Magmatic Province (CAMP) is a large igneous province (LIP) composed of basic dykes, sills, layered intrusions and lava flows emplaced before Pangea break-up and currently distributed on the four continents surrounding the Atlantic Ocean. One of the oldest, best preserved and most complete sub-provinces of the CAMP is located in Morocco. Geochemical, geochronologic, petrographic and magnetostratigraphic data obtained in previous studies allowed identification of four strato-chemical magmatic units, i.e. the Lower, Intermediate, Upper and Recurrent units. For this study, we completed a detailed sampling of the CAMP in Morocco, from the Anti Atlas in the south to the Meseta in the north. We provide a complete mineralogical, petrologic (major and trace elements on whole-rocks and minerals), geochronologic ($^{40}Ar/^{39}Ar$ and U–Pb ages) and geochemical set of data (including Sr–Nd–Pb–Os isotope systematics) for basaltic and basaltic–andesitic lava flow piles and for their presumed feeder dykes and sills. Combined with field observations, these data suggest a very rapid (<0·3 Ma) emplacement of over 95% of the preserved magmatic rocks. In particular, new and previously published data for the Lower to Upper unit samples yielded indistinguishable $^{40}Ar/^{39}Ar$ (mean age = 201·2 ± 0·8 Ma) and U–Pb ages (201·57 ± 0·04 Ma), suggesting emplacement

coincident with the main phase of the end-Triassic biotic turnover (*c.*201·5 to 201·3 Ma). Eruptions are suggested to have been pulsed with rates in excess of 10 km^3/year during five main volcanic pulses, each pulse possibly lasting only a few centuries. Such high eruption rates reinforce the likelihood that CAMP magmatism triggered the end-Triassic climate change and mass extinction. Only the Recurrent unit may have been younger but by no more than 1 Ma. Whole-rock and mineral geochemistry constrain the petrogenesis of the CAMP basalts. The Moroccan magmas evolved in mid-crustal reservoirs (7–20 km deep) where most of the differentiation occurred. However, a previous stage of crystallization probably occurred at even greater depths. The four units cannot be linked by closed-system fractional crystallization processes, but require distinct parental magmas and/or distinct crustal assimilation processes. EC-AFC modeling shows that limited crustal assimilation (maximum *c.*5–8% assimilation of e.g. Eburnean or Pan-African granites) could explain some, but not all the observed geochemical variations. Intermediate unit magmas are apparently the most contaminated and may have been derived from parental magmas similar to the Upper basalts (as attested by indistinguishable trace element contents in the augites analysed for these units). Chemical differences between Central High Atlas and Middle Atlas samples in the Intermediate unit could be explained by distinct crustal contaminants (lower crustal rocks or Pan-African granites for the former and Eburnean granites for the latter). The CAMP units in Morocco are likely derived from 5–10% melting of enriched peridotite sources. The differences observed in REE ratios for the four units are attributed to variations in both source mineralogy and melting degree. In particular, the Lower basalts require a garnet peridotite source, while the Upper basalts were probably formed from a shallower melting region straddling the garnet–spinel transition. Recurrent basalts instead are relatively shallow-level melts generated mainly from spinel peridotites. Sr–Nd–Pb–Os isotopic ratios in the CAMP units from Morocco are similar to those of other CAMP sub-provinces and suggest a significant enrichment of the mantle-source regions by subducted crustal components. The enriched signature is attributed to involvement of about 5–10% recycled crustal materials introduced into an ambient depleted or PREMA-type mantle, while involvement of mantle-plume components like those sampled by present-day Central Atlantic Ocean Island Basalts (OIB, e.g. Cape Verde and Canary Islands) is not supported by the observed compositions. Only Recurrent basalts may possibly reflect a Central Atlantic plume-like signature similar to the Common or FOZO components.

Key words: Central Atlantic Magmatic Province (CAMP); large igneous province (LIP); geochronology; basalt petrogenesis; crustal contamination; Morocco

INTRODUCTION

The Central Atlantic magmatic province (CAMP) is a large igneous province (LIP) composed almost exclusively of basic rocks (Marzoli *et al.*, 1999, 2018). These crop out as dykes, sills, a few layered intrusions and lava flows in the four continents surrounding the Atlantic Ocean (Fig. 1a) spanning an inferred original total surface area exceeding 10 million km^2, with an estimated total volume of more than 3 million km^3 (Marzoli *et al.*, 2018). Emplacement of the CAMP occurred in an extensional tectonic setting, heralding break-up of the megacontinent Pangea and opening of the Central Atlantic Ocean (Sahabi *et al.*, 2004; Labails *et al.*, 2010). CAMP magmatism was synchronous with one of the most severe environmental and biotic crises in Earth's history, which occurred during the latest Triassic (Hesselbo *et al.*, 2002; Marzoli *et al.*, 2004, 2008, 2011; Blackburn *et al.*, 2013; Davies *et al.*, 2017). CAMP is, therefore, one of the biggest LIP events ever recorded and its emplacement influenced the tectonics of Earth's continental plates and the evolution of life on our planet.

One of the oldest sub-provinces of the CAMP is located in Morocco where *c.*201 Ma volcanic and intrusive basaltic rocks are widespread and well exposed. Indeed, the first studies that recognized the existence and importance of a circum-Atlantic Triassic–Jurassic tholeiitic magmatic province were conducted in Morocco and in the once contiguous regions of North America (e.g. Manspeizer *et al.*, 1978; Bertrand *et al.*, 1982). Various aspects of the CAMP event in Morocco, including time-related evolution of the basaltic lavas, their age and their bearing on the end-Triassic mass extinction event have been investigated in the past (e.g. Bertrand *et al.*, 1982; Sebai *et al.*, 1991; Youbi *et al.*, 2003; Knight *et al.*, 2004; Marzoli *et al.*, 2004; Nomade *et al.*, 2007; Verati *et al.*, 2007; Deenen *et al.*, 2010; Dal Corso *et al.*, 2014). However, a comprehensive geochemical-petrologic-geochronologic study of CAMP magmatism from throughout Morocco has never been published. Here, we intend to fill this gap by providing and discussing a large number of mineralogical (including mineral trace elements), geochemical (including Sr–Nd–Pb–Os isotopes) and geochronologic data (including $^{40}Ar/^{39}Ar$ and U–Pb ages) for both intrusive and effusive mafic rocks from throughout Morocco to decipher their eruption mechanism and rate, mantle

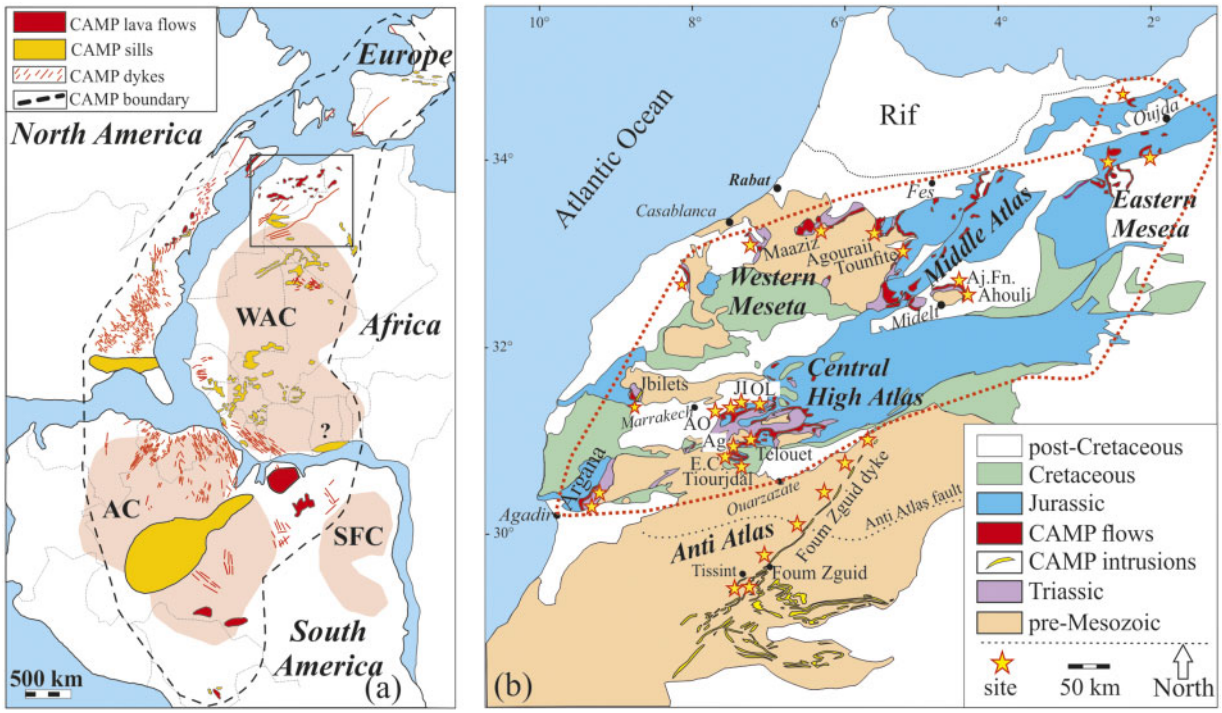

Fig. 1. (a) Schematic map of the western Pangea supercontinent at about 201 Ma showing the location of CAMP lava flows, sills and dykes. The dashed line shows the estimated global surface area of the CAMP. The pink areas indicate the approximate location of the West African craton (WAC), the Amazonian craton (AC) and the Sao Francisco craton (SFC). (b) Schematic geologic map of Morocco (for the area shown by the rectangle in Fig. 1a). The main sampling sites are shown by stars. Ag, Agouim; EC, Ec Cour; OL, Oued Lahr; JI, Jebel Imizar; AO, Ait Ourir; Aj. Fn., Ajoundou F'nouss. The thick dashed line represents the area probably covered by CAMP lava flows.

source and any temporal evolution. This work aims to improve our understanding of the global geodynamic and environmental consequence of CAMP magmatism in particular and potentially for LIPs in general. A companion paper (Tegner *et al.* in press) focuses on mantle dynamics of the Moroccan CAMP as constrained by their Platinum Group Element geochemistry.

Overview of CAMP magmatism

The CAMP shares common aspects with other continental LIPs, such as the Karoo, the Paranà–Etendeka, the Deccan, the Ethiopian Traps and the North Atlantic Igneous Province (Hofmann *et al.*, 1997; Peate, 1997; Tegner *et al.*, 1998; Melluso *et al.*, 2006; Jourdan *et al.*, 2007; Heinonen *et al.*, 2016; Parisio *et al.*, 2016; De Min *et al.*, 2018). Common features of these LIPs include the association with continental break-up events, the brief duration of the magmatism and the huge volume of magmatic rocks emplaced at high eruption rates. However, unlike the other cited LIPs, the CAMP lacks alkaline and silicic magmatism, with almost all the rocks analysed so far being basalts or basaltic andesites (and intrusive equivalents). On the other hand, near-primary magmatic compositions (e.g. picrites) are also virtually absent in the CAMP, with the exception of a few primitive basaltic dykes sampled in North Carolina (Callegaro *et al.*, 2013). A further significant peculiar feature of the CAMP is the abundance of shallow intrusive rocks (e.g. huge sill complexes in Brazil, Mali, Guinea, and prominent dyke swarms in Morocco, Spain, Mali, Liberia, Brazil, Guyana, USA; Fig. 1) compared to the relatively thin and dispersed volcanic successions. The best exposures of CAMP lava flows and the thickest lava piles have been observed in Canada, USA, Morocco and Brazil, but the preserved lava pile thickness never exceeds 400 m (e.g. Kontak, 2008), contrasting with thicknesses of a few kilometres observed in the other LIPs cited above. Lava piles in Portugal, Bolivia and Algeria are even thinner (<100 m; Martins *et al.*, 2008; Bertrand *et al.*, 2014; Callegaro *et al.*, 2014a; Meddah *et al.*, 2017).

CAMP magmatism was synchronous with the end-Triassic mass extinction event and probably triggered it (Marzoli *et al.*, 1999, 2004; Blackburn *et al.*, 2013; Callegaro *et al.*, 2014b; Davies *et al.*, 2017). CAMP magmatism may also have triggered widespread seismic activity recorded in seismites from northern Europe (Lindström *et al.*, 2015). The peak magmatic activity occurred between about 201·6 and 201·3 Ma throughout CAMP (Blackburn *et al.*, 2013; Davies *et al.*, 2017), but after this main event, discontinuous magmatism lasted possibly until ~196 Ma (Sinemurian), for example in Brazil, USA and Morocco (Marzoli *et al.*, 1999; 2011; Ruhl *et al.*, 2016).

CAMP basalts are represented by low-Ti and high-Ti tholeiites (below and above 2·0 wt % TiO_2, respectively; e.g. Merle *et al.*, 2011). Low-Ti basalts are largely

dominant in volume and crop out all over the province, while high-Ti ones are limited to a relatively small area comprising northeastern Brazil, Guyana and the once contiguous Sierra Leone and Liberia. Major and trace elements and Sr–Nd–Pb–Os isotopic compositions indicate that the basaltic magmas had an enriched composition compared to those of Mid-Ocean Ridge basalts and yet differed in composition from Atlantic Ocean Island basalts, for example in terms of incompatible trace elements such as Nb, Ti, Rb, Ba. The enriched composition of CAMP basalts is only in part attributable to crustal contamination (Marzoli *et al.*, 2014). High-Ti basalts were probably contaminated by metasomatic veins present in the continental lithospheric mantle of the Man and Amazonian cratons (e.g. Dupuy *et al.*, 1988; Deckart *et al.*, 2005; Merle *et al.*, 2011; Klein *et al.*, 2013; Callegaro *et al.*, 2017). On the contrary, the enriched signature of the low-Ti CAMP basalts is attributed to recycling of subducted continental crustal material that enriched the shallow upper mantle under the Pangea supercontinent (Callegaro *et al.*, 2013, 2014a; Merle *et al.*, 2014; Whalen *et al.*, 2015).

The origin of the CAMP remains controversial. Several authors (e.g. May, 1971; Hill, 1991; Oyarzun *et al.*, 1997; Ruiz-Martínez *et al.*, 2012) proposed a mantle-plume origin. However, geochemical and thermometric data (e.g. relatively low mantle potential temperatures; Herzberg & Gazel, 2009; Callegaro *et al.*, 2013, Whalen *et al.*, 2015) do not support this scenario. Moreover, the size and shape of the CAMP as well as the lack of any clear hot-spot track argue against a classical mantle-plume origin. Therefore, McHone (2000) and Coltice *et al.* (2007) proposed alternative scenarios based on continental thermal insulation under the Pangea super-continent to explain the near-synchronous melting over the entire province. Alternatively, a mantle-plume rising under a plate, which is already undergoing extension (Burov & Gerya, 2014), as was Pangea during the Triassic, would lead to an asymmetric distribution of magmatic rifts and amagmatic horst structures, consistent with the patterns in the CAMP in general. Delamination of the lithospheric keel would favor the rise and decompression melting of the mantle (e.g. Elkins-Tanton, 2005; Dinesen Petersen *et al.*, 2018). Paleomagnetic reconstructions support this model, since Morocco at 201 Ma was located above the margin of the African Large Low Shear Velocity Province (LLSVP), considered a plume-generation zone (Ruiz-Martínez *et al.*, 2012).

THE CAMP IN MOROCCO

Brief outline of the geology of Morocco

The geology of Morocco is characterized by three main orogenic cycles, the Eburnean (*c.*2 Ga), the Pan-African (*c.*0·6 Ga) and the Hercynian (*c.*0·3 Ga). These compressional events were intercalated with extensional phases, e.g. Triassic–Jurassic sedimentary rift-basin formation in the High and Middle Atlas regions associated with the CAMP.

The Anti Atlas in southern Morocco (Fig. 1b) formed at the northern margin of the West African Craton (WAC) chiefly during the Eburnean (*c.* 2·0 Ga; e.g. Abouchami *et al.*, 1990) and the Pan-African (*c.* 0·6 Ga; e.g. Gasquet *et al.*, 2005, 2008; Youbi *et al.*, 2013) orogenic events. Eburnean and Pan-African rocks are represented mainly by silicic intrusions. Most Eburnean granites crop out south of the Anti Atlas Major Fault, i.e. in the southern Anti Atlas. The northern border of the Pan-African belt occurs presently along the South Atlas Fault (the fault marking the southern limit of the Atlas mountain range). This boundary is also interpreted by some authors as being the northern border of WAC rocks at depth (Ennih & Liégeois, 2001). An oceanic magmatic belt (ophiolites) was accreted at about 0·7–0·8 Ga (Thomas *et al.*, 2002) and presently outcrops near Bou Azzer, Anti Atlas. After the Pan-African orogeny, during the Late Ediacaran and Paleozoic, the Anti Atlas experienced a period of subsidence with deposition of thick volcano-sedimentary sequences of Neoproterozoic–Cambrian to Carboniferous age (mainly represented by Ediacaran volcanics and Cambrian to Ordovician sandstones).

The basement of central-northern Morocco (Western and Eastern Meseta; Fig. 1b) is formed chiefly by Hercynian (Carboniferous to early Permian) granites, metamorphic rocks and quite rare basic intrusions. Post-orogenic alkaline rocks (lamprophyres) were intruded during the Permian west of Marrakech (Jbilets area). These lamprophyres host crustal xenocrysts dated at 0·3–2·0 Ga (Dostal *et al.*, 2005). Sparse Proterozoic gabbros and granites have been discovered in Central Morocco, north of the High Atlas (Baudin *et al.*, 2003; Pereira *et al.*, 2015), testifying to the existence of possible pre-Hercynian crustal roots also in this region.

From the Permian, sedimentary basins began developing in the Argana Valley (western High Atlas; Medina, 1991) and progressively expanded east and northwards into the present-day Central High Atlas and Middle Atlas regions. Triassic clastic sedimentary rocks in these basins are exclusively continental or lagoonal and were mainly derived from Pan-African and minor Eburnean source rocks (Marzoli *et al.*, 2017). Carbonate platforms formed after emplacement of the CAMP during the Early Jurassic.

Morocco experienced several episodes of anorogenic continental magmatism during the Proterozoic. Indeed, sparse basic dykes (*c.*1·8–1·4 Ga) were recently discovered in the Anti Atlas and attributed to Paleo- and Meso-Proterozoic LIPs (e.g. Youbi *et al.*, 2013). Post-CAMP Mesozoic and Cenozoic magmatism includes late-Jurassic to early Cretaceous transitional basalts from the Central High Atlas (Bensalah *et al.*, 2013), sparse Cenozoic lamproites and carbonatites (e.g. carbonatites of Taourirt, northeastern Morocco and Tamazert, High Atlas near Midelt; Wagner *et al.*, 2003;

Bouabdellah *et al.*, 2010). The most recent magmatic activity in Morocco took place during the Miocene to Quaternary, when alkaline (basalt to trachyte and phonolite) lava flows were emplaced in the Anti Atlas and Middle Atlas regions (e.g. El Azzouzi *et al.*, 2010; Berger *et al.*, 2014; Bosch *et al.*, 2014). The origin of this recent alkaline magmatism has been attributed to hotspot activity by some authors (e.g. Duggen *et al.*, 2009), although this interpretation is debated (e.g. Berger *et al.*, 2010).

The CAMP in Morocco: previous geochemical, geochronologic and biostratigraphic studies

The CAMP products are well exposed in Morocco (Bertrand *et al.*, 1982; Youbi *et al.*, 2003; Mahmoudi & Bertrand, 2007; Bensalah *et al.*, 2011) and include lava flow piles in the centre and north of the country in the High and Middle Atlas, as well as in the Eastern and Western Meseta (Fig. 1b). Intrusive CAMP rocks are mostly limited to southern Morocco, i.e. the Anti Atlas.

The pioneering work of Bertrand *et al.* (1982) recognized systematic stratigraphic geochemical changes of the Moroccan CAMP lava piles. Based on major and trace element analyses and on field-work observations, Bertrand *et al.* (1982) subdivided the lava piles into four units, the Lower, Intermediate, Upper and Recurrent lava flows. Lower to Upper units show an enriched geochemical character compared to Mid-Ocean-Ridge basalts (MORB), but the extent of this enrichment varies with stratigraphic height, a secular, up-section depletion of incompatible major (e.g. TiO_2) and trace elements being observed. The latest lava flows were named Recurrent basalts and crop out only locally in the Central High Atlas. Recurrent basalts were distinguished in particular by their low La/Yb. Bertrand *et al.* (1982) also highlighted the similarity of Moroccan CAMP flows in terms of major and trace element chemistry with those from the Newark Basin in eastern North America, proposing that these were related to the same LIP.

Geochronology ($^{40}Ar/^{39}Ar$ and U–Pb), paleomagnetism and biostratigraphy have constrained the age of the magmatism from the High Atlas and suggest pulsed emplacement mechanisms (Sebai *et al.*, 1991; Knight *et al.*, 2004; Marzoli *et al.*, 2004; Nomade *et al.*, 2007; Verati *et al.*, 2007; Palencia Ortas *et al.*, 2011; Blackburn *et al.*, 2013). A total of 22 $^{40}Ar/^{39}Ar$ plateau ages on plagioclase have been previously published for Moroccan CAMP volcanic rocks and comprise data for all four lava flow units. However, except for one sample from eastern Morocco (Oujda, Eastern Meseta) age data are limited to samples from the Central High Atlas (Sebai *et al.*, 1991; Knight *et al.*, 2004; Marzoli *et al.*, 2004; Nomade *et al.*, 2007; Verati *et al.*, 2007). The ages recalculated after Renne *et al.* (2011) are summarised in Marzoli *et al.* (2011). Even if cryptic alteration or excess ^{40}Ar may have affected some of the published data, for the Lower, Intermediate and Upper basalts $^{40}Ar/^{39}Ar$ plateau ages range from $202{\cdot}7 \pm 1{\cdot}6$ to $199{\cdot}3 \pm 0{\cdot}6$ Ma and are generally indistinguishable for these three units, defining a clear age peak at 201·3 Ma (Fig. 2). This is also supported by the U–Pb zircon age ($201{\cdot}56 \pm 0{\cdot}05$ Ma) obtained by Blackburn *et al.* (2013) for a sample from the Amelal sill, Argana Valley. This U–Pb dated sample is chemically correlated with the Intermediate unit basalts (Blackburn *et al.*, 2013). In contrast, Recurrent basalts yielded generally distinguishably younger $^{40}Ar/^{39}Ar$ plateau ages ($199{\cdot}6 \pm 2{\cdot}3$ Ma to $196{\cdot}3 \pm 2{\cdot}4$ Ma; Verati *et al.*, 2007) and define an age peak at *c.* 199 Ma. A significant eruption gap between Upper and Recurrent basalts is consistent with field evidence for deposition of 30–50 m thick sedimentary strata between these two basaltic units in the Central High Atlas.

The intrusive rocks of the Anti Atlas are poorly dated (unreliable K–Ar ages and one disturbed $^{40}Ar/^{39}Ar$ age spectrum; Sebai *et al.*, 1991; Youbi *et al.*, 2003 and references therein), but paleomagnetic studies support a *c.* 200 Ma intrusion age for the Foum Zguid dyke (Silva *et al.*, 2006; Palencia Ortas *et al.*, 2011). An attempt to date the Bas Draa sills (Anti Atlas near Foum Zguid village) by the $^{40}Ar/^{39}Ar$ method yielded disturbed age spectra, which are generally consistent with a CAMP-like age (Renne & Callegaro, unpublished data). More recently, Davies *et al.* (2017) obtained a zircon U–Pb age for a differentiated portion of the Foum Zguid sample AN733 ($201{\cdot}11 \pm 0{\cdot}07$ Ma), confirming that this dyke was emplaced during the CAMP peak activity.

Further constraints on the duration of the CAMP event in Morocco are given by magnetostratigraphic studies (Knight *et al.*, 2004; Marzoli *et al.*, 2004) of the Tiourjdal and Oued Lahr volcanic piles, showing that basaltic eruptions occurred in a series of five pulses, each of which lasted less than a secular variation cycle (about 450 years by analogy with the duration of these cycles in the Holocene; Schnepp *et al.*, 2003). The number of pulses calculated by Knight *et al.* (2004) was also based on the presence of a brief reversal event apparently recorded within a sedimentary interlayer. These authors estimated the duration of the Lower to Upper volcanism to be about 0·1 Ma, including the magnetic reversal event. Font *et al.* (2011) showed that this magnetic reversal event is probably not primary, but was induced by a much later overprint. Thus, if we exclude the magnetic reversal, the duration of volcanic activity at Tiourjdal may have been shorter than estimated by Knight *et al.* (2004) and the number of eruption pulses reduces from five to four. Therefore, the pulses were two for the Lower unit flows, one for the base of the Intermediate unit and one including the top of the Intermediate unit and all Upper flows. This suggests high eruption rates and has important consequences for the environmental impact of the volcanism, as well as for the formation and differentiation mechanisms of the basaltic magmas.

Biostratigraphic data indicate that the onset of CAMP volcanism and eruption of Lower to Upper basalts in

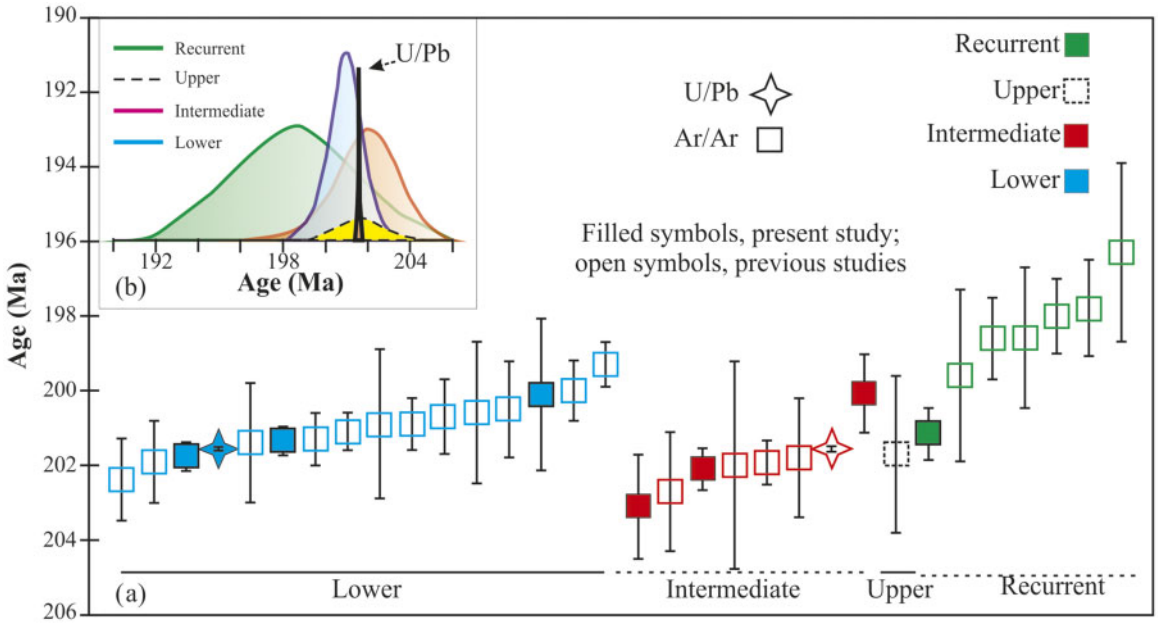

Fig. 2. (a) All available statistically robust $^{40}Ar/^{39}Ar$ plateau ages for the four lava flow units from the CAMP in Morocco (present study and ages from Sebai *et al.*, 1991; Knight *et al.*, 2004; Marzoli *et al.*, 2004; Nomade *et al.*, 2007; Verati *et al.*, 2007; all previous ages filtered after Marzoli *et al.* (2011) and recalculated after Renne *et al.* (2011)) and the U–Pb ages for the Amelal sill from Blackburn *et al.* (2013) and from this study. Ages are in millions of years, Ma. The vertical bars represent 2 sigma analytical uncertainties. Previous data are shown by open symbols, new data from this study are shown by filled symbols. The apparently slightly older ages for some Intermediate vs some Lower flows is most probably due to the effects of cryptic alteration or excess ^{40}Ar. (b) The inset shows a relative age probability plot for all available $^{40}Ar/^{39}Ar$ plateau ages for the four lava flow units and the two U/Pb ages.

Morocco occurred within the Rhaetian, the last stage of the Triassic. Such evidence is provided mainly by palynological data (Manspeizer *et al.*, 1978; Marzoli *et al.*, 2004; Dal Corso *et al.*, 2014; Panfili *et al.*, 2019). Despite being questioned by Whiteside *et al.* (2007; but see also Marzoli *et al.* 2008; Whiteside *et al.*, 2008), all sedimentary samples collected at the very base of the CAMP lava piles from the Central High Atlas (Oued Lahr, Tiourjdal), Argana, the Middle Atlas (Midelt, Tounfite, Agourai) and the Western Meseta (Maaziz) show a near-identical palynological assemblage that can be assigned to the Upper Rhaetian. Since the contact between the sedimentary layers and the overlying flows does not show a sedimentary hiatus at any of the sampled localities, the biostratigraphic data constrain the onset of the volcanism to the latest Triassic at all cited sites. Notably, the same biostratigraphic age can be attributed to sediments where the base of the lava pile is represented by the Lower basalt (e.g. at Tiourjdal or Oued Lahr, Central High Atlas) as well as where the first flow belongs to the Intermediate basalt (Agouraii, Middle Atlas). Recently, Panfili *et al.* (2019) detected an indistinguishable pollen and spore assemblage also within sedimentary strata occurring between the Upper and the Recurrent basalt in the northern Central High Atlas (at Oued Lahr and at Oued Amassine). Combined with carbon isotope data (Deenen *et al.*, 2010; Dal Corso *et al.*, 2014) and considering correlations with other end-Triassic sedimentary sequences (Lindström *et al.*, 2017), these new data suggest that the Lower to Upper basalts were emplaced in a very short time interval coincident with the onset of the end-Triassic mass extinction event (at *c.*201·5 Ma; Schoene *et al.*, 2010; Wotzlaw *et al.*, 2014). The sedimentary layers above the Recurrent flow at Telouet have been dated as Sinemurian (Lower Jurassic), based on palynological evidence (Courtinat & Algouti, 1985), consistent with the younger $^{40}Ar/^{39}Ar$ ages obtained for the Recurrent basalt flows (Verati *et al.*, 2007).

FIELD EVIDENCE AND SAMPLING

A total of about 200 samples from 14 lava piles, two main dykes and six sills was collected. Sampling sites are widespread in the High and Middle Atlas, the Western and Eastern Meseta, and the Anti Atlas (Fig. 1b). For each of the tectonically undisturbed volcanic sections, all fresh lava flows were sampled. For three sections from the Central High Atlas (Oued Lahr, Telouet and Tiourjdal) the samples collected for the magnetostratigraphic study of Knight *et al.* (2004) were used here for geochemical analysis. Coordinates of the main sampling sites are reported in Supplementary Data Electronic Appendix Table S1; supplementary data are available for downloading at http://www.petrology.oxfordjournals.org.

Lava sequences

As already mentioned, the striking feature of the CAMP event in Morocco is the occurrence of four stratigraphically sequenced lava flow units, the Lower, Intermediate, Upper and Recurrent flows, which are defined based on

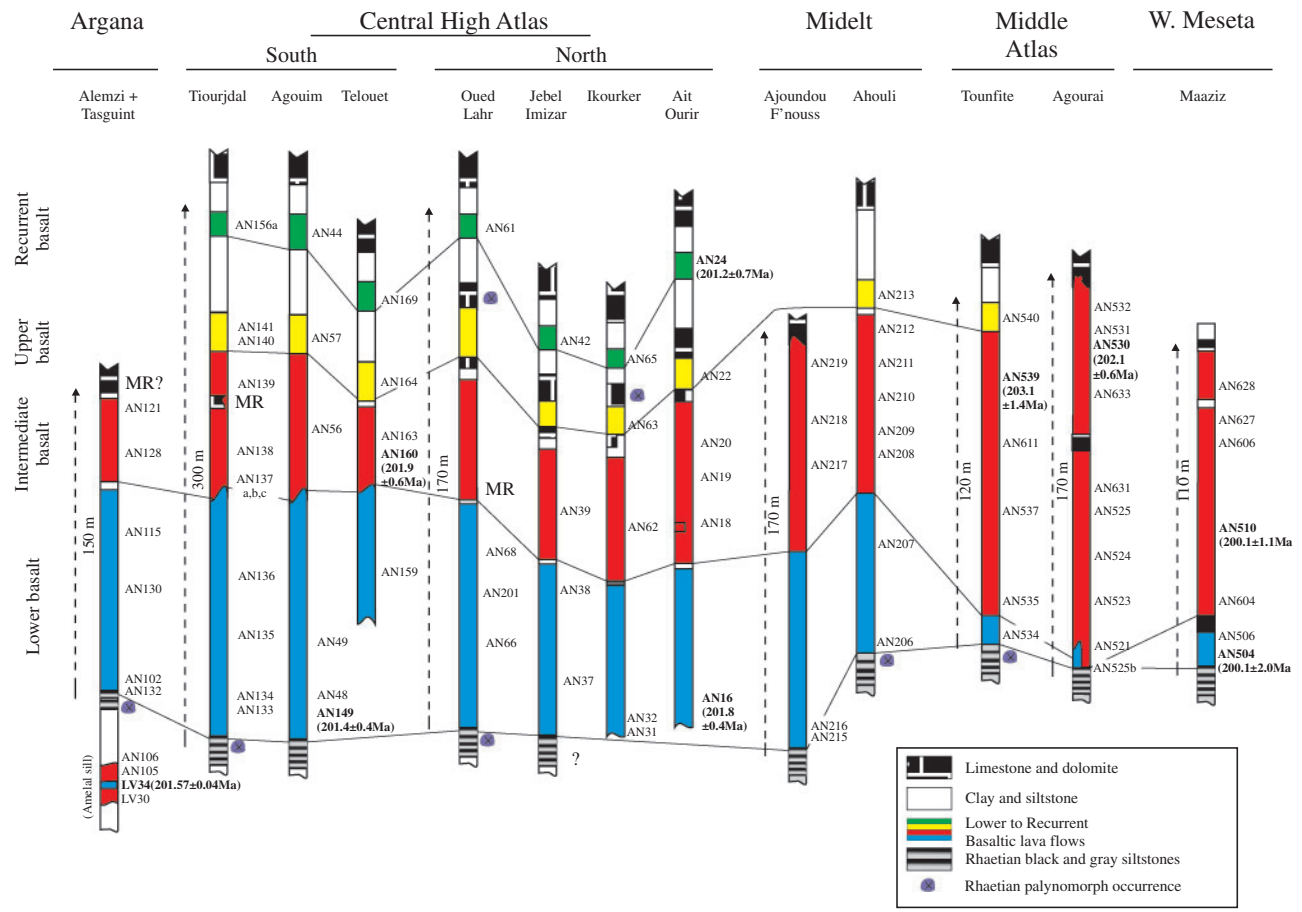

Fig. 3. Schematic logs of the main sampled and analysed volcanic sequences (see Fig. 1b for location of sites). Colour code: blue, Lower unit; red , Intermediate unit; yellow, Upper unit; green, Recurrent unit. Samples dated by U/Pb (LV34) and $^{40}Ar/^{39}Ar$ are in bold (ages in brackets; Ma, million years before present; see Table 1 and Figs 5 and 6 for detailed geochronological data). Sedimentary samples with Rhaetian palynomorph occurrence (purple symbols) are reported following Marzoli *et al.* (2004) and Panfili *et al.* (2019). MR, magnetic reversal (Knight *et al.*, 2004; Marzoli *et al.*, 2004). Sampling coordinates are reported in Supplementary Data Table S1; supplementary data are available for downloading at http://www.petrology.oxfordjournals.org.

field, petrographic and geochemical criteria (Bertrand *et al.*, 1982; Bertrand, 1991; Youbi *et al.*, 2003; Knight *et al.*, 2004; Marzoli *et al.*, 2004; Deenen *et al.*, 2010). Based on field observations alone, the relatively coarse-grained doleritic Lower and Intermediate compound pahoehoe lava flows are easily distinguishable from the slightly porphyric massive Upper and Recurrent sheet flows. Pillow lavas are quite abundant within the lower half of the Intermediate unit throughout Morocco, but are absent or very rare in the other units. Upper flows are the only ones characterized by well-developed columnar jointing the thin columns are probably indicative of sub-aqueous emplacement (Jerram *et al.*, 2016). Everywhere it crops out, the Recurrent basalt is a single massive simple sheet flow reaching up to 15 m in thickness locally. The Recurrent flow was emplaced on top of wet siltstones, which show signs of deformation (load casts) in response to the load imposed by the lava flow.

A total of 13 lava piles from the High Atlas, Middle Atlas and Western Meseta have been sampled in detail (Fig. 3). The sampled sections display several common features as well as some site-specific peculiarities (Fig. 4a–f). Generally, the lava piles are sub-horizontal or slightly tilted (10–30°) and tectonically undisturbed. The thickest lava pile is preserved at Tiourjdal (Central High Atlas, *c.*300 m), while at most other sites the total lava thickness ranges from 100 to 150 m. Except at a few sites where the base of the lava piles does not crop out, the first lava flows are emplaced on grey, black and red continental siltstones of latest Rhaetian age (Panfili *et al.*, 2019). These basal lava flows always belong to the Lower unit, except at the Middle Atlas section of Agourai, where the first lava flows belong to the Intermediate unit. Lower and Intermediate lava flows are present at all localities. The Lower flows make up *c.*30–50% of the total preserved lava thickness in the Central High Atlas, Argana and at Midelt, while they represent <10% of the total thickness in the Middle Atlas and Western Meseta. On the contrary, Intermediate flows are less abundant in central compared to northern Morocco (i.e. *c.*30 vol.% in the Central High Atlas and Argana vs > 90 vol.% in the Middle Atlas and Western Meseta).

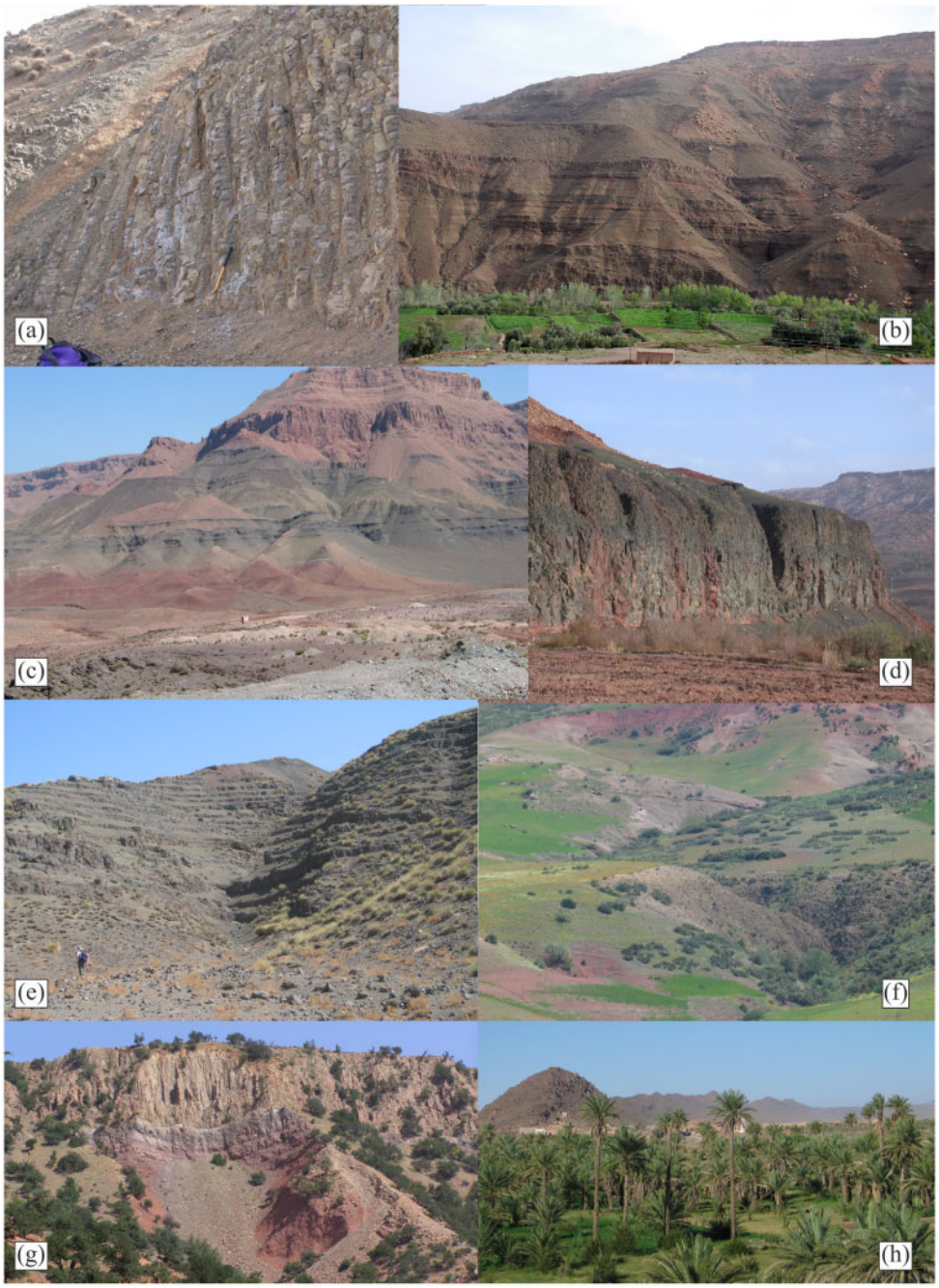

Fig. 4. Field photographs. (a) Columnar jointing in Upper basalts from Ait Ourir, northern Central High Atlas. (b) The Tiourjdal section, southern Central High Atlas. (c) The Ahouli section near Midelt. (d) The Recurrent basaltic flow near Agouim, southern Central High Atlas. (e) The Ajoundou F'nouss section near Midelt, Lower unit lava lobes. (f) The Agourai section, near Meknes, Middle Atlas. (g) The Amelal sill and its lower contact with Triassic red beds of the Bigoudine formation, Argana Valley. (h) The Foum Zguid dyke (behind the palm trees) near Foum Zguid village, Anti Atlas.

Upper flows are also quite widespread over Morocco (except at Argana and in the Western Meseta), but their volume never exceeds 10% of the preserved lava piles. The Recurrent unit is limited to the Central High Atlas lava piles and is absent in northern Morocco and at Argana.

Sedimentary interlayers are rare and thin from the base of the lava section to the top of the Upper unit. The nature of the sedimentary interlayers varies considerably. Sedimentary interlayers within the Lower and Intermediate units and between these units are very thin (<20 cm). Slightly thicker (up to 2–3 m) carbonate layers are for example observed between the Intermediate and Upper flows in the Central High Atlas. The most prominent carbonate and terrigenous sedimentary interlayers occur between the Upper and the Recurrent flows, where these flows are present (Central High Atlas). Sedimentary strata on top of the Upper

flows are still of Rhaetian age (Panfili *et al.*, 2019). On top of the Recurrent basalt quite thick (up to 60 m) red siltstones are followed by carbonates of Sinemurian age (Courtinat & Algouti, 1985). Further details on the sampled sections are given in the (Supplementary Data Electronic Appendix 1; supplementary data are available for downloading at http://www.petrology.oxfordjournals.org).

Intrusive rocks

Intrusive CAMP rocks are quite rare in Morocco (as opposed to North and South America or to other areas of northwest Africa, e.g. Mali, Mauritania). In particular, dykes and sills are absent (to our knowledge) in the Middle Atlas and in the Central High Atlas, while one small and fairly shallow level sill (the Amelal sill) occurs in the Argana Valley. The Amelal sill is about 80 metres thick and crops out over a distance of about 5 km. It intrudes Late Triassic lacustrine sediments (red siltstones), forming a small contact aureole at the base of the sill (Fig. 4g). The depth of intrusion of the sill was probably very shallow (about 0·5 km), as it is separated from the overlying lava flows by only a few hundred metres of siltstones. The basalt at the contact with the sediments is fine-grained, while the inner portions of the sill are coarse-grained and occasionally show granophyric textures. Alteration is pervasive throughout the sill and hinders recognition of intrusive structures and of possible multiple magma injections. Nevertheless, it can be observed that inner portions of the sill are fairly coarse-grained and feldspar-rich. The sample LV34, which yielded the U–Pb age (see below) was collected from this level. Alteration also hinders straightforward comparison of the geochemical composition of the eight analysed sill samples with that of the lava flows.

One dyke and one sill were sampled in the Jbilet Massif, northeast of Argana (Fig. 1b). Here, the intrusive rocks intrude the Paleozoic basement. The geometry of the outcrops in the rather flat Jbilet hills hinders definition of the morphological features of these intrusive rocks. However, aeromagnetic data suggest that the Jbilet dyke has a length of several tens of km and trends towards the Argana Valley where it may have fed the lava flows (Huvelin, 1971; Youbi *et al.*, 2003).

The most abundant outcrops of CAMP intrusive rocks occur in the Anti Atlas, southern Morocco (Bertrand *et al.*, 1982; Youbi *et al.*, 2003 and references therein). The most striking feature is the *c.* 200 km long and up to about 200 m thick, NE–SW trending Foum Zguid dyke (Silva *et al.*, 2006; Bouiflane *et al.*, 2017). The dyke intrudes Neoproterozoic to Palaeozoic sedimentary sequences and locally splits into multiple branches. We collected 16 samples from the dyke, from NE (Imiter) to SW (Bas Draa valley, near Foum Zguid village; Fig. 4h). Southeast of Foum Zguid village, we sampled small dykes approximately parallel to the main Foum Zguid dyke. In the same area, i.e. the Bas Draa valley, CAMP magmas intruded the lower Paleozoic sediments as sills, four of which have been sampled. The sills are up to about 50 m thick and are sometimes connected by small dykes. Further outcrops of probable CAMP sills occur towards and across the Algerian–Moroccan border, but are not accessible. On the contrary, the Ighrem dyke which is parallel to the Foum Zguid dyke and was tentatively attributed to the CAMP (e.g. Silva *et al.*, 2006; Palencia Ortas *et al.*, 2011), is composed of rocks, which are petrographically and geochemically clearly different from any known CAMP rock. Unlike most CAMP rocks, the Ighrem dyke rocks are moderately alkaline (i.e. most samples classify as trachybasalt or trachyandesite), yielding higher K than Na and are in general enriched in all incompatible trace elements (e.g. Nb$>$ 15 ppm, Zr $>$ 170 ppm; La $>$28 ppm) compared to any previously analysed CAMP rock. We also note that the paleomagnetic pole of the Ighrem dyke (Palencia Ortas *et al.*, 2011) is significantly displaced towards the north compared to that of the Foum Zguid dyke, arguing against a synchronous emplacement of these two dykes. Therefore, we conclude that the Ighrem dyke is not part of the CAMP and do not consider it further in this study.

The depth of intrusion of the sills and dykes in the Anti Atlas was probably 4–5 km below the surface, considering the thickness of the Proterozoic to Carboniferous sedimentary cover (Michard *et al.*, 2008). We also note that in the Newark basins, CAMP sills typically intruded at similar depths of about 5 km, below continental lacustrine-fluviatile sediments (e.g. Puffer *et al.*, 2009).

ANALYTICAL METHODS

The main features of the analytical methods are described here in summary. The complete description can be found in the (Supplementary Data Electronic Appendix 1; supplementary data are available for downloading at http://www.petrology.oxfordjournals.org).

Whole-rock major element and selected trace element contents were determined by X-ray fluorescence (XRF) at the University of Padova with a Philips PW2400 spectrometer, following methods described in Cal legaro *et al.* (2013). Trace elements were also analysed by Inductively Coupled Plasma–Mass Spectrometry (ICP-MS) at the University of Bretagne Occidentale, Brest (France), following analytical protocols described in Barrat *et al.* (1996). Analytical uncertainties are estimated at less than 5%.

Sr–Nd–Pb radiogenic isotope ratios were measured at the Department of Earth Sciences, University of Geneva (Switzerland) using a Thermo Neptune PLUS Multi-Collector ICP-MS. The method is described in detail in Chiaradia *et al.* (2011) and Béguelin *et al.* (2015).

Chemistry and mass spectrometry for Re–Os iso topic analyses were performed at the Centre de Recherches Pétrographiques et Géochimiques (CRPG-

CNRS, Vandoeuvre-les-Nancy, France) following methods outlined in Callegaro *et al.* (2013) and Merle *et al.* (2014). Osmium concentrations for the samples were determined by isotope dilution analysis of the same aliquot used for isotopic composition determination. Os isotopic compositions were measured by negative thermal ionization (N-TIMS, Creaser *et al.*, 1991; Volkening *et al.*, 1991) on a Finnigan MAT 262 mass spectrometer.

Mineral major element compositions were obtained using a CAMECA SX50 electron microprobe analysis at the CNR-IGG, Padova, Italy, following methods described in Callegaro *et al.* (2017). Trace element concentrations in minerals were determined with a LA-ICP-MS housed at IGG-C.N.R., Pavia (Italy), following methods described in Miller *et al.* (2012).

Argon geochronological analyses were carried out at the Western Australian Argon Isotope Facility (WAAIF) of the John de Laeter Centre, Curtin University (Perth, Australia) and at the Berkeley Geochronology Center (Berkeley, USA). Plagioclase separated from samples AN16, AN49, AN24, AN160, AN510, AN530, AN540 were analysed at Curtin, while plagioclase separates from samples AN216, AN219, AN504, AN525b, AN530, AN539, AN540 were analysed at Berkeley. GA1550 and FCs were used as neutron fluence monitors, adopting ages of 99·738 ± 0·100 Ma and 28·294 ± 0·036 Ma (1σ), respectively (Renne *et al.*, 2011). More details on the Ar analyses are reported in Renne *et al.* (1998) and Jourdan *et al.* (2009).

U–Pb geochronology was performed at the Department of Earth Sciences, University of Geneva (Switzerland). Zircon crystals from sample LV34 of the Amelal sill were extracted and analysed following a procedure similar to that of Davies *et al.* (2017).

Paleomagnetic analysis were performed at the Berkeley Geochronology Center (Berkeley, U.S.A.) following methods outlined in Knight *et al.* (2004).

RESULTS

$^{40}Ar/^{39}Ar$ and U–Pb geochronology

Nine new $^{40}Ar/^{39}Ar$ ages are presented in Fig. 5 and Table 1 (the complete data set is reported in the Supplementary Data Electronic Appendix Table S2; supplementary data are available for downloading at http://www.petrology.oxfordjournals.org). Seven of these are $^{40}Ar/^{39}Ar$ plateau ages, while two samples (AN504 and AN24) yielded mini-plateau ages defined by 67% and 55% of the released argon, respectively. The plateau ages are statistically quite robust (MSWD in the range 0·5–1·8, probability 6–93%). The Ca/K of the plateau steps (*c.*40–120), calculated from the $^{37}Ar/^{39}Ar$ isotope ratios, is generally consistent with the Ca/K measured by electron microprobe analysis (see below). Inverse isochron ages generally overlap the plateau and mini-plateau ages and yield initial $^{40}Ar/^{36}Ar$ values (252 ± 25 to 305 ± 25) overlapping or approaching atmospheric values (298·56). The only exception is sample AN525b, which yields an initial $^{40}Ar/^{36}Ar$ value (162 ± 9) implausibly below the atmospheric value. Therefore, we consider the apparent age of sample AN525b to be affected by post-eruption alteration and do not consider it as a valid crystallization age. Samples AN530 and AN510 were analysed both at Curtin University and at the BGC and yielded indistinguishable ages. The ages obtained at Curtin are slightly more precise (lower uncertainty) and are here retained. Furthermore, three more samples (AN216, AN219, AN540) were analysed, but did not provide plateau or isochron ages.

The seven retained $^{40}Ar/^{39}Ar$ plateau ages and the mini-plateau age (AN24) range from 200·10 ± 2·04 Ma to 203·10 ± 1·40 Ma. Three dated samples belong to the Lower unit from the Central High Atlas (AN16, AN49) and from the Western Meseta (AN504, mini-plateau age), while four belong to the Intermediate unit from the Central High Atlas (AN160), the Middle Atlas (AN530, AN539) and the Western Meseta (AN510). The only dated Recurrent basalt (AN24) yielded a mini-plateau (201·15 ± 0·70 Ma). The new ages for Lower and Intermediate basalts from the Central High Atlas, Middle Atlas and Western Meseta lava flows and previously published ones for the Central High Atlas and Eastern Meseta are near-synchronous, supporting a similar eruption age for CAMP basalts in all regions of Morocco. The Upper basalt previously dated (201·7 ± 2·1 Ma, Sebai *et al.*, 1991, age recalculated in Marzoli *et al.*, 2011) overlaps in age with the Lower and Intermediate lava flows. The only analysed Recurrent basalt (AN24) yielded a mini-plateau age (201·15 ± 0·70 Ma) that is indistinguishable from those of the other lava flow units. This value contrasts with previous studies that found younger $^{40}Ar/^{39}Ar$ ages for Recurrent basalts (196·3 ± 2·4 to 199·6 ± 2·3 Ma; Verati *et al.*, 2007; recalculated in Marzoli *et al.*, 2011). Our new age overlaps with the $^{40}Ar/^{39}Ar$ age for the Hook Mt. flows (200·3 ± 1·9 Ma; Marzoli *et al.*, 2011) from the Newark Basin, that are both stratigraphically and geochemically similar to the Recurrent flows from Morocco.

Sample LV34 from the Amelal sill yielded a few zircon crystals (Fig. 6; Table 2). Six of them were dated by ID-TIMS, with four grains producing a weighted mean age of 201·569 ± 0·042 Ma (MSWD = 1·1; probability = 34%). This age is identical to the U–Pb age obtained by Blackburn *et al.* (2013) for the Amelal sill (201·564 ± 0·054 Ma). Two of the zircon grains yielded slightly younger ages. However, these were interpreted as reflecting small amounts of Pb loss since the chemical abrasion procedure was only conducted at 180 °C (further details are reported in the Supplementary Data Electronic Appendix 1; supplementary data are available for downloading at http://www.petrology.oxfordjournals.org). Also, the calculated temperature for zircon saturation is 625 ± 10 °C (using the formula of Boehnke *et al.*, 2013). This low temperature and the mafic nature of the sample suggests that zircon xenocrysts should not be present in this sample, therefore,

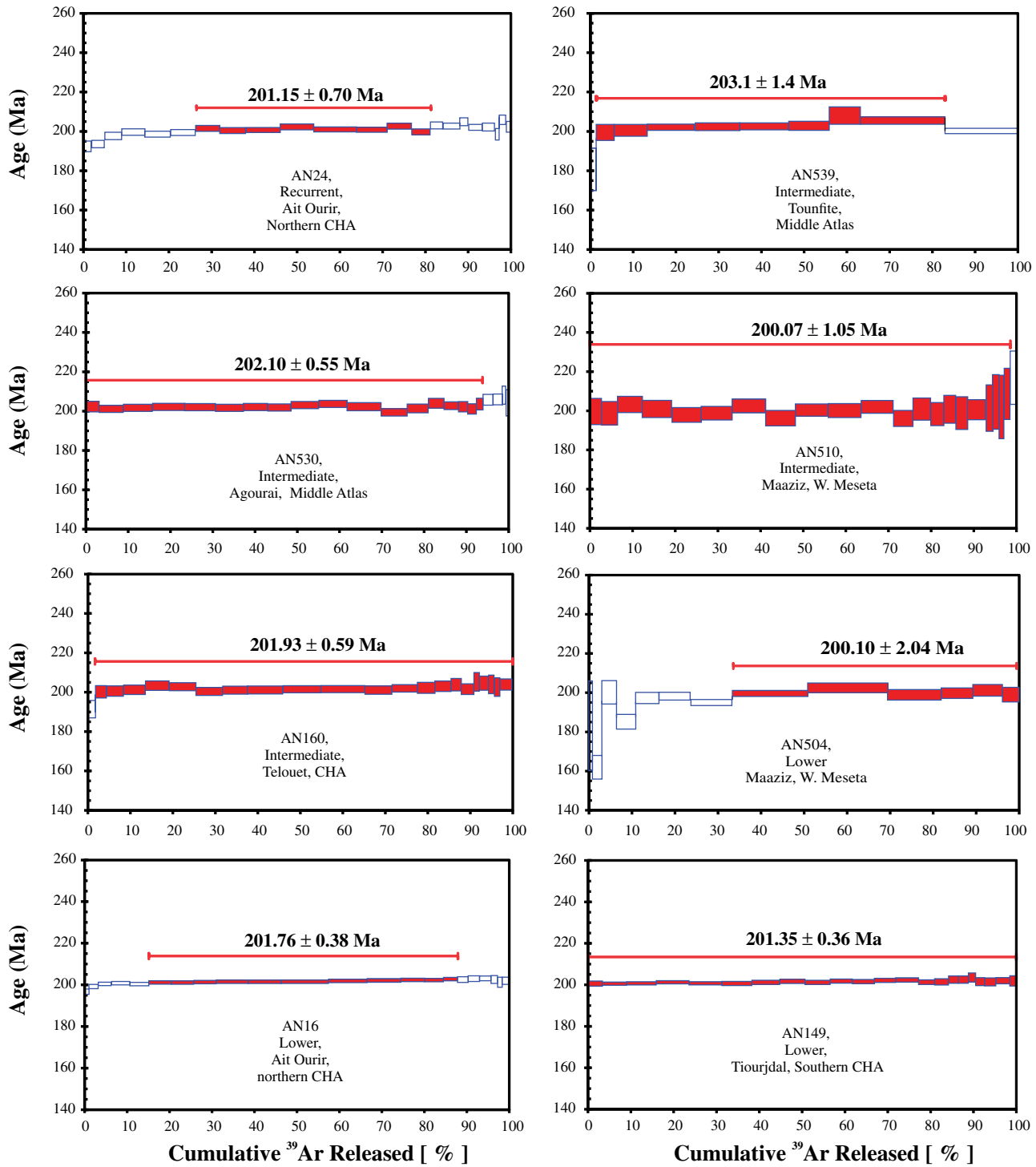

Fig. 5. $^{40}Ar/^{39}Ar$ plateau age spectra for plagioclase separates from 8 CAMP basalts from Morocco. The mini-plateau (AN504 and AN24) and plateau ages (in Ma, million years before present) are shown by the red bars with 2 sigma uncertainty. Plateau steps are shown by the filled boxes. Summary Argon age data are reported in Table 1, while the complete dataset can be found in the Supplementary Data Table S2; supplementary data are available for downloading at http://www.petrology.oxfordjournals.org.

the older zircon ages should more reliably record the crystallisation of this unit. Notably, as shown below, the sample dated here (LV34) has a composition approaching those of the Lower unit lava flows, while Blackburn *et al.* (2013) correlated their Amelal sample to the Intermediate unit.

Paleomagnetic results

Four lava piles from Midelt (Ahouli), the Middle Atlas (Tounfite and Agourai) and the Western Meseta (Maaziz) were investigated flow by flow (the detailed data and the virtual geomagnetic pole plots are reported in Supplementary Data Electronic Appendix

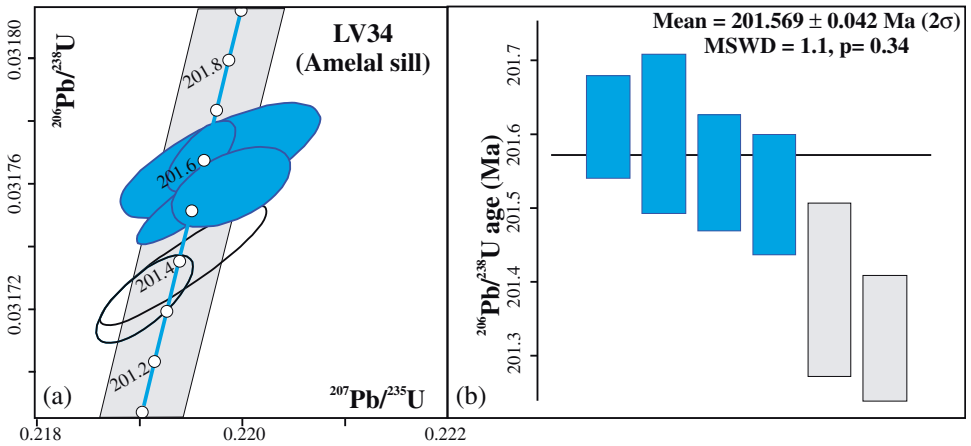

Fig. 6. (a) U–Pb Concordia and (b) $^{206}Pb/^{238}U$ weighted mean age of LV34, Amelal sill, Argana Valley. Ages on the Concordia diagram are in Ma, ellipses represent 2 sigma errors. In (b), the height of the boxes represents 2 sigma analytical uncertainty for single zircon $^{206}Pb/^{238}U$ ages. Retained ages are shown by blue rectangles. Data are reported in Table 2.

Table 1: $^{40}Ar/^{39}Ar$ plateau and isochron ages (± 2 sigma analytical uncertainty) and statistical data (MSWD and probability of fit, P)

Location	Sample	unit	Lab.	Plateau age (Ma) (±2σ)	MSWD	P	% ^{39}Ar in plateau steps	Isochron age (Ma) (±2σ)	Isochron $^{40}Ar/^{36}Ar$ intercept
Agouim CHA	AN149	Lower	1	**201·35±0·36**	1·35	0·13	100	201·62±0·45	281±19
Ait Ourir	AN24	Rec	1	***201·15±0·70***	1·95	0·06	55	200·80±2·57	310±91
CHA	AN16	Lower	1	**201·76±0·38**	1·74	0·07	73	202·41±0·47	252±25
Telouet CHA	AN160	Interm	1	**201·93±0·59**	0·96	0·51	98	203·03±1·21	287±11
Agourai Middle Atlas	AN530	Interm	1	**202·10±0·55**	1·28	0·19	94	202·04±0·87	299±8
			2	200·6±2·6	0·44	0·88	41	199±20	224±17
			2	199·6±1·0	1·58	0·14	79	205±13	239±11
	AN525 B	Lower?	2	197·5±1·0	1·36	0·24	84	205±16	162±9
Tounfite Middle Atlas	AN539	Interm	2	**203·1±1·4**	0·91	0·50	81	202±4	298±4
			2	199·0±2·8	0·88	0·49	74	195±7	281±7
Maaziz W. Meseta	AN510	Interm	1	**200·07±1·05**	0·93	0·55	99	199·7±1·9	303±25
			2	199·7±2·0	0·38	0·93	95	201±14	291±11
	AN504	Lower	2	**200.1±2.0**	0.27	0.93	67	200±4	292 3

Analyses were performed at Curtin University (Lab. 1) and at the Berkeley Geochronology Center (Lab. 2). Retained age data are in bold, mini-plateau age is in italics. The complete Ar isotopic dataset can be found in the Supplementary Data Electronic Appendix Table S2; supplementary data are available for downloading at http://www.petrology.oxfordjournals.org. CHA, Central High Atlas.

Table S3; supplementary data are available for downloading at http://www.petrology.oxfordjournals.org). All four sections have flow mean directions that are consistent with previous results from CAMP basalts. Within section resolution is not as high for this study as it was for previous ones (e.g. Knight *et al.*, 2004), but some directional groupings can be proposed based on within-section agreement of flow mean directions. At the Tounfite location, the lava flows were gently dipping due to numerous small faults. Finding a direct measurement of strike for the lava flows was very difficult due to the nature of the rocks, which were very fractured and due to the orientation of the outcrops along the roadside. In the field, we estimated the strike at ~50° and the dip at ~20° to the south. The flow mean directions from this locality have been rotated to correct for this tilting, which occurred after acquisition of the characteristic remanence magnetization.

The flow means can be placed into groups based on agreement of flow mean directions and stratigraphic patterns (Fig. 7). The groups are not very well constrained, but are distinct from one another by the Fisher mean of the flow means for samples from all sections (Fig. 7b). The small variations that differentiate directional groupings are a record of secular variation, which is a smooth and steady process. Therefore, distinct groupings suggest eruption in a pulsed manner in the Middle Atlas, which is consistent with the study on the Central High Atlas lava piles (Knight *et al.*, 2004).

Petrography and mineral compositions

The CAMP lavas from Morocco have textures ranging from intergranular or intersertal to porphyritic (Supplementary Data Electronic Appendix 1; supplementary data are available for downloading at http://www.petrology.oxfordjournals.org). The dominant phenocrysts in all four units are augitic clinopyroxene (mostly in the following range: Wollastonite 30–40%, Enstatite 40–60%, Ferrosilite 10–25%; mineral major element compositions are reported in the

Table 2: U–Pb geochronological data for sample LV34, Argana basin, Amelal sill

	Composition					Dates (Ma)								Isotopic Ratios							
Fraction	Th/U (a)	Pb* (pg)(b)	Pbc (pg)(c)	Pb*/Pbc(d)	Th/U (magma)(e)	$^{206}Pb/^{238}U$ <Th>(f)	±2σ abs	$^{207}Pb/^{235}U(g)$	±2σ abs	$^{207}Pb/^{206}Pb(g)$	±2σ abs	Corr. coef.	%disc (h)	$^{206}Pb/^{204}Pb$ (i)	$^{206}Pb/^{238}U(j)$	±2σ %	$^{207}Pb/^{235}U(j)$	±2σ %	$^{207}Pb/^{206}Pb(j)$	±2σ %
LV34																					
LV34_z1	2·03	25·10	0·09	290	10·15	201·61	0·071	201·58	0·28	202·20	3·00	0·690	0·32	11980	0·031755	0·036	0·2196	0·15	0·05018	0·13
LV34_z2	2·35	44·70	0·88	50	11·75	201·55	0·080	201·82	0·48	205·90	5·70	0·508	2·16	1980	0·031746	0·040	0·21989	0·26	0·05026	0·24
LV34_z3	2·16	61·40	2·25	27	10·80	201·60	0·110	201·73	0·81	204·20	9·30	0·729	1·32	1118	0·031754	0·058	0·21978	0·44	0·05022	0·40
LV34_z4	2·29	25·80	0·21	122	11·45	201·52	0·084	201·50	0·45	202·30	4·90	0·879	0·43	4824	0·031741	0·042	0·21951	0·25	0·05018	0·21
LV34_z8	2·91	10·20	0·14	75	14·55	201·40	0·120	201·43	0·67	202·80	7·30	0·912	0·72	2608	0·031722	0·060	0·21943	0·37	0·05019	0·31
LV34_z9	2·76	14·30	0·10	147	13·85	201·33	0·087	201·12	0·39	199·60	4·30	0·736	−0·84	5295	0·031711	0·044	0·21905	0·21	0·05012	0·18

Supplementary Data Electronic Appendix Tables S4–6; supplementary data are available for downloading at http://www.petrology.oxfordjournals.org) and plagioclase (anorthite component, An = 40–88; orthoclase < 3; Fig. 8a). Oxides (titanomagnetite, mostly and rare ilmenite) are also present in all rocks as microphenocrysts or groundmass crystals and frequently show exsolution patterns. Olivine, when present, is generally strongly altered and the few available optically fresh patches have low forsterite contents ($Fo_{64–76}$), which is probably the result of late- or post-magmatic modification. Olivine is relatively frequent in Lower unit flows, while it is rare (Intermediate and Recurrent) or absent (Upper) in the other units. Low-Ca clinopyroxene (pigeonite, $Wo_{5–10}$, $En_{50–70}$, $Fs_{15–30}$) can be abundant and present as phenocrysts, notably in the Intermediate lava flows, while it is limited to groundmass crystals in the Upper and Recurrent units. Pigeonite is sometimes found rimming augite cores.

Systematic textural and mineralogical variations are observed through the lava piles, as previously shown by Bertrand (1991). The Lower and Intermediate basalts have generally intergranular or intersertal textures with grain sizes depending on the lava flow thickness or on the distance of the sample from the lava crust. For example, the thin Lower flows at Maaziz are fine grained, whereas the Lower flows at Tiourjdal yield mm-sized crystals. A few samples (e.g. AN132, Argana and AN31, AN32, Central High Atlas) show large aggregates of mafic minerals and thus have a cumulitic whole-rock composition. Upper and Recurrent flows are always slightly porphyritic to glomeroporphyritic, i.e. they carry mm-sized phenocrysts of augite and plagioclase set in a fine-grained matrix.

Intrusive rocks display mineral compositions similar to those of the lava flows, with the exception that pigeonite is found in an intrusive Recurrent-unit sill only (AN724, Anti Atlas). The textures of sills and dykes range from porphyritic at the chilled margins of the Foum Zguid dyke and of the Amelal sill, to coarse doleritic and occasionally gabbroic and granophyric textures within the central portions of the intrusions.

Mineral major element composition

Forty plagioclase phenocrysts from 20 samples (lava flows and intrusive rocks) were investigated in detail by electron microprobe analysis (Fig. 8; Supplementary Data Electronic Appendix Table S5; supplementary data are available for downloading at http://www.petrology.oxfordjournals.org). The analysed plagioclase for Lower and Recurrent samples have Ca/Na similar to those of their host-rocks, while some Intermediate and most Upper basalt plagioclase cores have substantially higher Ca/Na than the whole-rock compositions. Plagioclase phenocrysts from the Lower and Recurrent units are mostly labradorite (An_{50-75}), while those from the Intermediate unit are both labradorite and bytownite ($An_{55–83}$) and Upper basalt plagioclases are mostly

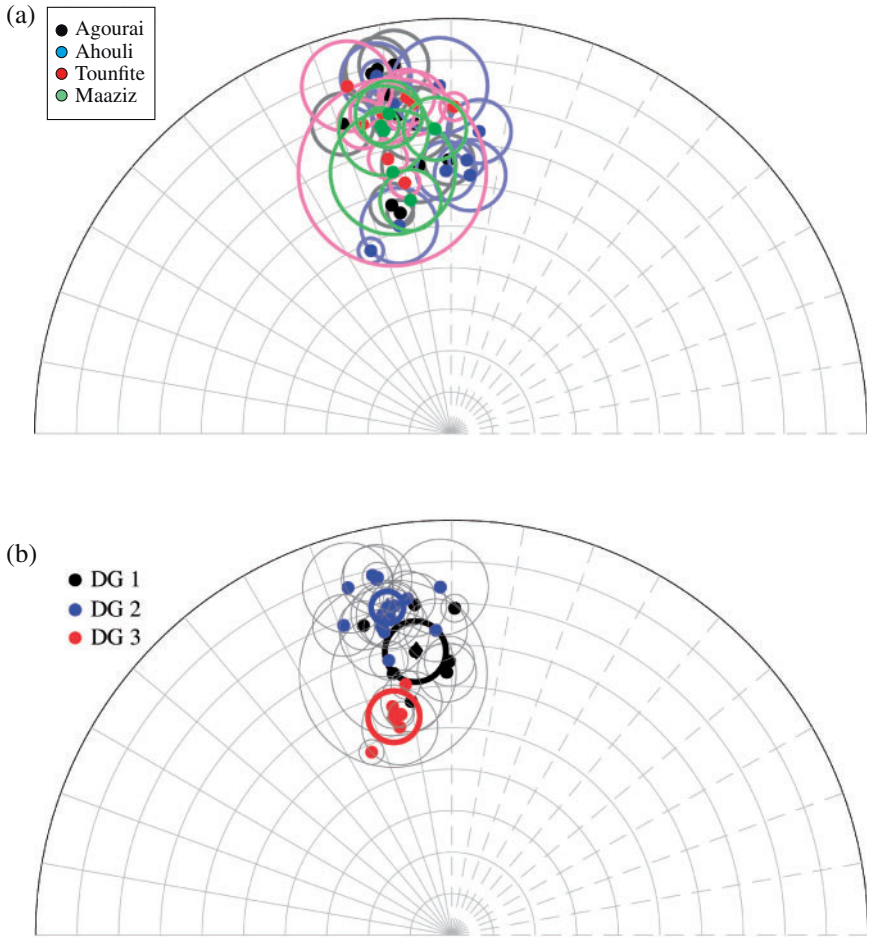

Fig. 7. (a) Paleomagnetic flow mean directions for the 4 sections, Agourai (black), Ahouli (blue), Tounfite (red) and Maaziz (green). Flow means and 95% confidence cones are shown. (b) Directional groupings (DG) made based on geochemical and directional correlations between sections are statistically different from one another at 95% confidence. Directional groups are the Fisher mean of the flow means for each directional group from all sections and are shown with their 95% confidence cone (the data are reported in Supplementary Data Table S3; supplementary data are available for downloading at http://www.petrology.oxfordjournals.org).

bytownite ($An_{70–88}$). Recurrent plagioclase is systematically depleted in K_2O compared to Lower and Intermediate unit samples at a similar An content.

The majority of the over 40 plagioclase phenocrysts analysed by detailed core-rim compositional traverses are normally zoned, with An decreasing towards the crystal rims (Fig. 8c). However, inverse zoning occurs in some Recurrent unit plagioclase phenocrysts (2 of 6 analysed crystals) and is frequent in Intermediate unit samples (6/9), while it is rare in the Upper unit (2/9) and absent in the Lower one. Upper basalts occasionally contain resorbed, high-An cores, surrounded by relatively low-An external zones. Notably, the zoning is much smoother in intrusive rocks, where plagioclase shows a nearly continuous decrease in An from core to rim (Fig. 8c). This suggests a prolonged evolution at relatively high temperature and at equilibrium conditions.

Augite phenocrysts are found in nearly all CAMP rocks from Morocco and 28 crystals have been analysed by detailed electron microprobe traverses (representative data are reported in the Supplementary Data Electronic Appendix Table S4; supplementary data are available for downloading at http://www.petrology.oxfordjournals.org). Most augite cores have compositions at or close to equilibrium with their whole-rock (Fig. 8d), for example in terms of Mg# (for Kd Fe^{2+}/Mg of about 0·25–0·30; cf. Putirka *et al.*, 1996; Villiger *et al.*, 2004; Putirka, 2008). Only augites from Upper basalt lava flows and from the Foum Zguid Intermediate unit samples yield slightly higher Mg# than expected for equilibrium conditions. These augite cores may be antecrysts that crystallized from a magma more mafic than the host whole-rock. On the contrary, a few Lower and Intermediate augite cores yield Mg# lower than expected, suggesting that the whole-rock is enriched in Mg due to accumulation of mafic minerals (Fig. 8d). Most augite cores analysed in Recurrent basalts are close to equilibrium with their whole-rock, while their rim compositions are progressively depleted in Mg#.

Bertrand (1991) also highlighted systematic minor element differences in the compositions of augite and pigeonite for the four lava flow units. In general, our data confirm these differences, such as distinct Ti and

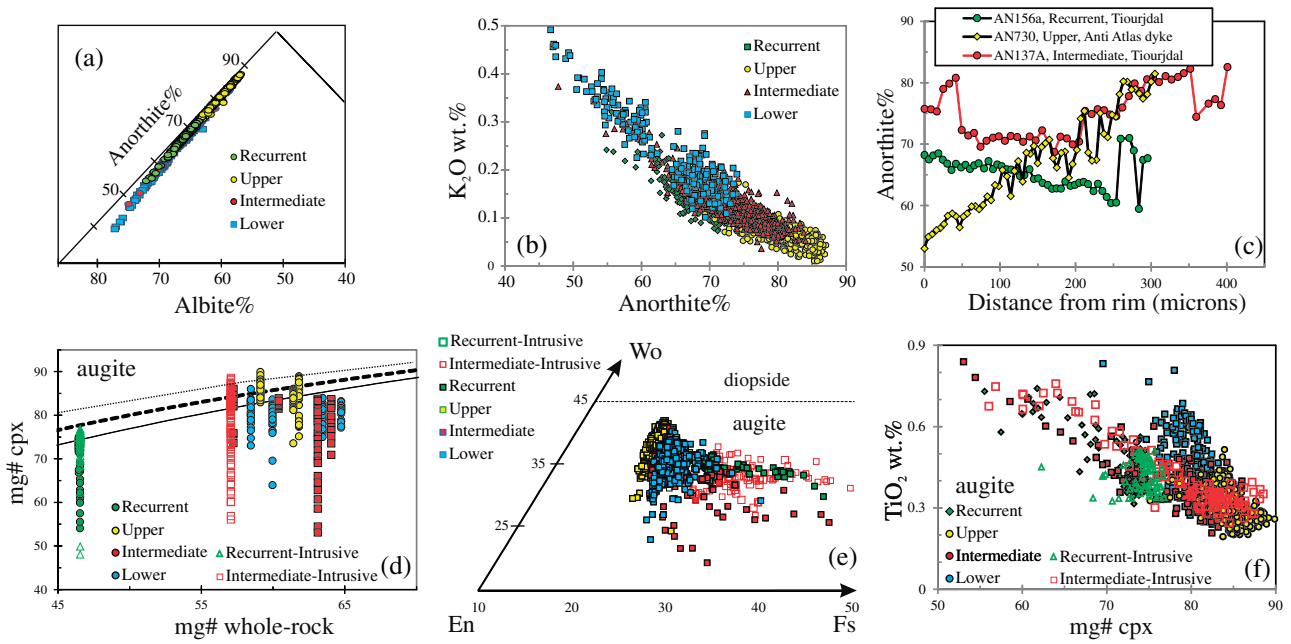

Fig. 8. Plagioclase and augitic clinopyroxene compositions of CAMP samples from Morocco. (a) Feldspar classification diagram for forty crystals from twenty samples of the four units. (b) Plagioclase K_2O wt % vs anorthite%. (c) Anorthite% core–rim variation of representative plagioclase crystals from lava flows of the Intermediate (AN137A) and Recurrent units (AN156a; both samples from Tiourjdal, Central High Atlas) and of an Anti Atlas sill (AN730) with Upper unit composition. (d–f) Augite major element compositions of all analysed Moroccan CAMP augites. (d) Whole-rock mg# (= 100*Mg/(Mg+Fe^{2+}), where Fe^{2+} is calculated assuming $Fe^{3+}/Fe^{2+} = 0{\cdot}15$ consistent with the poorly oxidized composition of the CAMP tholeiitic magmas) vs augite mg# (same as for whole-rock, Fe^{2+} calculated according to Papike *et al.* (1974); it should be noted that calculated Fe^{3+} in augites is generally zero), Kd = Fe/Mg in mineral divided by Fe/Mg in equilibrium magma. Continuous, dashed and dotted lines represent Kd values of 0·30, 0·27, 0·24, respectively. (e) Pyroxene classification, following Morimoto *et al.* (1988). (f) Augite TiO_2 (wt %) vs augite mg# content. In all diagrams blue symbols are the Lower unit, red are Intermediate, yellow are Upper, green are Recurrent.

Al contents of augite cores that reflect largely whole-rock compositional differences (i.e. Lower and Recurrent augites yield highest TiO_2). However, in detail, we observe a large overlap in TiO_2 content between Intermediate (TiO_2 = 0·2–0·5 wt %) and Upper basalt augites (TiO_2 = 0·2–0·4 wt %).

A further systematic difference among the four units concerns augite zoning. Lower unit augites are generally unzoned in terms of major (e.g. Mg#) and minor elements (Ti, Al, Cr). On the contrary, Intermediate (5/11 analysed phenocrysts) and Upper unit (4/8) augites are frequently sector zoned, with abrupt variations of Ti, Al and Cr at near-constant Mg# suggesting rapid disequilibrium crystallization (Brophy *et al.*, 1999). Augite and pigeonite from intrusive rocks are normally zoned.

Mineral trace element data

A few plagioclase and augite crystals from two of each of the lava flow units were analysed by laser ablation ICP-MS (data are reported in the Supplementary Data Electronic Appendix Table S7; supplementary data are available for downloading at http://www.petrology.oxfordjournals.org). Only the elements showing concentrations well above the detection limit are considered in this study. These are LREE (La to Eu), Y, LILE (Rb, Ba, Sr) and Ti for plagioclase, and all REE, Sr, Zr, Y, in addition to Ti (measured also by electron microprobe) and transition metals (Cr, Ni, V), for augites.

Trace element contents both in plagioclase and augite show systematic differences among the four units. In general, plagioclase and augite crystals in Lower basaltic andesites are those with the highest LREE, LILE and Zr contents, while Recurrent basalt crystals yield the highest Y and HREE and the lowest Sr and Eu. Therefore, Lower and Recurrent unit augites are those with the highest and lowest La/Yb, respectively. Intermediate and Upper unit augites have quite similar trace element contents, including similar La/Yb. On the contrary, plagioclases from the Intermediate unit yield slightly higher LREE, Y, Ba and Ti relative to Upper unit plagioclase crystals. In general, La contents are similar in plagioclases and augites from the same rocks, except for the two analysed Intermediate unit basaltic andesites, where La is slightly higher in plagioclase (0·49–1·45 ppm; mean 0·71 ppm) than in augite (0·29–0·64 ppm; mean 0·48 ppm).

Chondrite-normalized REE and primitive mantle normalized (McDonough & Sun, 1995) trace element patterns for the augites (Fig. 9 a and b) show depleted light vs heavy REE and negative Zr and Ti anomalies. Eu anomalies are in general moderate in most Intermediate, Upper and Recurrent unit augites (Eu/Eu* = 0·8–1·1) while Lower unit augites always display negative Eu anomalies (Eu/Eu* = 0·6–0·8). The analysed augite and plagioclase crystals yield, in general, trace element contents and patterns similar to those obtained

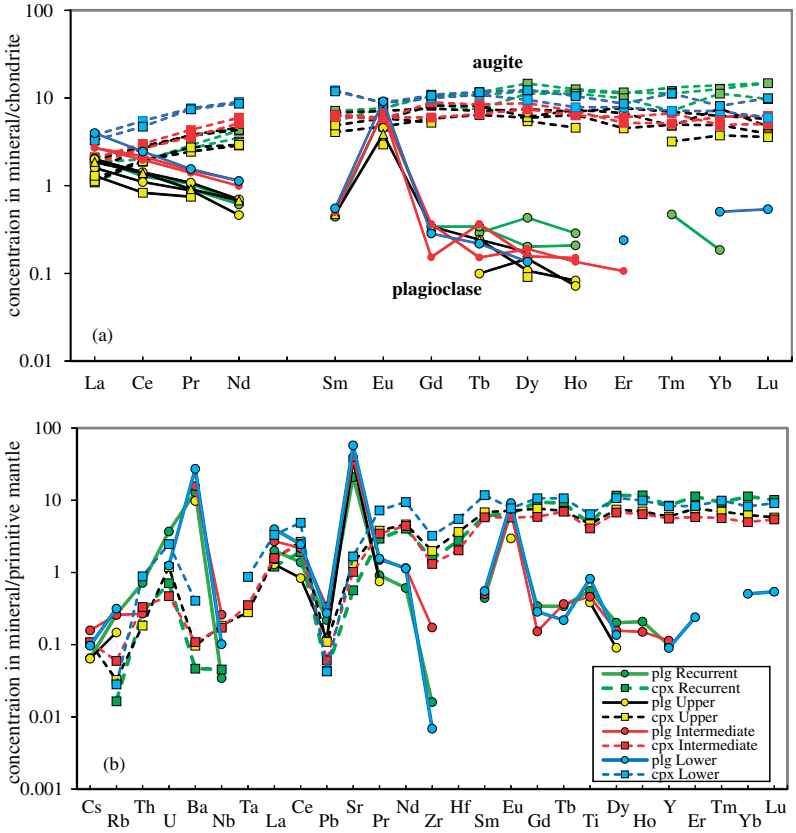

Fig. 9. Representative augite (dashed lines) and plagioclase (continuous lines) (a) rare earth element REE and (b) incompatible trace element compositions normalized to chondritic values (McDonough & Sun, 1995) and to Primitive mantle values (McDonough & Sun, 1995). Complete LA-ICP-MS data are reported in Supplementary Data Table S7; supplementary data are available for downloading at http://www.petrology.oxfordjournals.org.

on minerals from other CAMP rocks (Dorais & Tubrett, 2008; Marzoli *et al.*, 2014).

Whole-rock compositions

Alteration

Secondary minerals such as iddingsite, sericite, chlorite, celadonite, zeolites, quartz and calcite, replacing primary minerals or filling voids, are rare in most rocks, but may be abundant in some samples (notably in most Argana, some Middle Atlas and Anti Atlas samples). Selection of the freshest samples for geochemical investigation is thus necessary and is based both on petrographic observations and geochemical criteria. The optically and mineralogically most altered samples yield generally high LOI (loss on ignition $>$ 2·0 wt %), Na_2O ($>$ 2·4 wt %) and K_2O ($>$ 1·2 wt %) and low CaO ($<$ 9 wt %). However, in order to discriminate between secondary (alteration) and primary (magmatic differentiation) effects it is necessary to consider the systematic chemical differences among the four units (see below), i.e. the generally higher alkali content of the Lower basalts and the generally higher CaO of the Upper basalts. Accounting for such differences, 28 (Argana lava flows and sill, and Anti Atlas dyke samples, mostly) of the total set of 159 analysed samples yield anomalously high alkalis and low CaO in addition to high LOI and are thus not considered further. Nonetheless, more subtle alteration cannot be ruled out completely for several samples and is evidenced, for example, by the presence of sericite lamellae in plagioclase or by altered interstitial glass. Such alteration affects particularly the mobile elements such as the LILE, which indeed show a relatively larger scatter than immobile elements such as REE or HFSE (see below).

Whole-rock classification and major and trace element variations

The majority of the analysed CAMP rocks from Morocco have MgO contents varying between 10 and 6 wt % and Mg# (=100 Mg/(Mg+Fe^{2+}), calculated for Fe^{3+}/Fe^{2+}= 0·15) ranging from 66 to 56, indicating that they are moderately evolved (representative rock compositions are reported in Table 3, the complete dataset can be found in the Supplementary Data Electronic Appendix Table S8; supplementary data are available for downloading at http://www.petrology.oxfordjournals.org). The evolved compositions are confirmed by moderate Ni (140–40 ppm) and Cr contents (400–100 ppm). Only a few samples (three Lower flows, one Intermediate and one Upper flow, and two dyke samples with Upper affinity) have high MgO ($>$ 10 wt %), Mg# (69–73), Cr (530–753 ppm) and Ni (181–380 ppm).

Table 3: Whole-rock major and trace element and Sr–Nd–Pb isotopic data

Sample	AN 16	AN 32	AN 37	AN 49	AN 134	AN 135	AN 136	AN 137 C	AN 102
Unit	lower	lower	lower	lower	lower	lower	lower	lower	lower
area	N-CHA	N-CHA	N-CHA	S-CHA	S-CHA	S-CHA	S-CHA	S-CHA	Argana
locality	Ait Ourir	Ikourker	J. Imizar	Tiourjdal	Tiourjdal	Tiourjdal	Tiourjdal	Tiourjdal	Alemzi
SiO_2 wt %	53·59	50·97	50·95	52·22	53·57	54·31	53·89	53·44	52·63
TiO_2	1·40	1·23	1·21	1·27	1·43	1·39	1·42	1·42	1·32
Al_2O_3	14·42	11·68	11·47	13·55	14·26	14·14	14·09	14·77	14·04
FeOt	9·87	11·39	11·60	10·50	10·02	9·36	10·24	9·35	10·49
MnO	0·18	0·19	0·19	0·15	0·18	0·17	0·17	0·13	0·17
MgO	7·17	12·92	12·88	9·30	7·23	7·90	7·35	7·30	8·44
CaO	10·05	9·01	9·06	10·11	9·96	9·27	9·41	10·09	9·43
Na_2O	2·41	1·64	1·66	1·90	2·14	2·12	2·17	2·23	2·16
K_2O	0·66	0·71	0·71	0·74	0·98	1·12	1·06	1·02	1·08
P_2O_5	0·18	0·13	0·13	0·14	0·17	0·16	0·16	0·18	0·16
Total	99·94	99·87	99·87	99·89	99·94	99·94	99·95	99·94	99·93
LOI	0·44	0·99	0·67	0·41	0·91	2·38	1·34	2·2	1·77
Mg# (0·15)	59·81	69·93	69·46	64·49	59·66	63·36	59·52	61·54	62·24
Ni (ppm)	76	236	157	60	92	85	84	104	97
Cr	294	609	502	331	288	267	267	305	351
Rb	28·39	22·39	23·48	28·26	28·40	33·54	20·36	23·99	14·17
Sr	215·79	176·32	207·48	239·12	237·45	222·95	204·46	184·85	189·06
Y	24·98	20·40	21·03	23·39	25·96	19·97	24·28	23·27	23·24
Zr	143·46	110·71	110·42	126·45	147·20	121·00	133·45	100·00	125·88
Nb	12·89	10·41	10·77	11·94	13·25	10·22	12·46	7·83	11·69
Cs	1·26	1·32	0·73	1·00	0·91		0·77		0·45
Ba	213·99	171·28	174·64	202·64	239·66	211·54	196·71	175·95	193·64
La	16·12	12·13	12·53	14·86	15·45	15·30	14·86	13·07	15·64
Ce	35·09	26·42	26·90	31·35	34·32	33·28	32·23	28·73	32·47
Pr	4·41	3·42	3·50	4·01	4·55	4·12	4·20	3·59	4·07
Nd	18·21	14·38	14·41	16·96	18·68	17·53	17·77	15·53	16·74
Sm	4·41	3·54	3·71	4·17	4·61	4·21	4·44	3·92	3·85
Eu	1·32	1·13	1·17	1·32	1·41	1·36	1·31	1·26	1·28
Gd	4·56	3·83	3·85	4·38	4·89	4·58	4·56	4·40	4·17
Tb	0·72	0·63	0·62	0·69	0·78	0·81	0·77	0·82	0·66
Dy	4·16	3·51	3·44	4·06	4·64	4·23	4·34	4·63	3·79
Ho	0·88	0·73	0·74	0·84	0·92	0·84	0·91	0·94	0·80
Er	2·36	1·99	1·96	2·39	2·55	2·41	2·57	2·78	2·20
Tm	0·21					0·29		0·30	0·25
Yb	2·05	1·85	1·84	1·93	2·30	2·14	2·21	2·54	1·86
Lu	0·30	0·26	0·25	0·28	0·31	0·28	0·32	0·33	0·28
Hf	3·53	2·92	2·84	3·20	3·65	3·43	3·53	3·19	3·05
Ta	0·79	0·62	0·62	0·70	0·78	0·99	0·82	0·83	0·70
Pb	4·96	4·41	3·31	4·24	4·55	4·29	4·69	4·89	1·86
Th	3·44	2·58	2·59	2·99	3·40	3·46	3·70	2·65	3·18
U	0·70	0·59	0·59	0·72	0·73	0·84	0·84	0·61	0·65
$^{87}Sr/^{86}Sr$ meas.	0·707329	0·707263	0·707312	0·707324	0·706812	0·707728	0·706832	0·707267	0·707111
$^{87}Sr/^{86}Sr_{\ 201\ Ma}$	0·706246	0·706218	0·706381	0·706351	0·705828	0·706490	0·706012	0·706199	0·706494
$^{143}Nd/^{144}Nd$ meas.	0·512520	0·512543	0·512567	0·512565	0·512578	0·512562	0·512573	0·512531	0·512563
$^{143}Nd/^{144}Nd_{\ 201\ Ma}$	0·512328	0·512348	0·512363	0·512371	0·512383	0·512372	0·512376	0·512331	0·512381
$\varepsilon Nd_{\ 201\ Ma}$	−1·01	−0·62	−0·33	−0·18	0·06	−0·15	−0·08	−0·95	0·02
$^{206}Pb/^{204}Pb$ meas.		18·631		18·691	18·620				
$^{207}Pb/^{204}Pb$ meas.		15·658		15·643	15·633				
$^{208}Pb/^{204}Pb$ meas.		38·659		38·751	38·742				
$^{206}Pb/^{204}Pb_{\ 201\ Ma}$		18·363		18·354	18·301				
$^{207}Pb/^{204}Pb_{\ 201\ Ma}$		15·644		15·626	15·617				
$^{208}Pb/^{204}Pb_{\ 201\ Ma}$		38·277		38·291	38·254				

(Continued)

However, the Lower lava samples display up to 30 vol.% of olivine, suggesting accumulation of mafic minerals and cannot be considered as magmatic liquid compositions.

Lava flows

According to the TAS diagram (Le Bas *et al.*, 1986), the Moroccan CAMP rocks can be classified as basalts and basaltic andesites (Fig. 10). In particular, most Lower and Intermediate samples are basaltic andesites, Upper lava flows straddle the basalt and basaltic andesite fields and Recurrent samples are all basalts. The TAS diagram also shows that the Lower basaltic andesites are slightly higher in alkalis than the other samples. The Moroccan CAMP samples are all low-TiO_2 basalts ($TiO_2 <$ 2·0 wt %; Fig. 11), as are the vast majority of CAMP rocks in general (Marzoli *et al.*, 2018).

Table 3: Continued

Sample	AN 115 B	AN 130	AN 132	AN 206	AN 215	AN504	AN 174 B	AN 18	AN 39
Unit area locality	lower Argana Alemzi	lower Argana Tasguint	lower Argana Argana	lower M. Atlas Midelt	lower M. Atlas Midelt	lower M. Atlas Maaziz	lower East Meseta Oujda	Intermediate N-CHA Ait Ourir	Interm N-CHA J Imizar
SiO_2 wt %	53·14	54·76	49·23	54·48	53·51	53·48	53·28	53·30	53·26
TiO_2	1·37	1·44	0·94	1·63	2·02	1·54	1·40	1·22	1·25
Al_2O_3	14·07	13·84	9·89	14·09	13·67	13·93	14·38	14·69	14·51
FeOt	10·01	10·05	14·15	10·07	11·90	9·74	9·65	10·06	10·28
MnO	0·14	0·18	0·21	0·14	0·32	0·16	0·14	0·18	0·17
MgO	7·24	6·67	16·5	6·24	5·96	8·25	7·63	7·35	7·14
CaO	8·11	9·51	7·49	9·50	8·85	9·83	10·17	10·44	10·74
Na_2O	3·52	2·31	1·32	2·35	2·47	2·23	2·17	2·15	2·09
K_2O	2·23	1·07	0·64	1·25	1·01	0·64	0·95	0·41	0·36
P_2O_5	0·16	0·17	0·12	0·21	0·23	0·19	0·17	0·15	0·14
Total	99·99	100·00	100·49	99·97	99·95	100·00	99·94	99·95	99·95
LOI	2·16	1·53	1·74	0·59	0·98	1·12	1·97	0·55	0·35
Mg# (0·15)	59·71	57·63	70·50	55·93	50·66	63·45	61·83	59·95	58·75
Ni (ppm)	84	65	377	85	61	45	74	72	79
Cr	303	240	538	262	125	354	285	200	233
Rb	34·91	16·48	21·98	44·99	41·40	26·54	26·73	25·02	36·10
Sr	302·90	162·34	159·80	272·14	305·70	252·06	225·14	172·49	172·45
Y	23·27	20·54	18·71	29·25	34·91	25·71	22·79	24·37	24·29
Zr	126·45	134·71	96·71	185·23	189·32	131·27	131·22	108·70	105·17
Nb	11·28	11·54	8·65	17·36	20·85	11·36	12·97	8·41	8·12
Cs	0·59	0·51	1·83	3·80	8·43	1·14	0·65	1·49	2·09
Ba	329·52	189·19	141·71	316·59	345·26	192·73	214·30	137·25	139·57
La	13·20	13·94	10·62	22·70	25·62	16·86	15·40	11·40	10·85
Ce	28·66	31·73	23·76	49·69	56·73	35·90	33·00	24·98	23·98
Pr	3·66	3·96	3·02	6·01	6·87	4·65	4·27	3·27	3·14
Nd	15·34	16·72	12·60	26·07	30·11	19·68	17·82	13·87	13·40
Sm	3·85	4·08	3·13	6·21	7·21	4·95	4·34	3·54	3·37
Eu	1·22	1·17	0·91	1·56	1·85	1·57	1·35	1·09	1·09
Gd	4·06	4·26	3·28	5·42	6·43	5·17	4·63	3·87	4·11
Tb	0·66	0·68	0·53	0·98	1·13	0·87	0·74	0·64	0·63
Dy	3·83	3·94	3·28	6·04	7·06	5·24	4·33	3·87	3·96
Ho	0·81	0·85	0·64	1·15	1·34	1·03	0·86	0·83	0·84
Er	2·20	2·38	1·78	3·34	3·91	2·75	2·33	2·33	2·41
Tm	0·26	0·24		0·46	0·53	0·39			
Yb	1·92	2·03	1·64	3·00	3·51	2·32	2·22	2·20	2·01
Lu	0·28	0·29	0·22	0·44	0·50	0·36	0·33	0·33	0·30
Hf	3·09	3·45	2·40	4·85	5·44	3·68	3·54	2·72	2·73
Ta	0·68	0·76	0·55			0·76	0·85	0·50	0·48
Pb	6·56	15·88	4·81	10·84	16·05	3·49	4·52	3·88	3·27
Th	3·15	2·85	2·51	4·75	5·28	3·54	3·66	2·46	2·24
U	0·63	0·71	0·55	1·18	1·35	0·84	0·80	0·54	0·52
$^{87}Sr/^{86}Sr$ meas.	0·709932	0·707437	0·707382	0·707309	0·706979	0·707211	0·706930	0·707250	0·707710
$^{87}Sr/^{86}Sr_{\ 201\ Ma}$	0·708984	0·706601	0·706250	0·705948	0·705865	0·706345	0·705953	0·706056	0·705987
$^{143}Nd/^{144}Nd$ meas.	0·512581	0·512566	0·512511	0·512567	0·512585	0·512573	0·512581	0·512455	0·512490
$^{143}Nd/^{144}Nd_{\ 201\ Ma}$	0·512383	0·512373	0·512314	0·512379	0·512396	0·512374	0·512388	0·512253	0·512291
$\varepsilon Nd_{\ 201\ Ma}$	0·05	-0·14	-1·28	-0·02	0·31	-0·12	0·16	-2·47	-1·73
$^{206}Pb/^{204}Pb$ meas.			18·620			18·258		18·627	18·670
$^{207}Pb/^{204}Pb$ meas.			15·658			15·641		15·673	15·674
$^{208}Pb/^{204}Pb$ meas.			38·810			38·245		38·822	38·707
$^{206}Pb/^{204}Pb_{\ 201\ Ma}$			18·392			18·250		18·348	18·390
$^{207}Pb/^{204}Pb_{\ 201\ Ma}$			15·646			15·640		15·659	15·658
$^{208}Pb/^{204}Pb_{\ 201\ Ma}$			38·470			38·235		38·408	38·268

(Continued)

Nevertheless, TiO_2 decreases from the Lower basaltic andesites (average 1·45 wt %) to Intermediate (average 1·22 wt %) and then to the Upper flows (average 1·05 wt %) and is again high in the Recurrent basalts (average 1·63 wt %). Na_2O and P_2O_5 as well as Zr and Hf display a similar concentration decrease from the Lower to the Upper units (Figs 11 and 12), though little or no increase is observed in the Recurrent samples. The Lower flows are also characterized by the highest LILE (K_2O, Sr, Ba, Rb), HFSE (Nb, Ta, Th, U) and LREE (La to Eu) concentrations, but tend to have slightly lower FeO concentrations than the other units. By contrast, the Upper flows have extreme compositions in terms of high CaO and Al_2O_3, and low P_2O_5, K_2O and low concentrations of most incompatible trace elements, including REE, HFSE and LILE (with the exception of Sr and, to some extent, Pb). As shown in Figs 11 and 12, Intermediate flows are intermediate also in terms of major and trace element

Table 3: Continued

Sample	AN 137 A	AN 138	AN 160	AN 128	AN 212	AN 219	AN537	AN611	AN525B
Unit area locality	Interm S-CHA Tiourjdal	Interm S-CHA Tiourjdal	Interm S-CHA Telouet	interm Argana Tasguint	interm M. Atlas Midelt	interm M. Atlas Midelt	interm M. Atlas Tounfite	interm M. Atlas Tounfite	interm M. Atlas Agourai
SiO_2 wt %	53·14	53·53	52·51	52·94	53·22	52·91	53·96	52·33	53·01
TiO_2	1·16	1·16	1·21	1·26	1·15	1·31	1·20	1·30	1·48
Al_2O_3	13·91	13·39	14·06	14·38	14·43	14·16	14·32	14·36	13·79
FeOt	10·47	10·20	10·40	11·43	10·30	10·79	9·25	9·76	10·84
MnO	0·18	0·17	0·17	0·16	0·18	0·19	0·14	0·13	0·19
MgO	7·77	8·50	8·05	7·26	7·14	7·03	8·57	8·92	7·44
CaO	10·68	9·94	11·25	9·94	10·94	10·91	10·01	10·94	10·46
Na_2O	2·00	1·90	1·77	1·96	2·03	2·10	1·98	1·80	1·99
K_2O	0·38	0·84	0·28	0·51	0·40	0·39	0·45	0·25	0·57
P_2O_5	0·14	0·17	0·12	0·15	0·13	0·13	0·15	0·15	0·16
Total	99·83	99·81	99·82	99·99	99·93	99·92	100·03	99·95	99·93
LOI	2·24	1·13	1·46	1·84	0·64	0·65	1·31	1·18	0·37
Mg# (0·15)	60·34	63·08	61·34	56·55	58·70	57·16	65·51	65·19	58·45
Ni (ppm)	69	104	93	69	86	64	109	77	98
Cr	110	326	402	204	257	210	325	477	365
Rb	16·65	26·83	26·18	11·00	15·94	23·29	28·60	9·25	25·69
Sr	166·58	156·75	165·62	248·94	179·33	192·93	170·21	170·63	164·53
Y	23·62	26·72	23·18	23·06	19·96	24·29	21·93	20·44	25·06
Zr	105·55	129·22	101·54	109·28	92·83	112·85	96·76	92·69	108·44
Nb	7·96	9·95	6·36	7·68	6·64	7·38	6·45	5·75	7·13
Cs	1·36	0·75	1·34	6·68	7·48	5·70	1·08	0·67	1·04
Ba	143·00	188·17	99·94	109·94	127·46	131·60	133·49	78·31	160·09
La	11·07	13·08	9·28	10·56	10·33	11·38	11·63	10·07	12·00
Ce	24·25	29·09	21·32	23·64	23·22	26·13	24·90	22·52	26·35
Pr	3·19	3·75	2·82	3·07	2·92	3·39	3·26	3·02	3·48
Nd	13·56	15·63	12·95	13·03	12·95	15·24	14·11	13·62	15·28
Sm	3·56	3·88	3·44	3·25	3·38	4·11	3·74	3·80	4·09
Eu	1·12	1·15	1·05	1·05	0·98	1·22	1·19	1·26	1·29
Gd	3·99	4·23	3·93	3·71	3·44	4·29	4·06	4·15	4·60
Tb	0·65	0·71	0·64	0·62	0·60	0·75	0·73	0·72	0·81
Dy	4·01	4·34	3·98	3·69	3·91	4·78	4·48	4·31	5·01
Ho	0·85	0·95	0·82	0·80	0·77	0·94	0·89	0·87	1·02
Er	2·42	2·74	2·29	2·26	2·28	2·75	2·44	2·29	2·72
Tm				0·22	0·32	0·38	0·35	0·32	0·39
Yb	2·12	2·38	1·93	2·02	2·10	2·48	2·13	1·97	2·35
Lu	0·32	0·35	0·31	0·30	0·31	0·36	0·33	0·30	0·36
Hf	2·65	3·24	2·58	2·72	2·51	3·12	2·81	2·68	3·13
Ta	0·48	0·61	0·41	0·50			0·44	0·39	0·50
Pb	3·07	3·66	2·73	3·12	12·03	10·76	2·62	1·28	3·44
Th	2·20	2·87	1·98	2·35	2·25	2·37	2·37	1·96	2·65
U	0·48	0·65	0·42	0·48	0·54	0·56	0·54	0·46	0·63
$^{87}Sr/^{86}Sr$ meas.	0·706964	0·707600	0·707379	0·707588	0·707018	0·706922	0·707647	0·706962	0·707061
$^{87}Sr/^{86}Sr_{\ 201\ Ma}$	0·706142	0·706191	0·706078	0·707225	0·706287	0·705929	0·706264	0·706516	0·705776
$^{143}Nd/^{144}Nd$ meas.	0·512485	0·512465	0·512556	0·512548	0·512510	0·512551	0·512504	0·512592	0·512516
$^{143}Nd/^{144}Nd_{\ 201\ Ma}$	0·512277	0·512269	0·512346	0·512351	0·512303	0·512338	0·512295	0·512372	0·512304
$\varepsilon Nd_{\ 201\ Ma}$	-2·00	-2·17	-0·67	-0·57	-1·49	-0·82	-1·67	-0·17	-1·48
$^{206}Pb/^{204}Pb$ meas.		18·637	18·710				18·622	18·700	18·626
$^{207}Pb/^{204}Pb$ meas.		15·662	15·687				15·674	15·653	15·650
$^{208}Pb/^{204}Pb$ meas.		38·812	38·896				38·852	38·844	38·795
$^{206}Pb/^{204}Pb_{\ 201\ Ma}$		18·282	18·400				18·216	17·986	18·263
$^{207}Pb/^{204}Pb_{\ 201\ Ma}$		15·644	15·671				15·653	15·617	15·632
$^{208}Pb/^{204}Pb_{\ 201\ Ma}$		38·300	38·420				38·266	37·841	38·291

(Continued)

concentrations between Lower and Upper flows and sometimes overlap with them. Notably, most samples from these three units have similar MgO contents and Mg# as well as compatible element contents (Ni, Cr, Sc, Co). By contrast, the Recurrent basalts are slightly more evolved than the other rocks, i.e. they yield slightly lower MgO (about 5·5–6·2 wt %), Mg# (54–46) and Cr (about 100 ppm). The Recurrent basalts plot outside the general field of the other basalts and basaltic andesites and have higher TiO_2, FeO_{tot}, V, Sc, HREE (from Gd to Lu) contents and lower SiO_2, Rb and Sr, as well as low LREE (La to Sm) and HFSE (except Zr) contents.

Regional-scale geochemical trends and unit-specific characteristics are further highlighted by comparing the geochemical compositions of the different units in multi-element diagrams (Fig. 13). Lower, Intermediate and Upper units have broadly similar incompatible element patterns, with progressively lower absolute

Table 3: Continued

Sample	AN631	AN633	AN510	AN627	AN 22	AN 57	AN 63	AN 140	AN 141
Unit area locality	interm M. Atlas Agourai	interm M. Atlas Agourai	interm M. Atlas Maaziz	interm M. Atlas Maaziz	upper N-CHA Ait Ourir	upper N-CHA Agouim	upper N-CHA Ikourker	upper S-CHA Tiourjdal	upper S-CHA Tiourjdal
SiO_2 wt %	54·81	52·98	53·74	53·65	51·57	51·74	51·66	51·34	52·05
TiO_2	1·27	1·14	1·36	1·40	1·05	1·10	1·09	1·00	1·04
Al_2O_3	14·38	14·34	13·92	14·05	15·12	15·07	15·05	15·01	14·85
FeOt	9·07	10·13	10·77	10·30	9·88	9·76	9·76	9·95	9·97
MnO	0·14	0·24	0·17	0·18	0·17	0·17	0·16	0·18	0·18
MgO	8·20	7·14	7·03	7·36	8·01	8·09	8·20	8·25	7·74
CaO	9·46	11·39	10·20	10·24	11·85	11·74	11·82	12·01	11·43
Na_2O	2·01	2·00	2·03	2·02	1·92	1·96	1·86	1·78	1·90
K_2O	0·41	0·42	0·60	0·54	0·27	0·23	0·24	0·21	0·58
P_2O_5	0·16	0·14	0·16	0·16	0·11	0·11	0·11	0·11	0·11
Total	99·92	99·93	99·98	99·92	100·00	100·00	100·00	99·85	99·85
LOI	1·17	0·32	0·49	0·70	0·12	0·26	0·51	1·32	0·58
Mg# (0·15)	64·95	59·12	57·24	59·42	62·43	62·95	63·26	62·96	61·39
Ni (ppm)	56	63	106	59	87	87	89	108	91
Cr	309	273	289	362	217	212	205	328	229
Rb	17·39	14·10	23·28	16·98	11·79	5·51	12·29	1·55	12·75
Sr	173·78	176·14	170·39	180·26	163·15	172·92	163·96	106·68	158·81
Y	21·14	21·99	24·97	23·90	20·42	21·32	21·09	16·77	20·12
Zr	103·62	81·57	112·87	111·67	76·04	80·82	79·04	71·87	78·05
Nb	6·94	5·11	7·58	7·40	5·03	5·17	5·14	4·52	4·99
Cs	0·87	0·59	1·13	2·51	0·83	0·72	0·95	0·21	0·40
Ba	139·78	113·10	177·89	268·73	92·47	102·82	84·27	83·57	111·89
La	10·67	8·91	12·75	12·31	7·19	7·58	7·48	6·32	7·17
Ce	23·65	19·84	27·72	26·86	16·45	17·62	16·79	14·68	16·59
Pr	3·12	2·70	3·63	3·58	2·28	2·36	2·34	1·98	2·30
Nd	13·50	11·93	15·55	15·59	9·97	10·36	10·22	8·74	10·35
Sm	3·58	3·33	4·11	4·14	2·70	2·80	2·75	2·37	2·79
Eu	1·23	1·13	1·31	1·37	0·87	0·94	0·92	0·79	0·93
Gd	3·95	3·90	4·52	4·51	3·12	3·15	3·20	2·83	3·14
Tb	0·69	0·67	0·79	0·79	0·54	0·58	0·54	0·48	0·54
Dy	4·26	4·26	4·95	4·89	3·11	3·26	3·23	2·87	3·40
Ho	0·86	0·88	1·02	0·97	0·71	0·73	0·73	0·63	0·72
Er	2·30	2·39	2·74	2·64	1·94	2·06	1·92	1·74	2·03
Tm	0·33	0·35	0·39	0·37				0·23	
Yb	2·04	2·07	2·36	2·23	1·84	2·02	1·83	1·55	1·87
Lu	0·31	0·33	0·36	0·34	0·29	0·30	0·28	0·23	0·28
Hf	3·01	2·40	3·21	3·18	2·00	2·04	1·90	1·79	2·08
Ta	0·48	0·34	0·53	0·49	0·31	0·30	0·30	0·27	0·31
Pb	2·82	2·09	3·64	3·37	1·73	2·39	1·68	1·72	2·41
Th	2·67	1·64	2·87	2·69	1·23	1·28	1·18	0·86	1·27
U	0·62	0·40	0·67	0·63	0·29	0·32	0·28	0·23	0·30
$^{87}Sr/^{86}Sr$ meas.	0·707191	0·706368	0·707393	0·706937	0·706115	0·705849	0·706103		0·706248
$^{87}Sr/^{86}Sr_{\ 201\ Ma}$	0·706367	0·705709	0·706269	0·706162	0·705520	0·705587	0·705486		0·705587
$^{143}Nd/^{144}Nd$ meas.	0·512485	0·512505	0·512490	0·512526	0·512543	0·512564	0·512539	0·512561	0·512547
$^{143}Nd/^{144}Nd_{\ 201\ Ma}$	0·512275	0·512284	0·512281	0·512316	0·512329	0·512350	0·512326	0·512347	0·512334
$\varepsilon Nd_{\ 201\ Ma}$	-2·042	-1·872	-1·935	-1·253	-0·99	-0·58	-1·04	-0·65	-0·90
$^{206}Pb/^{204}Pb$ meas.	18·660	18·523	18·607	18·640	18·571				18·515
$^{207}Pb/^{204}Pb$ meas.	15·658	15·610	15·638	15·647	15·629				15·624
$^{208}Pb/^{204}Pb$ meas.	38·843	38·499	38·753	38·793	38·680				38·485
$^{206}Pb/^{204}Pb_{\ 201\ Ma}$	18·221	18·146	18·239	18·269	18·236				18·272
$^{207}Pb/^{204}Pb_{\ 201\ Ma}$	15·635	15·591	15·619	15·628	15·612				15·612
$^{208}Pb/^{204}Pb_{\ 201\ Ma}$	38·223	37·989	38·238	38·271	38·218				38·145

(Continued)

values of LREE and MREE from Lower to Upper basalts. Common features are negative Nb and Ta (vs Th, U and LREE) and positive Pb (vs LREE) anomalies, whereas a negative anomaly of Sr is observed in most Lower and Intermediate flows but is lacking in the Upper basalts (except one sample). The LILE (particularly K and Rb) show a large scatter of data, which may in part be related to secondary processes even for the selected and apparently slightly altered samples. The difference among these three flow units is obvious for the LREE (La to Sm), whereas it is negligible for HREE (from Dy to Lu), resulting in broadly parallel REE patterns with a progressive decrease of LREE/HREE ratios from Lower (i.e. La/Yb_{CN} = 4·4–5·6, except for two outliers; chondrite normalized after McDonough & Sun, 1995) to Intermediate (La/Yb_{CN} = 2·9–3·8) and Upper basalts (La/Yb_{CN} = 2·5–2·8). The highest La/Yb and REE concentrations as well as the

Table 3: Continued

Sample	AN 213	AN540	AN24	AN 44	AN 156 A	AN 169	AN 730	AN 734	AN 704
Unit	upper	upper	rec	rec	rec	rec	Interm	Interm	Upper
area	M. Atlas	M. Atlas	N-CHA	N-CHA	S-CHA	S-CHA	A Atlas	A Atlas	A Atlas
locality	Midelt	Tounfite	Ait Ourir	Agouim	Agouim	Telouet	B. D. sill	F. Z. dyke	F. Z. dyke
SiO_2 wt %	51·54	51·88	50·39	50·68	51·33	51·32	52·76	53·29	50·52
TiO_2	1·08	1·09	1·62	1·63	1·63	1·56	1·19	1·14	1·00
Al_2O_3	15·04	14·77	13·71	13·57	13·60	13·59	14·07	14·37	14·52
FeOt	10·38	10·01	14·72	14·85	14·04	14·22	10·86	10·87	9·87
MnO	0·16	0·15	0·34	0·28	0·22	0·30	0·18	0·18	0·19
MgO	7·15	7·90	6·13	5·77	5·93	6·02	6·34	6·19	7·72
CaO	11·37	11·75	10·47	10·45	10·42	10·29	10·06	9·78	10·96
Na_2O	2·37	1·85	2·09	2·19	2·13	2·00	2·39	2·31	1·79
K_2O	0·71	0·39	0·33	0·39	0·34	0·35	0·73	0·87	1·19
P_2O_5	0·11	0·13	0·17	0·17	0·17	0·16	0·14	0·12	0·10
Total	99·93	99·92	100·00	100·00	99·82	99·83	98·72	99·12	97·86
LOI	1·25	0·85	0·34	-0·26	1·51	0·51	0·81	0·05	0·24
Mg# (0·15)	58·54	61·80	46·06	44·32	46·42	46·47	57·06	56·45	64·03
Ni (ppm)	87	115	72	71	90	67	53	48	91
Cr	214	267	105	100	235	118	36	21	199
Rb	15·93	14·03	4·32	7·52	6·13	6·30	24·20	23·14	21·71
Sr	181·79	174·25	103·86	92·94	95·52	102·25	207·96	210·71	235·28
Y	20·03	20·61	46·27	43·10	41·04	42·99	26·75	25·12	21·90
Zr	81·65	73·07	126·09	115·68	114·85	123·35	101·06	105·78	77·78
Nb	5·55	4·66	5·68	5·27	5·21	5·59	7·04	7·03	5·04
Cs	1·52	0·52	0·31	0·50	0·78	0·59	1·86	1·13	1·83
Ba	149·36	94·32	123·26	178·50	164·33	120·81	177·16	261·72	135·82
La	8·12	7·71	8·89	8·61	8·57	8·76	11·58	11·07	7·32
Ce	19·03	17·58	20·87	19·62	19·85	20·47	25·46	24·27	16·67
Pr	2·51	2·42	2·87	2·72	2·77	2·78	3·37	3·20	2·27
Nd	11·47	10·89	13·22	13·03	12·70	13·44	14·72	13·78	10·40
Sm	3·19	3·05	4·02	3·89	3·92	4·09	3·72	3·50	2·78
Eu	0·96	1·08	1·27	1·24	1·24	1·28	1·20	1·15	0·99
Gd	3·43	3·45	5·60	5·36	5·49	5·45	4·28	3·95	3·36
Tb	0·60	0·63	1·00	0·99	1·00	1·05	0·70	0·66	0·57
Dy	3·91	4·07	6·68	6·41	6·68	6·86	4·45	4·18	3·62
Ho	0·79	0·82	1·53	1·49	1·49	1·53	0·93	0·87	0·77
Er	2·33	2·24	4·54	4·44	4·44	4·63	2·63	2·48	2·15
Tm	0·33	0·32					2·30	2·11	2·33
Yb	2·17	1·99	4·52	3·97	4·22	4·18	2·42	2·30	1·97
Lu	0·32	0·30	0·63	0·62	0·64	0·68	0·35	0·34	0·29
Hf	2·28	2·12	3·24	3·05	3·07	3·26	2·55	2·63	1·94
Ta		0·30	0·35	0·33	0·34	0·35	0·43	0·46	0·31
Pb	10·57	1·82	4·21	3·26	3·32	2·69	3·16	4·07	1·81
Th	1·39	1·31	2·31	2·08	2·14	2·16	2·12	2·33	1·12
U	0·35	0·32	0·57	0·62	0·55	0·57	0·51	0·57	0·27
$^{87}Sr/^{86}Sr$ meas.	0·706371	0·706117	0·705263	0·705950	0·705569	0·705569	0·707575	0·708103	0·707335
$^{87}Sr/^{86}Sr_{\ 201\ Ma}$	0·705650	0·705454	0·704920	0·705284	0·705040	0·705062	0·706618	0·707199	0·706575
$^{143}Nd/^{144}Nd$ meas.	0·512559	0·512572	0·512683	0·512683	0·512724	0·512689	0·512464	0·512436	0·512599
$^{143}Nd/^{144}Nd_{\ 201\ Ma}$	0·512339	0·512351	0·512443	0·512447	0·512480	0·512448	0·512264	0·512235	0·512388
$\varepsilon Nd_{\ 201\ Ma}$	-0·799	-0·574	1·22	1·31	1·95	1·33	-2·259	-2·838	0·150
$^{206}Pb/^{204}Pb$ meas.		18·522	18·922	18·828	18·938	18·979	18·562	18·591	18·653
$^{207}Pb/^{204}Pb$ meas.		15·607	15·658	15·676	15·670	15·679	15·647	15·651	15·634
$^{208}Pb/^{204}Pb$ meas.		38·510	38·856	38·834	38·963	39·038	38·591	38·650	38·712
$^{206}Pb/^{204}Pb_{\ 201\ Ma}$		18·178	18·650	18·450	18·605	18·551	18·243	18·319	18·359
$^{207}Pb/^{204}Pb_{\ 201\ Ma}$		15·590	15·644	15·657	15·653	15·657	15·630	15·637	15·619
$^{208}Pb/^{204}Pb_{\ 201\ Ma}$		38·044	38·496	38·416	38·538	38·511	38·154	38·284	38·311

(Continued)

highest contents of most other incompatible trace and major elements (e.g. TiO_2 and P_2O_5) are shown by the Lower basalts from the Midelt section (AN206 and AN215; Figs 11 and 12). The outlier of the Lower flows which yields low La/Yb (3·5), similar to those of Intermediate flows is sample AN137C from Tiourjdal (southern Central High Atlas), which is instead characterized by relatively high TiO_2 (1·43 wt %).

By contrast, Recurrent basalts, which are all remarkably similar, yield markedly different incompatible element and particularly REE contents and patterns compared to the other flows. The most significant difference concerns the almost flat REE patterns (La/Yb_{CN}=1·4–1·3, Sm/Yb_{CN} = 1·04–0·95), which resemble those of E-MORB, even if E-MORB have much lower REE contents (Sun & McDonough, 1989). Unlike most

Table 3: Continued

Sample	AN 709	AN 711	AN 725	AN 726	AN 728	AN 724
Unit area locality	Upper A Atlas F. Z. dyke	Upper A Atlas F. Z. dyke	Upper A Atlas B. D. sill	Upper A Atlas B. D. sill	Upper A Atlas B. D. sill	Rec A Atlas B. D. sill
SiO_2 wt %	50·63	50·76	50·63	51·48	50·88	50·21
TiO_2	0·98	1·00	0·82	0·93	0·92	1·42
Al_2O_3	14·63	14·54	11·53	14·93	14·59	13·14
FeOt	9·80	9·96	9·89	9·57	9·48	14·90
MnO	0·17	0·17	0·18	0·17	0·17	0·25
MgO	7·95	7·96	11·91	8·01	8·91	5·70
CaO	11·68	11·50	12·30	12·05	12·14	9·96
Na_2O	1·87	1·89	1·48	1·97	1·85	2·24
K_2O	0·45	0·71	0·31	0·39	0·40	0·50
P_2O_5	0·10	0·10	0·08	0·09	0·09	0·13
Total	98·26	98·59	99·13	99·59	99·43	98·45
LOI	0·14	0·22	0·06	-0·16	0·38	0·01
Mg# (0·15)	64·87	64·53	73·27	65·59	68·16	46·55
Ni (ppm)	97	91	181	87	114	53
Cr	195	216	753	236	320	51
Rb	12·50	18·67	8·76	10·85	10·85	17·03
Sr	180·67	209·12	137·47	174·78	194·27	125·27
Y	21·32	21·80	18·48	20·12	19·70	42·28
Zr	49·85	78·38	63·44	72·13	69·76	107·64
Nb	5·04	5·00	4·05	4·62	4·54	4·88
Cs	0·86	1·42	0·56	0·50	0·50	1·77
Ba	124·87	132·53	105·36	107·26	111·28	117·55
La	7·23	7·21	6·04	6·71	6·57	8·05
Ce	16·70	16·56	13·84	15·50	15·11	18·55
Pr	2·28	2·27	1·91	2·12	2·08	2·54
Nd	10·40	10·38	8·76	9·66	9·44	11·92
Sm	2·79	2·81	2·41	2·65	2·57	3·68
Eu	0·97	0·97	0·81	0·92	0·89	1·26
Gd	3·37	3·36	2·90	3·12	3·06	5·11
Tb	0·57	0·58	0·49	0·53	0·52	0·95
Dy	3·61	3·67	3·15	3·38	3·30	6·50
Ho	0·76	0·77	0·67	0·72	0·69	1·44
Er	2·14	2·18	1·90	2·03	1·98	4·25
Tm	2·27	2·26	2·07	2·39	2·33	2·80
Yb	1·93	2·00	1·74	1·86	1·81	4·10
Lu	0·28	0·29	0·25	0·27	0·26	0·60
Hf	1·43	2·00	1·67	1·86	1·78	2·78
Ta	0·32	0·32	0·26	0·29	0·29	0·31
Pb	2·15	4·61	2·04	2·33	2·00	6·36
Th	1·14	1·19	1·02	1·14	1·06	1·95
U	0·25	0·29	0·25	0·28	0·26	0·53
$^{87}Sr/^{86}Sr$ meas.	0·706212	0·707187	0·706071	0·706055	0·706567	0·707165
$^{87}Sr/^{86}Sr_{\ 201\ Ma}$	0·705642	0·706453	0·705546	0·705545	0·706107	0·706046
$^{143}Nd/^{144}Nd$ meas.	0·512599	0·512596	0·512599	0·512577	0·512589	0·512724
$^{143}Nd/^{144}Nd_{\ 201\ Ma}$	0·512387	0·512382	0·512381	0·512360	0·512374	0·512480
$\varepsilon Nd_{\ 201\ Ma}$	0·135	0·038	0·023	-0·396	-0·113	1·958
$^{206}Pb/^{204}Pb$ meas.	18·450	18·494	18·452	18·448	18·519	18·752
$^{207}Pb/^{204}Pb$ meas.	15·614	15·632	15·608	15·609	15·641	15·675
$^{208}Pb/^{204}Pb$ meas.	38·456	38·517	38·454	38·430	38·564	38·745
$^{206}Pb/^{204}Pb_{\ 201\ Ma}$	18·217	18·371	18·208	18·211	18·263	18·585
$^{207}Pb/^{204}Pb_{\ 201\ Ma}$	15·603	15·626	15·596	15·597	15·628	15·667
$^{208}Pb/^{204}Pb_{\ 201\ Ma}$	38·111	38·350	38·130	38·113	38·219	38·545

Major elements, Cr and Ni analysed by X-Ray fluorescence, other trace elements by ICP-MS. Mg# = 100x [Mg/(Mg+Fe^{2+})], for Fe^{3+}/Fe^{2+} = 0·15. Sampling coordinates are given in Supplementary Data Table S1; supplementary data are available for downloading at http://www.petrology.oxfordjournals.org. The complete whole-rock data set is reported in the Supplementary Data Electronic Appendix Table S8; supplementary data are available for downloading at http://www.petrology.oxfordjournals.org. CHA, Centra High Atlas; B. D., Bas Draa; F. Z., Foum Zguid.

other samples, all Recurrent basalts display a marked negative Eu (Eu/Eu* = 0·8) and negative Sr and Ti anomalies (relative to LREE and HREE, respectively), which are moderate to absent in most Lower, Intermediate and Upper flows. Recurrent basalts are also relatively enriched in Th and U relative to Nb and Ta (Th/Nb = 0·39–0·41, U/Ta = 1·6–1·9 vs 0·19–0·40 and 1·3–0·7 for the other rocks).

Intra-unit variations are rather scattered and do not display clear trends, which might be due to the somewhat restricted MgO (i.e. differentiation) range of each unit. Nonetheless, for the Lower unit there is a tendency

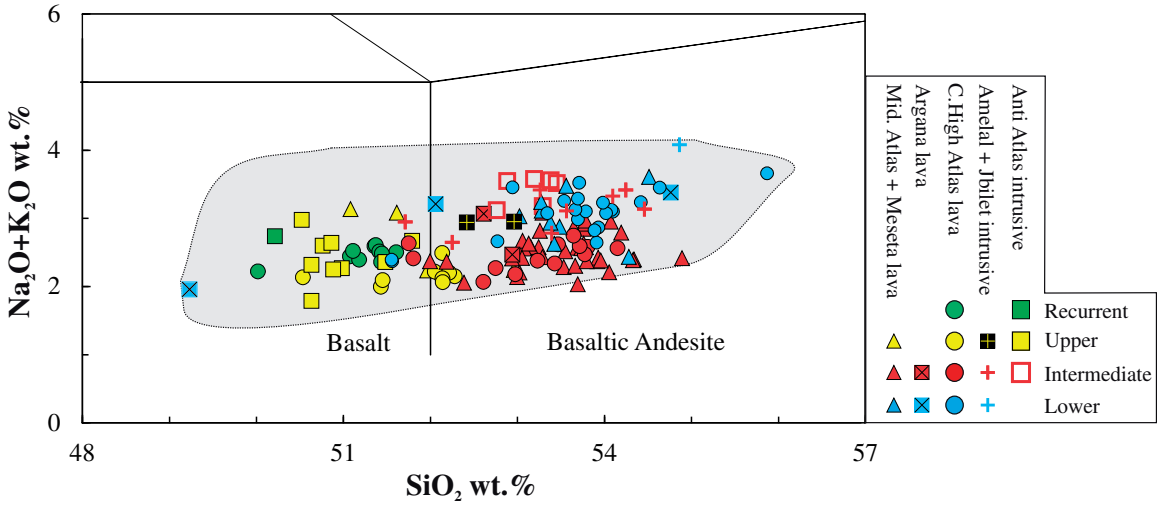

Fig. 10. Total alkalis vs silica (TAS) classification diagram (Le Bas *et al.*, 1986) of CAMP lava flows from the Central High Atlas, Argana, Middle Atlas (including Midelt) and Meseta and intrusive rocks from the Jbilets, Amelal sill (Argana) and from the Anti Atlas. Blue symbols, Lower unit; red, Intermediate; yellow, Upper; green, Recurrent. The grey field shows the compositional range composition of over 500 CAMP low-Ti basalts from throughout the province (Marzoli *et al.*, 2018 and references therein).

for the most differentiated samples (MgO< 6 wt %) to yield slightly higher SiO_2, Na_2O and incompatible element contents (including TiO_2) and La/Yb. Intermediate lava flows show a restricted range of composition and of differentiation (e.g. MgO generally in the range 9–7 wt %), while Intermediate intrusive rocks from the Anti Atlas and parts of the Amelal sill tend to be more evolved (MgO as low as 4 wt %). Most Upper unit rocks plot in a fairly restricted range in terms of major and trace element concentrations, except for one lava flow from the Middle Atlas (AN540) and two sill samples from the Anti Atlas (MOR1015, AN725), which are MgO-rich (10·5–11·9 wt %). The regional variations within each lava flow unit, for example between the High Atlas and the Middle Atlas and Meseta, are negligible and not systematic. Instead, subtle geochemical differences are revealed within some of the sections analysed in most detail (Fig. 14). As an example, the Tiourjdal section of the southern Central High Atlas shows in general significant compositional jumps between the four lava units. However, in some cases, such abrupt discontinuities between the different units do not coincide for all chemical elements. For instance, the basaltic andesite AN137C sampled about halfway up the Tiourjdal section may be regarded either as the last of the Lower flows because of its high TiO_2 (1·43 wt %) similar to those of the Lower flows, or as the first of the Intermediate flows because of its low Zr (105 ppm), Nb (7·8 ppm), La/Yb (5·1) and highly incompatible trace element contents (Zr and Nd isotopic variations are shown in Fig. 14 a and e). Similar features apply for the Telouet, southern Central High Atlas and Agourai (Middle Atlas) sections (not shown in Fig. 14), where samples AN159 and AN525b yield Lower unit-like major elements and Intermediate unit-like incompatible trace elements. The Midelt samples (Fig. 14c and g) show among the highest incompatible trace element contents, in particular for the Lower unit, yet the general up-section variations are similar to those from the Central High Atlas. The most marked difference and compositional jump from the Lower to the Intermediate unit is instead shown for the Maaziz section (Western Meseta). However, here the topmost Intermediate samples show an increase of TiO_2, but not of incompatible trace elements. We note a similar increase in TiO_2 towards the top of the Intermediate unit at Tounfite (Middle Atlas). Finally, the Agourai section (not shown in Fig. 14) of the Middle Atlas consists of flows with Intermediate unit-like geochemical affinities, except for the previously cited sample AN525b and for sample AN633, collected towards the top of the section, with major and trace element compositions approaching those of Upper unit samples (e.g. TiO_2 = 1·14 wt %; La/Yb_{CN} = 2·3).

Geochemical data obtained for samples previously collected for magnetostratigraphic analyses (Knight *et al.*, 2004) at Tiourjdal, Telouet and Oued Lahr in the Central High Atlas offer further insights into both the temporal and spatial variability of the units. Even if slightly altered, poorly mobile elements such as Ti and other HFSE can be readily used to describe the up-section variation of these densely-sampled lava piles (Fig. 15). Based on these data, correlations can be established among these three sections. These show that the Lower unit seems to be complete only at Tiourjdal, while at Telouet and Oued Lahr about the lower half of the Lower unit is missing (or not cropping out). By contrast, the transition from the Lower to the Intermediate units is well expressed in all sections, with a general clear compositional shift (with the exceptions described above).

Intrusive rocks

Direct comparison of effusive and intrusive rocks can be hampered by the (partially) cumulative nature of the

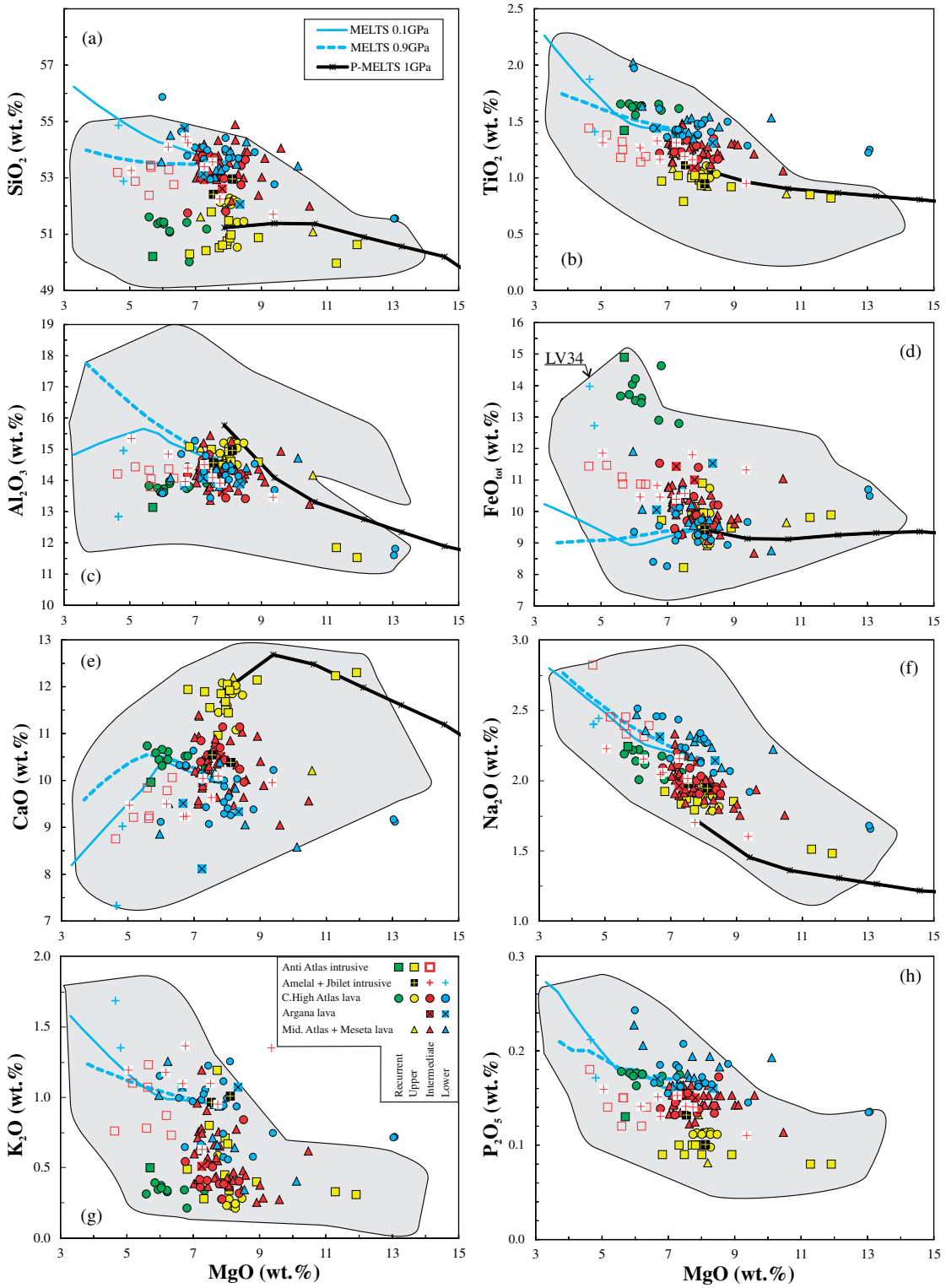

Fig. 11. Whole-rock major element compositions of CAMP lava flows and intrusives from Morocco. Same symbols and abbreviations as in Fig. 10. Grey field is the compositional range of CAMP basalts from other parts of the province. MELTS (Ghiorso & Sack, 1995) liquid lines of descent have been calculated starting from AN133 (Lower unit) as the parental magma composition at 0·9 GPa (dashed line) and 0·1 GPa (full line), 0·5 wt % H_2O in the starting magma, fO_2 at the QFM buffer. The most evolved composition on the MELTS lines corresponds to about 25 and 35 wt % fractionation at 0·9 and 0·1 GPa, respectively. The pMELTS (Ghiorso *et al.*, 2002) liquid line of descent (black lines with tick marks) is calculated at 1 GPa, the parental magma (MgO = 15·5 wt %, off-scale on diagrams) is a *c.*8% melt of KLB-1 peridotite (Hirose & Kushiro, 1993) calculated for 1·5 GPa, 1400 °C. Tick marks on the pMELTS lines represent 5% increments of fractional crystallization at T decreasing from 1350 to 1200 °C, i.e. the most evolved composition corresponds to about 35 wt % fractionation. Note: pMELTS lines are not shown for K_2O and P_2O_5, as these are trace elements that are not properly modelled with this program.

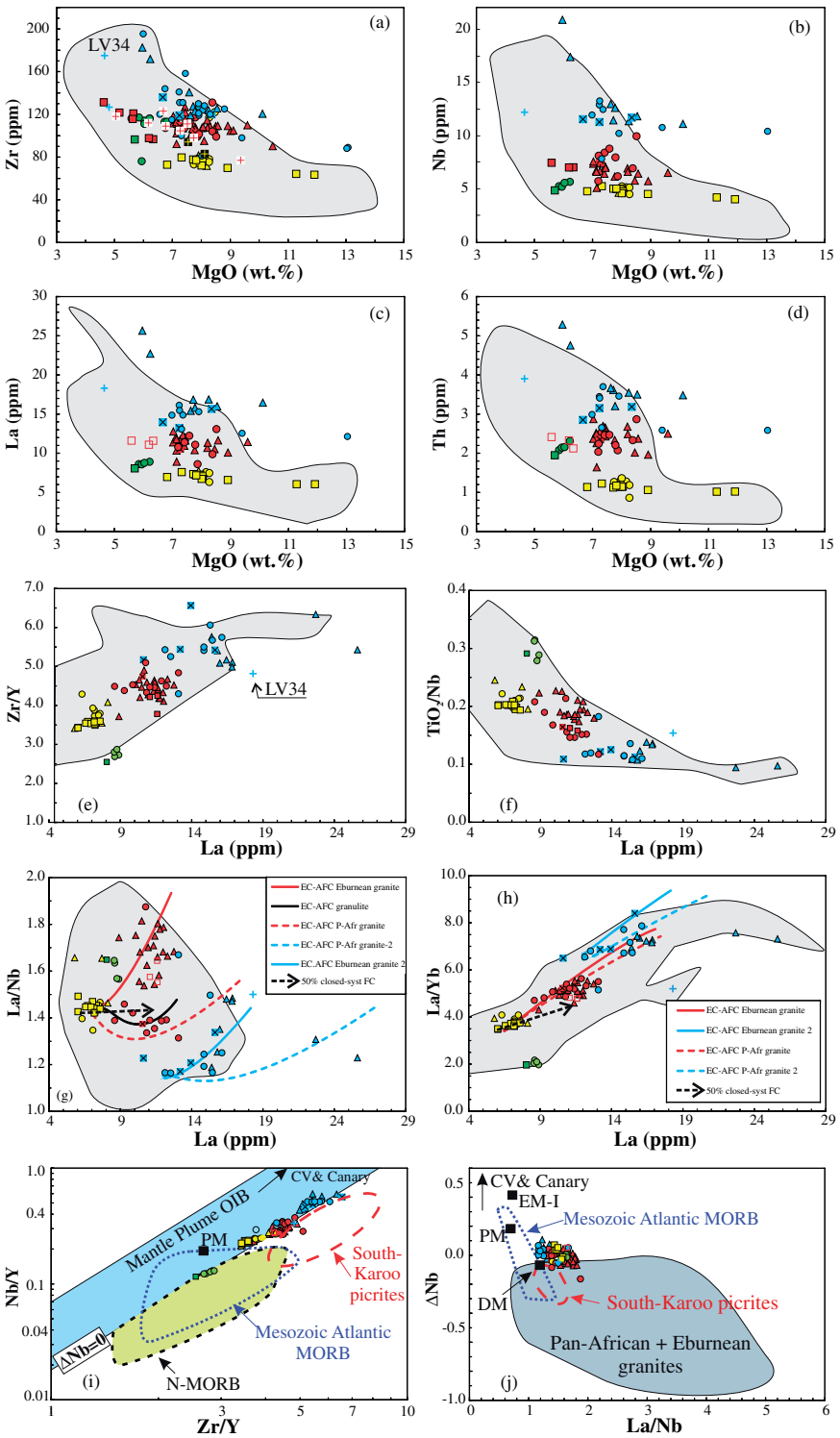

Fig. 12. (a–h) Selected trace element variation vs MgO (wt %) and La (ppm). Same symbols as in Fig. 10. Zr measured by X-ray fluorescence, La, Nb, Th by ICP-MS. EC-AFC paths (Spera & Bohrson, 2001) in (g) and (h) are calculated starting from an Upper and from a Lower initial composition, considering the following rocks as crustal contaminants: an Eburnean granite (more enriched), a Pan-African granite (slightly less enriched) and a lower crustal granulite (in (e) only; in (d) the granulite EC-AFC curve overlaps with the Eburnean granite curve). Parameters used in EC-AFC are reported in Table 5. Grey field is CAMP basalts from other parts of the province (data from Marzoli *et al.*, 2018 and references therein). In (g) and (h), the closed system FC (fractional crystallization) line represents 50% fractionation from a hypothetical parental Upper magma (black arrow) and has been calculated assuming 40% augite and 10% plagioclase fractionation (partition coefficients from Aigner-Torres *et al.* (2007) and Bédard (2014)). (i, j) Zr/Y vs Nb/Y (logarithmic scale) and La/Nb vs delta-Nb (= 1·74+log(Nb/Y) - 1·92 x log(Zr/Y); see text for explanation; Fitton *et al.*, 1997) for Moroccan CAMP basalts. The grey field represents the Icelandic mantle array as defined in Fitton *et al.* (1997); Mesozoic Atlantic MORB data are from Janney & Castillo (2001); southern Karoo picrites are from Heinonen *et al.* (2010) and Luttinen (2018); Pan-African and Eburnean granite compositions are from Toummite *et al.* (2013) and from Ennih & Liégeois (2008).

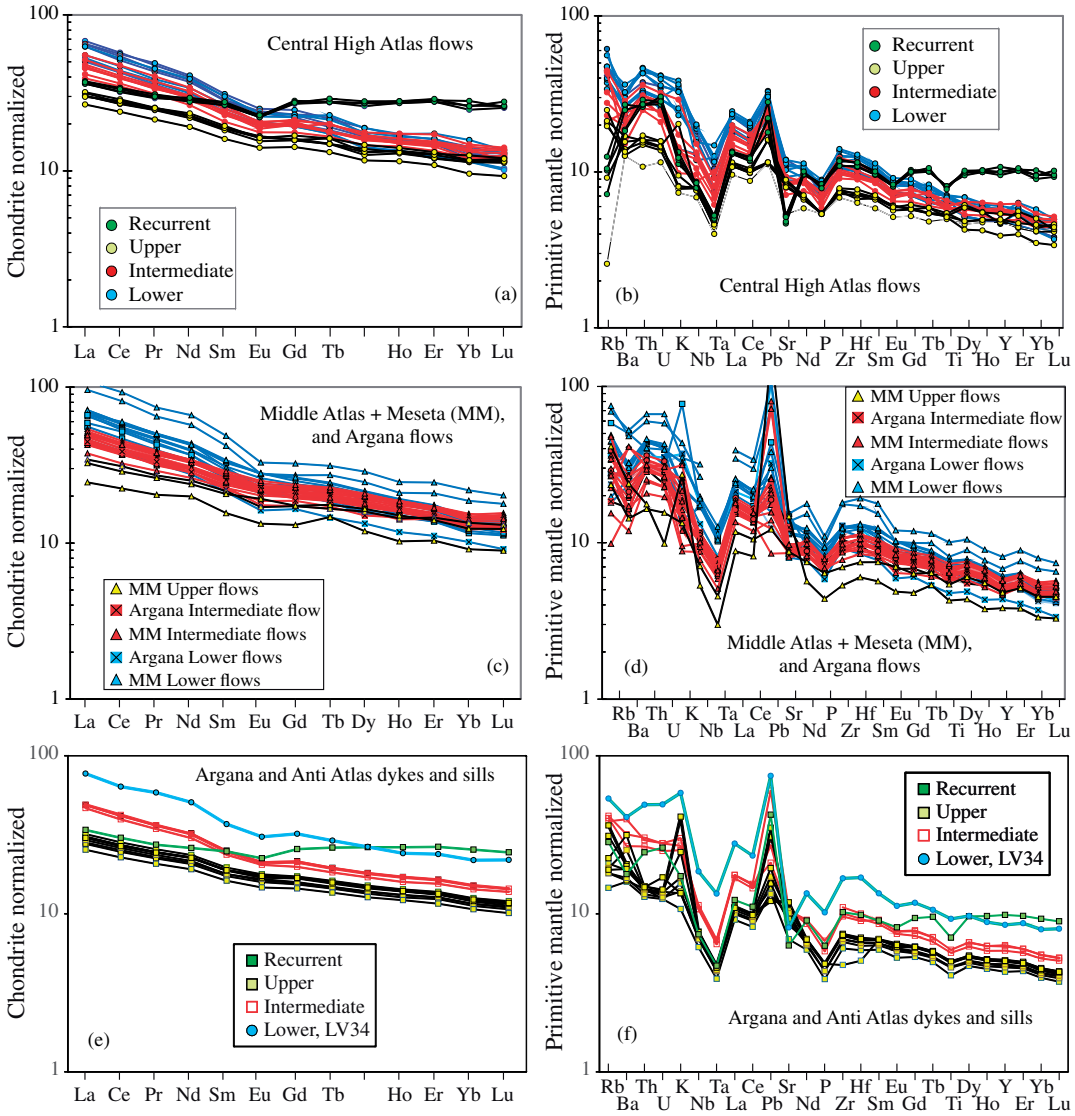

Fig. 13. Chondrite normalized REE (McDonough & Sun, 1995) and primitive mantle (McDonough & Sun, 1995) normalized incompatible element patterns of Central High Atlas (a, b), Argana and Middle Atlas lava flows (c, d) and of Anti Atlas and Argana intrusive rocks (e, f).

latter samples, as they may not reflect magmatic liquid compositions. In the case of the Amelal sill, these difficulties are enhanced by the pervasive alteration of the sill. Nevertheless, relying mainly on immobile incompatible minor and trace element compositions, Moroccan CAMP intrusive rocks can be assigned to the four main magmatic units.

Most of the sampled rocks from the Amelal sill have major and trace element compositions similar to Intermediate unit lava flows (Figs 11 and 12). However, a few samples are relatively depleted in Ti and other incompatible elements, as observed for Upper unit basalts (e.g. sample LV37). One sample from the Amelal sill, LV34, is compositionally rather distinct from the remainder of the sill. LV34 is in general enriched in incompatible minor and trace elements, approaching the composition of Lower basaltic andesitic lava flows. The similarity between LV34 and Lower lava flows is also evidenced by incompatible element ratios, such as TiO_2/Y or Zr/Y (Fig. 12e and f). The Jbilet intrusives include a dyke sample with Lower unit composition (AN320), as well as one dyke and one sill with Intermediate composition.

Intrusive rocks from the Anti Atlas (Foum Zguid dyke and Bas Draa sills) can be readily assigned to three (out of the four) magmatic units as they share strong similarities with the lava flows at least in terms of incompatible major and trace elements and trace element ratios. Most Foum Zguid dyke samples overlap the compositional field defined by Intermediate lava flows, for example in TiO_2, P_2O_5, La/Yb etc. By contrast, four Foum Zguid dyke samples also have Upper-unit like compositions and one small dyke parallel to the main Foum Zguid dyke has a Recurrent-like composition. The Foum Zguid dyke appears to be a composite dyke, intruded by Intermediate and Upper magmas. In fact, at two

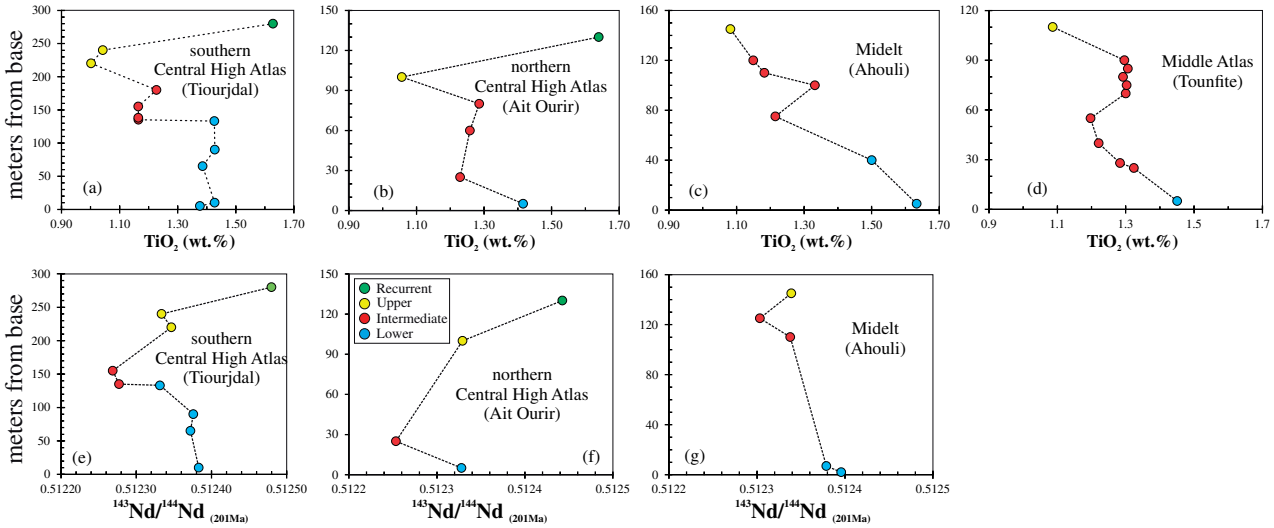

Fig. 14. Stratigraphic variations of major (TiO_2, wt %), trace element (Zr, ppm) and initial Sr–Nd isotopic ratios of Moroccan lava sequences from the Central High Atlas (Tiourjdal and Ait Ourir), Midelt (Ahouli) and Middle Atlas (Tounfite; isotopic data are too few for this section and are thus not shown). Colour code as in Fig. 10, i.e.: blue, Lower flows; red, Intermediate flows; yellow, Upper flows; green, Recurrent flow.

sampling localities both Intermediate and Upper-like rocks have been encountered in the same dyke. In particular, near Bou Azzer, the central part of the dyke has an Intermediate-like composition while its margin has an Upper-like composition. The opposite is observed at Tanzirt, where the core has Upper-like and the rim Intermediate-like composition. Sampled Bas Draa sills have compositions similar to Intermediate (1 sill) and Upper unit flows (3 sills).

Sr–Nd–Pb–Os isotopic compositions. For this study, we obtained 52 $^{87}Sr/^{86}Sr$ and $^{143}Nd/^{144}Nd$, 33 Pb and 13 Os isotope analyses on whole-rock samples. The selected samples belong to the four lava flow units and intrusive rocks and represent the various CAMP localities of Morocco. Initial isotopic compositions were back-calculated to 201 Ma to correct the measured isotopic ratios for *in situ* decay of the radioactive element. Initial Sr–Nd–Pb isotopic compositions of CAMP basalts from Morocco (Table 3) fall in the field of typical low-Ti basalts of the CAMP (Fig. 16), with $^{87}Sr/^{86}Sr_i$ in the range 0·705–0·707, $^{143}Nd/^{144}Nd_i$= 0·5125–0. ·5122 (εNd_i from +2 to -3) and high $^{207}Pb/^{204}Pb_i$ (15·59–15·67) and $^{208}Pb/^{204}Pb_i$ (37·8–38·8) at moderate $^{206}Pb/^{204}Pb_i$ (18·0–18·9), resulting in high Δ7/4 (10–18) and Δ8/4(32–61) values (Δ values indicating difference with respect to the Northern Hemisphere Reference Line, NHRL; Hart, 1984). One Argana Lower flow (AN115b), one Argana Intermediate flow (AN128) and one Intermediate Anti Atlas (Foum Zguid) dyke sample (AN734) yield higher $^{87}Sr/^{86}Sr_i$ (0·7072–0·7089), plotting off the field of other Lower and Intermediate basaltic andesites at similar $^{143}Nd/^{144}Nd_i$ (0·51238 and 0·51235). This shift to higher $^{87}Sr/^{86}Sr_i$ ratios reflects a secondary alteration fingerprint rather than a primary compositional feature, as also suggested by the higher Sr contents of these same samples (enrichment excess by *c.*50–70 ppm) compared to samples of the same unit.

Systematic differences in Sr and Nd initial isotopic ratios characterize the four Moroccan CAMP lava flow units and their intrusive equivalents (Fig. 16). With the exception of the sample thought to be altered (AN115b), Lower flows yield relatively high $^{87}Sr/^{86}Sr_i$ (0·7058–0·7066) and moderate $^{143}Nd/^{144}Nd_i$ (0·51231–0·51239). Intermediate flows trend to lower $^{143}Nd/^{144}Nd_i$ (0·51225–0·51237) with similar $^{87}Sr/^{86}Sr_i$ (0·7057–0·7065), again excluding altered samples. Pb isotopic compositions for Lower and Intermediate flows overlap, even if these latter show a slightly larger spread ($^{206}Pb/^{204}Pb_i$ 18·0–18·4) and plot at slightly higher $^{207}Pb/^{204}Pb_i$ and $^{208}Pb/^{204}Pb_i$ for a given $^{206}Pb/^{204}Pb_i$. Upper basalt lava flows and half of the Upper unit intrusive rocks yield a restricted Sr-Nd isotopic range (0·7055–0·7056, 0·51235–0·51233, respectively) having lower $^{87}Sr/^{86}Sr_i$ compared to Lower and Intermediate flows. Upper unit basalts plot towards the less radiogenic end in Pb isotopic space for low-Ti CAMP basalts.

Recurrent basalts can be clearly distinguished from the other CAMP units. They show limited variations of Nd and Sr initial isotopic compositions and have lower $^{87}Sr/^{86}Sr_i$ (0·7049–0·7053) and higher $^{143}Nd/^{144}Nd_i$ (0·51244–0·51248) compared to the other units. In addition, they yield the highest $^{206}Pb/^{204}Pb_i$ (18·45–18·65) and $^{208}Pb/^{204}Pb_i$ (38·42–38·54) of all magmatic units. Recurrent basalts are also characterized by correlated Sr and Pb isotopic compositions, a feature that is not observed in other units. They also yield slightly decreasing $^{207}Pb/^{204}Pb_i$ (15·66–15·64) at increasing $^{206}Pb/^{204}Pb_i$ and slightly lower Δ8/4 (32–48) compared to the other samples (43–60).

Thirteen of the freshest samples from the four Moroccan CAMP lava flow units were analysed also for

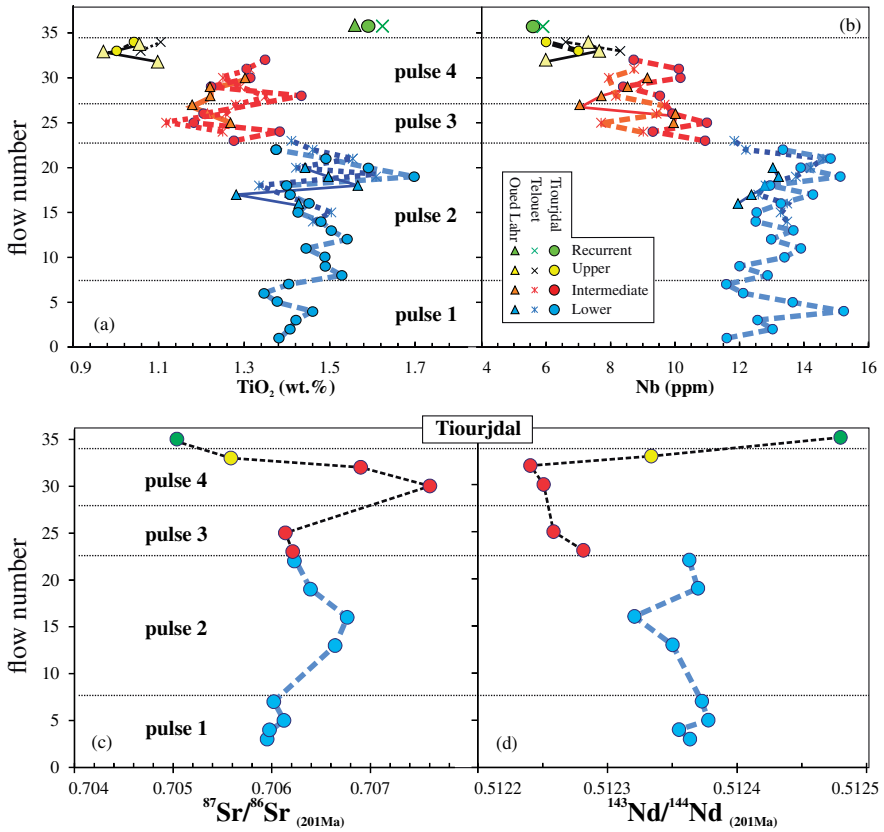

Fig. 15. Detailed time-related variations of (a)TiO_2 wt %, (b) Nb (ppm) and (c, d) initial Sr–Nd isotopic compositions (back-calculated to 201 Ma) for Moroccan lava sequences from the Central High Atlas (Tiourjdal, Telouet, Oued Lahr). Analysed samples were originally collected for magnetostratigraphic investigations (Knight *et al.*, 2004). Isotopic data for the Tiourjdal section only. Colour code as in Fig. 10, i.e.: blue, Lower flows; red, Intermediate flows; yellow, Upper flows; green, Recurrent flow.

Re–Os isotopic compositions (Fig. 17; Table 4). Re contents range from 130 to 678 ppt, with the exception of samples AN44 and AN24 from the Recurrent basalts, which contain 1953 and 5502 ppt, respectively. Re has the lowest content in the Lower basaltic andesites and by far the highest one in the Recurrent basalts. Os contents range from 22 to 482 ppt. The lowest Os concentrations are found in Upper and Recurrent basalts and are in general correlated with MgO, Cr and Ni. Measured $^{187}Os/^{188}Os$ is roughly correlated with $^{187}Re/^{188}Os$ (MSWD = 62) in all analysed samples except one (Recurrent basalt AN24) and yields an apparent Re–Os age (202·3 ± 5·8 Ma, 2σ uncertainty) indistinguishable from the $^{40}Ar/^{39}Ar$ ages of the Moroccan CAMP, with a $^{187}Os/^{188}Os$ intercept of 0·1236 ± 0·0089. While this apparent age has no geochronologic significance, Fig. 17a suggests that the Re/Os isotopic system remained nearly closed since the eruption of the lava flows at about 201 Ma. Initial $^{187}Os/^{188}Os_i$ ranges from 0·109 ± 0·004 to 0·136 ± 0·017 for all samples except the Recurrent sample AN24, which has an initial ratio of 0·453 ± 0·077. In detail, Lower flows have relatively uniform $^{187}Os/^{188}Os_i$ (0·127 ± 0·03, 1σ) compared to the heterogeneous Intermediate and Upper flows. These latter units yield the lowest (*c.*0·11) and highest $^{187}Os/^{188}Os_i$ (*c.*0·14) values among the studied units. This may reflect the fact that the Lower basalts have the highest Os contents and thus the lowest $^{187}Re/^{188}Os$ ratios and so are subject to the smallest corrections for radiogenic ingrowth, leading to the most robust estimates of initial ratio. In general, Os isotopic compositions are poorly correlated with Sr–Nd–Pb isotopic compositions, with the exception of Lower unit samples which show a relatively good correlation for Os vs Nd and Pb isotopic ratios (Fig. 17).

The differences in isotopic composition among the four units are also highlighted for some sections analysed in detail (Figs 14 and 15). In particular, at Tiourjdal, Sr–Nd–Pb–Os isotopic data are available for all the four units and show a similar $^{87}Sr/^{86}Sr_i$ for Lower and Intermediate flows and then a decrease for Upper and Recurrent samples; $^{143}Nd/^{144}Nd_i$ is slightly higher for Lower and Upper flows compared to Intermediate ones, whereas the Recurrent basalt yields the highest value. Although not shown in the figures, Pb and Os isotopes show comparable variations, with almost indistinguishable isotopic ratios in Lower and Intermediate flows, showing the lowest values for the Upper basalt and the highest values for the Recurrent basalt. Similar variations can also be seen for the Ait Ourir (northern central High Atlas), Ahouli (Midelt) and Maaziz (western

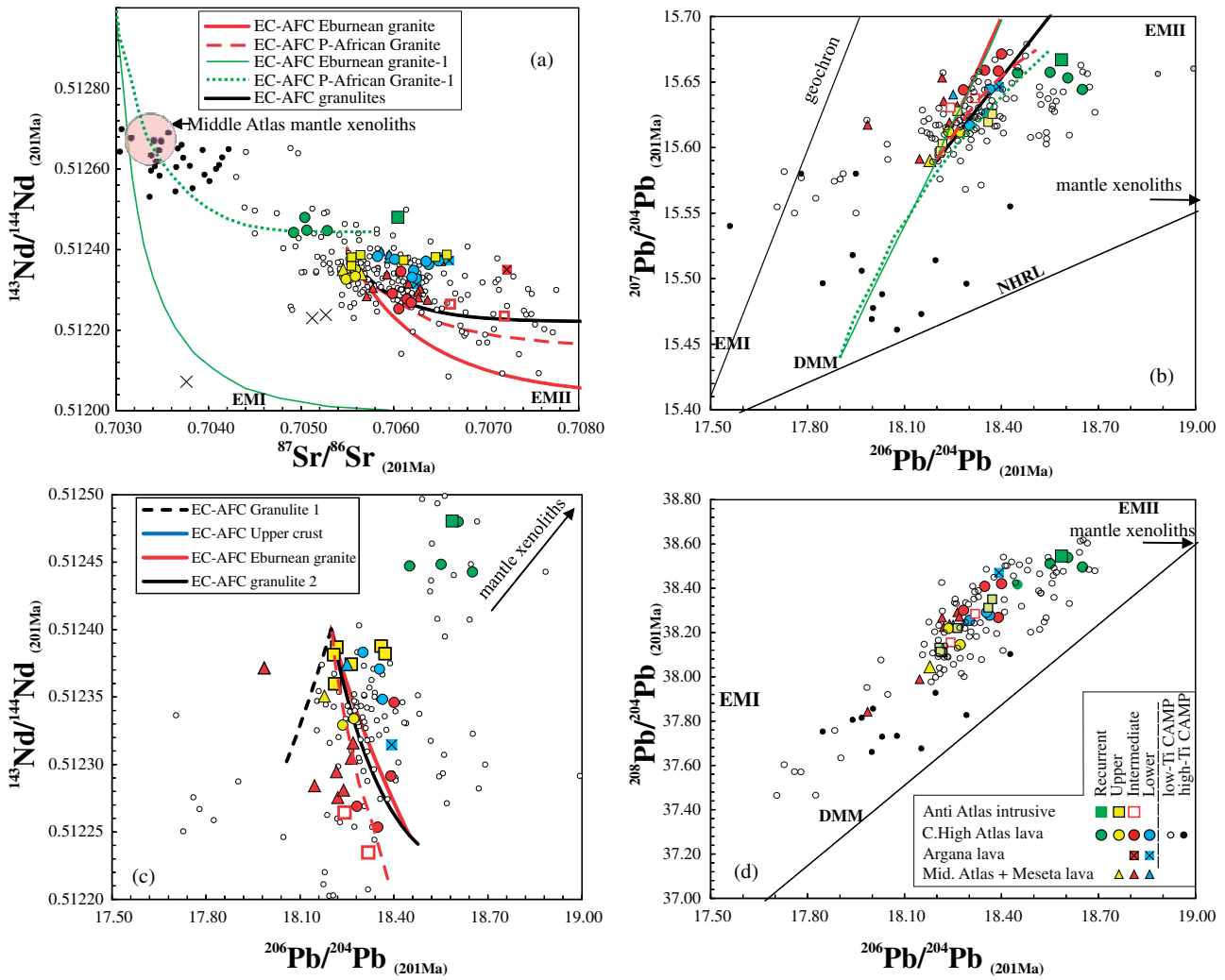

Fig. 16. Initial (at 201 Ma) Sr–Nd–Pb isotopic compositions of Moroccan CAMP lava flows and intrusives. Data for other CAMP low-Ti ($TiO_2 < 2{\cdot}0$ wt %) and high-Ti ($TiO_2 > 2{\cdot}0$ wt %) samples are from Alibert (1985); Dupuy *et al.* (1988); Pegram (1990); Puffer (1992); Heatherington & Mueller (1999); De Min *et al.* (2003); Jourdan *et al.* (2003); Verati *et al.* (2005); Deckart *et al.* (2005); Merle *et al.* (2011, 2014); Callegaro *et al.* (2013, 2014a); Whalen *et al.* (2015). EC-AFC (Spera & Bohrson, 2001) crustal assimilation and fractional crystallization paths are calculated from an initial MORB (dashed curves) and from an initial CAMP basalt (solid curves). Crustal assimilants used in modelling are given in Table 5.

Meseta), although the isotopic data are sparser for these sections.

Isotopic compositions are in general poorly correlated with major and trace element concentrations and ratios. The best, although still scattered, correlations are shown between $^{87}Sr/^{86}Sr_i$ and SiO_2 and La/Yb (Supplementary Data Electronic Appendix 1; supplementary data are available for downloading at http://www.petrology.oxfordjournals.org), which is consistent with the cited differences among the four lava flows units. No correlations are observed with MgO, Mg# or any incompatible element variations, neither at global or intra-unit variation scales.

Comparison with other CAMP basalts

Compared to other CAMP basalts, those from Morocco plot within the field of low-Ti samples from Africa, Europe, North and South America in terms of major and trace element contents and of Sr, Nd and Pb isotopic compositions (Figs 16 and 18). Marzoli *et al.* (2018) identified six main geochemical groups of magmatic compositions from the entire CAMP (Fig. 18). In detail, Moroccan Lower basalts belong to the Tiourjdal group along with some dykes and sills from Mali (Taoudenni Basin; Verati *et al.*, 2005) and with Lower lava flows from Algeria (Meddah *et al.*, 2017). Samples of this group are significantly more enriched in terms of incompatible trace element contents and have higher ratios of strongly vs moderately incompatible elements (e.g. La/Yb) than any other group of low-Ti CAMP rocks from the circum-Atlantic basins (Portugal, Canada, U.S.A.; Tollo & Gottfried, 1992; Callegaro *et al.*, 2013, 2014a; Merle *et al.*, 2014) or from Brazil and Bolivia (De Min *et al.*, 2003; Merle *et al.*, 2011; Bertrand *et al.*, 2014; Marzoli *et al.*, 2018). However, the Sr–Nd–Pb isotopic compositions of Moroccan Lower flows and of the

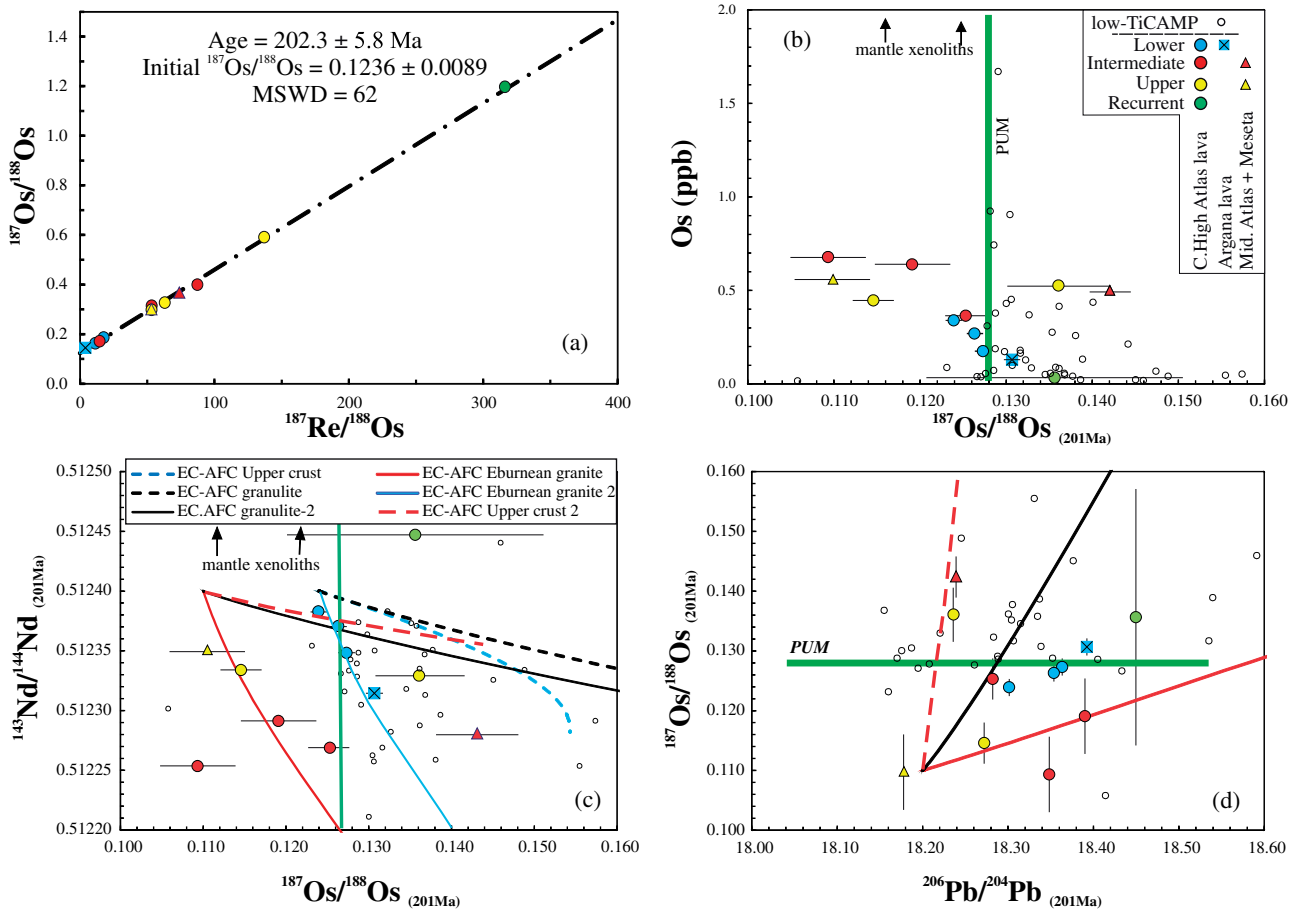

Fig. 17. Re–Os isotopic compositions of CAMP lava flows from Morocco. (a) $^{187}Os/^{188}Os$ vs $^{187}Re/^{188}Os$ diagram showing alignment of all analysed points (except Recurrent basalt AN24) in a pseudo-isochron which yields an apparent age of 202·3 ± 5·8 Ma. Isochron calculated using Isoplot (Ludwig, 2003); uncertainties on $^{187}Re/^{188}Os$ and $^{187}Os/^{188}Os$ are listed in Table 5. The apparent age does not have statistical validity (MSWD 62, probability close to zero), but indicates that the Re–Os systematics of the analysed rocks (except AN24, not included in the diagram) were not greatly modified by post-crystallization processes. (b) Initial Os content (in ppb) vs $^{187}Os/^{188}Os$. (c–d) Nd and Pb vs Os isotopic compositions. EC-AFC assimilation paths starting from two different initial compositions are shown; parameters reported in Table 5. The green vertical lines in (b) and (c) and the horizontal line in (d) represent the $^{187}Os/^{188}Os$ of the primitive upper mantle (PUM) calculated for 201 Ma (0·1281 ± 0·0008, derived from the present-day value of PUM of 0·1296; Meisel *et al.*, 2001). Black bars on symbols represent uncertainties on calculated initial $^{187}Os/^{188}Os$.

Table 4: Re–Os isotopic data. Os isotopic ratios were normalized to $^{192}Os/^{188}Os = 3.08271$

	Unit	[Re] (ppt)	[Os] (ppt)	^{188}Os M g^{-1}	$^{187}Os/^{188}Os$	2σ	$^{187}Re/^{188}Os$	2σ	$^{187}Os/^{188}Os_{201Ma}$	2σ
AN 49	lower	269	75·6	5·24E-14	0·18427	0·00055	17·3	0·333	0·1263	0·0012
AN 32	lower	176	321·8	2·24E-13	0·13615	0·00034	2·6	0·065	0·1273	0·0004
AN 134	lower	340	108·5	7·53E-14	0·17481	0·00058	15·2	0·306	0·1239	0·0012
AN 132	lower	130	482·1	3·36E-13	0·13507	0·00063	1·3	0·050	0·1307	0·0007
AN 18	intermediate	678	39·3	2·66E-14	0·39718	0·00123	85·8	1·256	0·1093	0·0044
AN 138	intermediate	365	152·6	1·06E-13	0·16408	0·00050	11·6	0·243	0·1253	0·0010
AN 39	intermediate	639	44·7	3·04E-14	0·35646	0·00130	70·8	1·032	0·1191	0·0037
AN 510	intermediate	465	50·7	3·46E-14	0·29484	0·00148	45·2	0·602	0·1431	0·0025
AN 141	upper	446	35·1	2·40E-14	0·32465	0·00132	62·6	1·022	0·1146	0·0037
AN 22	upper	526	22·3	1·47E-14	0·53935	0·00301	120·2	1·538	0·1361	0·0060
AN 540	upper	559	57·4	3·93E-14	0·27114	0·00097	47·9	0·563	0·1105	0·0021
AN 44	recurrent	1953	33·7	2·07E-14	1·1994	0·0060	317·1	4·735	0·136	0·017
AN 24	recurrent	5502	34·2	1·51E-14	4·564	0·037	1225·4	20·153	0·453	0·077

All uncertainties are 2σ. Uncertainties listed for the measured $^{187}Os/^{188}Os$ ratios include those related to in-run statistics, standard reproducibility and blank variability. Initial ratios were calculated using a decay constant l = 1·666 x10-11 (Smoliar *et al.*, 1996). Uncertainties on initial ratios include those related to in-run errors, blank corrections and weighing errors. Uncertainties on age and ^{187}Re decay constant are not included as these produce systematic rather than random errors on initial ratios.

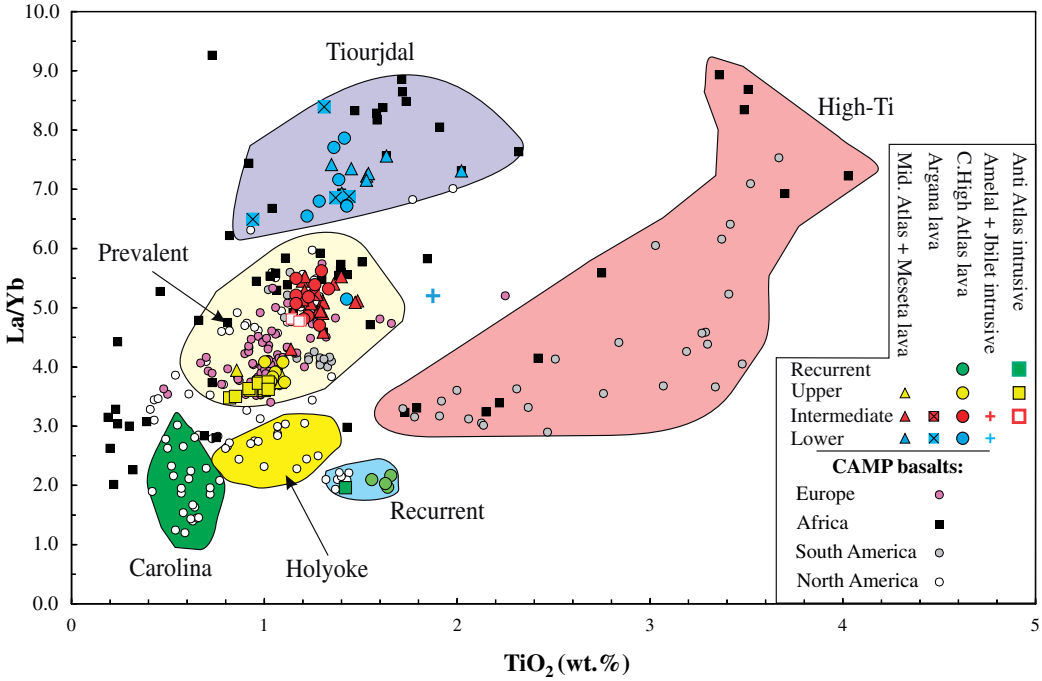

Fig. 18. La/Yb vs TiO_2 (wt %) variation for whole-rocks from the Moroccan CAMP units (same symbols as Fig. 10) and CAMP rocks from Europe, Africa, North America and South America. The contoured fields highlight the compositions of the six main geochemical groups of CAMP basalts defined by Marzoli *et al.* (2018): Prevalent, Tiourjdal, Holyoke, Carolina, Recurrent, High-Ti.

Tiourjdal group samples in general fall in the field of most other low-Ti CAMP rocks.

Intermediate and Upper basalts belong to the Prevalent group (Marzoli *et al.*, 2018) and share incompatible element contents and ratios with the oldest basalts from the Newark basins (e.g. Orange Mt. basalt), all CAMP basalts from SW Europe and some Taoudenni dykes from Mali (Cebriá *et al.*, 2003; Verati *et al.*, 2005; Martins *et al.*, 2008; Callegaro *et al.*, 2014; Merle *et al.*, 2014). Intermediate Moroccan basaltic andesites display some of the highest $^{207}Pb/^{204}Pb_i$ and thus $\Delta 7/4$ of all CAMP rocks and the Moroccan Upper basalts yield among the least radiogenic Pb isotopic compositions of CAMP low-Ti samples (except for SE-USA dykes; Callegaro *et al.*, 2013).

Finally, Recurrent basalts from Morocco along with the Hook Mt. and Hampden basalts from the U.S.A. (Merle *et al.*, 2014) belong to the Recurrent group (Marzoli *et al.*, 2018) and yield among the lowest Sr and highest Nd and Pb isotopic ratios of all CAMP low-Ti basalts. This rock group is also characterized by similar systematics in trace element contents and ratios, for example little fractionated MREE/HREE patterns.

Several of the Moroccan samples show lower $^{187}Os/^{188}Os_i$ than the great majority of CAMP rocks so far. In particular, four samples (two Intermediate and two Upper basalts) display $^{187}Os/^{188}Os_i$ lower than 0·120, implying derivation from a mantle source that experienced melt extraction more than 1·3 billion years ago (assuming that the $^{187}Re/^{188}Os$ ratios of these samples have been unperturbed). This has rarely been observed elsewhere in the CAMP province. On the other hand, the Lower basalt samples, which have the highest Os concentrations, have $^{187}Os/^{188}Os_i$ values fairly close to those analysed so far within the CAMP and close to the Primitive Upper Mantle (PUM) value at 201 Ma (0·1281 ± 0·0008, derived from the present-day value of PUM of 0·1296; Meisel *et al.*, 2001).

DISCUSSION

The CAMP in Morocco: age, duration, volcanostratigraphic correlations

Geochemical data show that the lava flow sequences share similar time-related variations throughout Morocco (Figs 14 and 15). In particular, throughout Morocco, lava flows of the Lower and Intermediate units are nearly ubiquitous. The thickness of Lower basalts diminishes from south (Central High Atlas, Argana) to north (Middle Atlas and Meseta), while that of Intermediate basalts increases. Upper flows are relatively less abundant but can be found in the Central High Atlas and Middle Atlas, while they are (to our knowledge) absent in the Eastern and Western Meseta and at Argana. Recurrent lava flows are limited to the Central High Atlas.

Combined with previously published geochronologic, magnetostratigraphic and palynological data (Sebai *et al.*, 1991; Knight *et al.*, 2004; Marzoli *et al.*, 2004; Nomade *et al.*, 2007; Verati *et al.*, 2007; Blackburn *et al.*, 2013; Davies *et al.*, 2017; Panfili *et al.*, 2019) the ages presented in this study, paleomagnetic and geochemical data constrain the emplacement history of the CAMP in Morocco. The new $^{40}Ar/^{39}Ar$ ages for the

Middle Atlas and Meseta lava flows are similar to those for the Central High Atlas (previous and new data) and suggest a synchronous eruption all over Morocco with peak activity at *c.*201·4 Ma (Figs 2 and 6). The now quite large set of $^{40}Ar/^{39}Ar$ ages for the Lower and Intermediate unit lava flows (15 and 8 ages, respectively) suggests also that Lower and Intermediate lavas were erupted over a short time span. These findings are consistent with new palynological data (Marzoli *et al.*, 2004; Deenen *et al.*, 2010; Panfili *et al.*, 2019), which show that Lower to Upper basalts from throughout Morocco were emplaced on sedimentary strata with an identical palynological association, i.e. with identical biostratigraphic age. Combined with carbon isotope data on the associated sedimentary strata (Deenen *et al.*, 2010; Dal Corso *et al.*, 2014), the palynological data suggest that the Lower to Upper basalts were erupted at the very beginning of the end-Triassic extinction interval (c.201·51 ± 0·15 Ma) and ceased their activity before the Triassic-Jurassic boundary (c.201·36 ± 0·15 Ma; U/Pb ages from Schoene *et al.*, 2010, recalculated by Wotzlaw *et al.*, 2014). The new magnetostratigraphic data for the Middle Atlas and Meseta sections, even if slightly more scattered than similar data for the Central High Atlas (Knight *et al.*, 2004), confirm that lava flows from northern Morocco were also erupted in short successive pulses. Following Knight *et al.* (2004) and Font *et al.* (2011), five volcanic pulses may have occurred in Morocco. Finally, the new U/Pb age for the Amelal sill sample LV34 (201·569 ± 0·042 Ma), which we correlate to the Lower unit, constrains the onset of the CAMP volcanism in Morocco. This age is identical to the U–Pb age (201·564 ± 0·054 Ma) obtained by Blackburn *et al.* (2013) for an Amelal sill sample, which those authors attributed to the Intermediate unit. These ages suggest that emplacement of Lower and Intermediate basalts was essentially synchronous, given that their age difference is less than *c.*0·1 Ma considering the uncertainty on the ages. Based on field evidence and on previous geochronologic data, only Recurrent basalts seem to be significantly younger than the main peak of CAMP activity in Morocco, consistent with the separation by about 50 m of sediments. However, our new mini-plateau age for the Recurrent basalt AN24 (201·15 ± 0·70 Ma) suggests that the time interval between emplacement of the peak volcanic activity (Lower to Upper flows) and emplacement of the Recurrent basalt may have been relatively short (<1 Ma).

The global picture that emerges, based on paleomagnetic, palynological, geochronologic data, is that of a very rapid emplacement (possibly in less than 0·1 Ma) of over 95 vol. % (i.e. Lower to Upper units) of the basaltic lava flows. All over Morocco, lavas of each unit have near-identical composition and lava piles display near-identical stratigraphic evolution. CAMP lava flows were probably present in the entire High Atlas basin, even if in Eastern Morocco they are probably buried under the Jurassic and Cretaceous sedimentary cover. On the other hand, there are no observations demonstrating that CAMP lavas ever flowed out of the basins, i.e. that they flooded over the Hercynian basement. It also remains unclear if CAMP magmas were erupted in the Anti Atlas (see next section). Taking into account the area shown by the dashed line in Fig. 1b, the CAMP in Morocco may have reached a total surface area of about 0·13 million km^2. Considering an average thickness of the lava piles of 100 m, the total erupted volume would be around 10^4 km^3 and the average eruption rate about 0·1 km^3/year, assuming a duration of 0·1 Ma. Such an eruption rate is comparable to that at Hawaii (Lipman *et al.*, 2006; Jourdan *et al.*, 2012). However, if we consider that Lower to Upper CAMP flows in Morocco were erupted in four pulses each lasting about 400 years (Knight *et al.*, 2004; Font *et al.*, 2011), the eruption rate during the pulses would be about 8 km^3/year. Such an eruption rate is over one order of magnitude higher than at Hawaii and similar to e.g. the Laki eruption in Iceland (15 km^3 in 9 months during the years 1783–1784), which had a considerable effect on the climate in the northern hemisphere (Thordarson & Self, 1993).

Magmatic plumbing system: dykes and sills from the Anti Atlas, Argana and the Jbilets Mts

Correlations of intrusive rocks from the Anti Atlas, the Argana Valley (Amelal sill) and the Jbilets Mountains with effusive rocks are based on geochemical analyses. In particular, the best constraint is provided by comparison of minor (Ti and P) and trace element (e.g. HFSE and REE) contents and ratios. The overlap of major element compositions of intrusive and effusive rocks is not perfect. This is probably due to the fact that, unlike most of the lava flows, dykes and sills are significantly different from near-liquidus melt compositions. Isotopic data are also useful to correlate intrusive and effusive rocks, even if the $^{87}Sr/^{86}Sr_i$ of the intrusive rocks seems to be slightly modified by alteration effects.

Our geochemical data and field observations indicate that the large dykes and sills were formed mainly by magmas of the Intermediate and Upper units. In the Anti Atlas, multiple intrusions of magmas with Intermediate and Upper composition occurred at some localities along the ~200 km long Foum Zguid dyke (e.g. near Bou Azzer or near Tanzirt, Fig. 1b). This indicates that the Foum Zguid dyke was intruded by compositionally distinct magmas probably during successive magma injection events. Near Tissint, a small dyke paralleling the main Foum Zguid dyke can be assigned to the Recurrent unit, while the main body of the Foum Zguid dyke corresponds to the Intermediate unit. However, it remains unclear if the Anti Atlas dyke system ever fed any lava flows. It is notable that the *c.* N30 orientation of the Foum Zguid dyke does not intersect the areas where CAMP lava flows crop out in the High Atlas. Notably, the Foum Zguid dyke runs along the main axis of the Anti Atlas Paleozoic basins and and

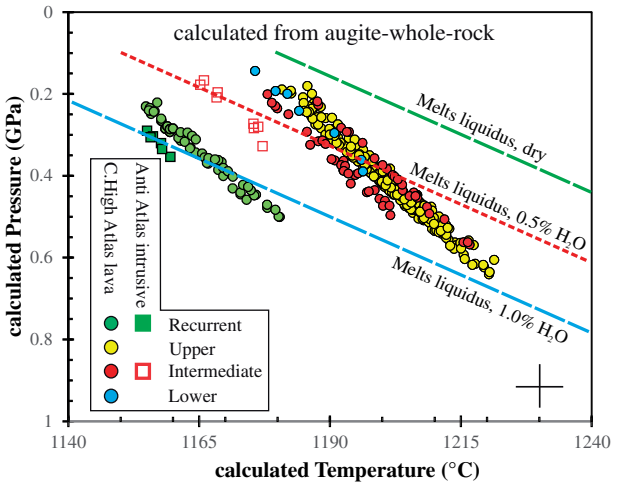

Fig. 19. Pressure (GPa) – temperature (°C) conditions calculated after Putirka *et al.* (1996) and Putirka (2008) from augite and whole-rock compositions for the four magmatic units. A test for equilibrium of augite and whole-rock has been done following criteria outlined in Putirka *et al.* (2009). The parameters have been calculated for two Lower, four Intermediate, three Upper and two Recurrent samples. The cross indicates approximate uncertainties on pressure and temperature estimates, due to analytical uncertainties and uncertainties related to the thermobarometer.

intrudes Proterozoic basement and Paleozoic sediments. It follows the direction intruded by a late Proterozoic dyke.

The few samples from the Jbilet dyke (except sample AN320 akin to the Lower basalts) and NNE–SSW orientation of the dyke, pointing towards the Argana Valley, suggest that this rather large (even if poorly outcropping) dyke fed the Intermediate lava flows of the Argana basin. The Amelal sill in the Argana basin was mainly formed by Intermediate-type magmas (Fig. 12). Only one sample (LV37) approaches the Upper magma composition, even if it should be considered that pervasive alteration of this rock hinders a clear correlation with lava flow compositions. One sample from the central part of the Amelal sill (LV34) has a composition quite different from the rest of the Amelal rocks; LV34 is similar to Lower lava flows, even if its geochemical overlap with the Lower basaltic lava flows is not perfect. Sample LV34 is of major importance, since it contains zircon and yielded a U/Pb age. LV34 has an evolved composition (MgO = 4·66 wt %, SiO_2 = 54·86 wt %) and relatively high contents of incompatible major (TiO_2 1·87 wt %, P_2O_5 0·21 wt %) and incompatible trace elements (e.g. Th = 3·9 ppm; Nb = 12·2 ppm; La = 18·3 ppm; Zr = 175 ppm), as well as high values for most ratios of strongly to moderately incompatible elements (e.g. TiO_2/Y, Zr/Y; Fig. 12). These values are similar to those of the Lower lava flows and clearly higher than those shown by even the most evolved Intermediate lava samples. They are also different from the values of all other Amelal sill samples, which instead are of Intermediate or Upper affinity. However, LV34 differs from Lower basalts in terms of its relatively low La/Yb (5·19, while most Lower basalts have La/Yb >6·2). In general, it may be concluded that the Amelal sill is composite in composition, i.e. it was formed by multiple intrusions of distinct magma batches. However, the Amelal sill is not only quite altered but also coarse-grained, making the comparison with lava flow samples difficult.

In general, one pattern that emerges is that intrusive rocks with compositions pertaining to the Lower unit are virtually absent in Morocco with the possible exception of the U/Pb dated Amelal sill sample LV34 and of a Jbilet dyke sample (AN320). The reason for the lack of outcropping Lower-type dykes and sills is unclear and we can only propose tentative interpretations. For example, it may be suggested that during the initial stages the magmatism was focused mainly in the Triassic rift basins, where the extension was strongest. Therefore, Lower basalts are present only in those basins and are thickest in the High Atlas in particular. Later, during more mature extension, Intermediate to Upper basalts were also emplaced outside the Triassic basins.

Pressure, temperature, H_2O content and oxygen fugacity of CAMP magmas

Clinopyroxene phenocryst compositions can be used to constrain the pressure–temperature conditions of the magmas before eruption or intrusion. However, it should be noted that none of the investigated magmatic rocks corresponds to a primary (or near-primary) magmatic composition, i.e. all the samples are evolved and their calculated temperatures and pressures are most probably lower than those of their parental magmas. Equilibrium temperature and pressure were calculated after Putirka *et al.* (1996; see also Putirka, 2008; Neave & Putirka, 2017) for augite compositions that are considered in equilibrium with their host rock (Fig. 19). Following criteria outlined, for example, in Putirka *et al.* (2009), equilibrium augites should have Fe^{2+}/Mg, which ranges between 0·27 and 0·33 that of the whole-rock (assuming that Fe^{2+} equals to Fe_{tot} in augites and is 87% of Fe_{tot} in the whole rocks). Moreover, the difference between calculated and observed clinopyroxene components should not exceed 5% relative error. According to these criteria, few augites from the Lower basaltic andesites are in equilibrium with their host rock, while a large number of augites from the other three units could be selected for pressure-temperature calculation. It should also be noted that the calculated pressure and temperature is strongly controlled by the Na concentration measured in the augites (Na_2O ranges generally between 0·15 and 0·25 wt % for all analysed augites). Since the analytical uncertainty for electron microprobe analysis of this relatively volatile element is conservatively estimated at ca. 10%, this propagates uncertainties of *c.*0·1 GPa and *c.*15 °C to the calculated pressures and temperatures, respectively.

Calculated pressures (*c.*0·2–0·6 GPa) and temperatures (*c.*1180–1220 °C) obtained from augite

compositions are broadly similar for effusive rocks from the Lower, Intermediate and Upper units. In detail, a subset of the Intermediate flows are characterized by slightly lower calculated pressures for a given temperature, relative to both Lower, Upper and other Intermediate lavas (Fig. 19). The Lower unit has the smallest *P–T* range of all units, slightly displaced on average toward both higher equilibrium depths and lower temperatures relative to those of Intermediate and Upper units (Fig. 19). Although Recurrent lavas are equilibrated in a pressure range encompassed by those (*c.*0·2–0·4 GPa) of Lower, Intermediate and Upper samples, they have significantly lower equilibrium temperature (*c.*25 °C less for a given pressure). With regard to intrusive rocks, the T-ranges calculated for an Intermediate unit sample from the Foum Zguid dyke and for a small Recurrent-unit dyke from the Anti Atlas are shifted toward lower values than those of their eruptive counterparts at similar pressure ranges, which is most probably due to the slow cooling of the intrusions. Calculated pressure ranges obtained for augites from intrusive rocks are roughly consistent with estimated thickness of the sedimentary strata (about 5 km) under which these magmas intruded in the Anti Atlas, as well as with the depth range of CAMP sill intrusions in eastern North America (*c.*5 km, e.g. Weems *et al.*, 2016).

The geobarometric data suggest that crystallization of most augites mainly happened at mid-crustal depths (7 to 20 km). This indicates that Moroccan CAMP basalts were mainly erupted from a mid-crustal plumbing system, assuming that the crust was not significantly thinned due to extensional tectonics. At the regional scale, it is important to notice that mid-crustal plumbing depths (10–20 km) have also been estimated for the Freetown layered complex (Chalokwu, 2001; Callegaro *et al.*, 2017). In addition, since none of the analysed rocks can be considered as primary and since most analysed augites would be in equilibrium with a relatively evolved magma (Mg#<60), it is likely that significant early fractionation may have occurred at depths higher than those yielded by the analysed augites. Such high pressure fractionation may have been located at or close to the Moho, or even within the uppermost mantle, where it is generally considered that primary LIP magmas may differentiate to more evolved compositions by fractionation of mafic minerals (cf. Cox, 1980; Hole, 2018).

Pigeonite crystallization temperatures have also been calculated following Ishii (1975). The calculated values range between *c.*1050 and 1180 °C for most analysed pigeonite crystals. A slightly lower crystallization temperature for pigeonite compared to augite seems consistent with petrographic observations, which indicate that pigeonite is a relatively late crystallizing mineral. Among all pigeonites, those from the Recurrent basalts yield the lowest temperatures (<1080 °C).

Plagioclase crystallization temperatures calculated after Thy *et al.* (2013) range between 1100 and 1220 °C for most analysed crystals. Again, Recurrent basalts yield the lowest values (<1170 °C), while most Upper basalts yield temperature higher than 1170 °C. Similar temperatures have been obtained with the plagioclase-melt geothermometer of Putirka (2005).

MELTS modelling (Ghiorso & Sack, 1995) further constrains the liquidus temperature for the Moroccan samples. Representative samples from the four units yield liquidus temperatures of about 1180 to 1220 °C at 0·1 GPa, rising to 1250–1280 °C at 0·5 GPa and 1320–1350 °C at 0·9 GPa for dry conditions (Fig. 19). Slightly hydrous conditions (1 wt % H_2O) would decrease the liquidus temperature by about 60 °C. The liquidus temperatures provided by MELTS at pressures of 0·1 and 0·7 GPa are compared to the *P–T* estimates for the augites, based on Putirka's (1996) geothermobarometer. Assuming that the augites crystallized at temperature slightly lower than the liquidus temperature, dry to weakly hydrous conditions (e.g. 0–0·5 wt % H_2O) may be suggested for the Lower and Intermediate magmas. On the contrary, a slightly higher depth of crystallization and slightly more hydrous conditions (approximately 1·0 wt %) may be suggested for some Upper basalts in order to fit both their liquidus temperature calculated with MELTS and their calculated clinopyroxene crystallization temperatures. The high anorthite component in plagioclase from the Upper basalts may support relatively high water contents in these magmas. The hygrometer of Putirka (2005) indicates the presence of higher H_2O contents in Upper and Recurrent basalts compared to Intermediate basalts and Lower basaltic andesites. However, the water contents estimated using the Putirka (2005) hygrometer (*c.*2·0 wt % for Upper and Recurrent basalts; *c.*1·0–1·5 wt % for Intermediate and Lower samples) seem to be too high for the tholeiitic basalt compositions of the studied rocks. Moreover, these calculated water contents appear higher than those obtained with MELTS modelling.

Pairs of unexsolved Ti-magnetite and ilmenite microphenocrysts analysed in some Lower, Intermediate and Recurrent flows and one sill from Argana (geochemically similar to the Intermediate flows) yielded equilibrium temperatures ranging from about 1350 to 790 °C. The calculated oxygen fugacity values range from 10^{-8} to 10^{-16} bar, corresponding to slightly more reduced values than the QFM buffer (the highest T and fO_2 values refer to the Amelal sill from the Argana valley). Such relatively low fO_2 values are typical of low-Ti CAMP basalts in general (Marzoli *et al.*, 2018) as well as of other low-Ti LIP basalts (e.g. Melluso *et al.*, 1995).

Mineral trace element contents and calculated magmas

Mineral minor and trace element contents contribute to our interpretation of the genesis of the CAMP magmas in Morocco. The first observation is that augite and plagioclase have minor and trace element contents and trace element ratios that are generally consistent with the distinct whole-rock compositions of the four respective units. For example, Lower unit augites have

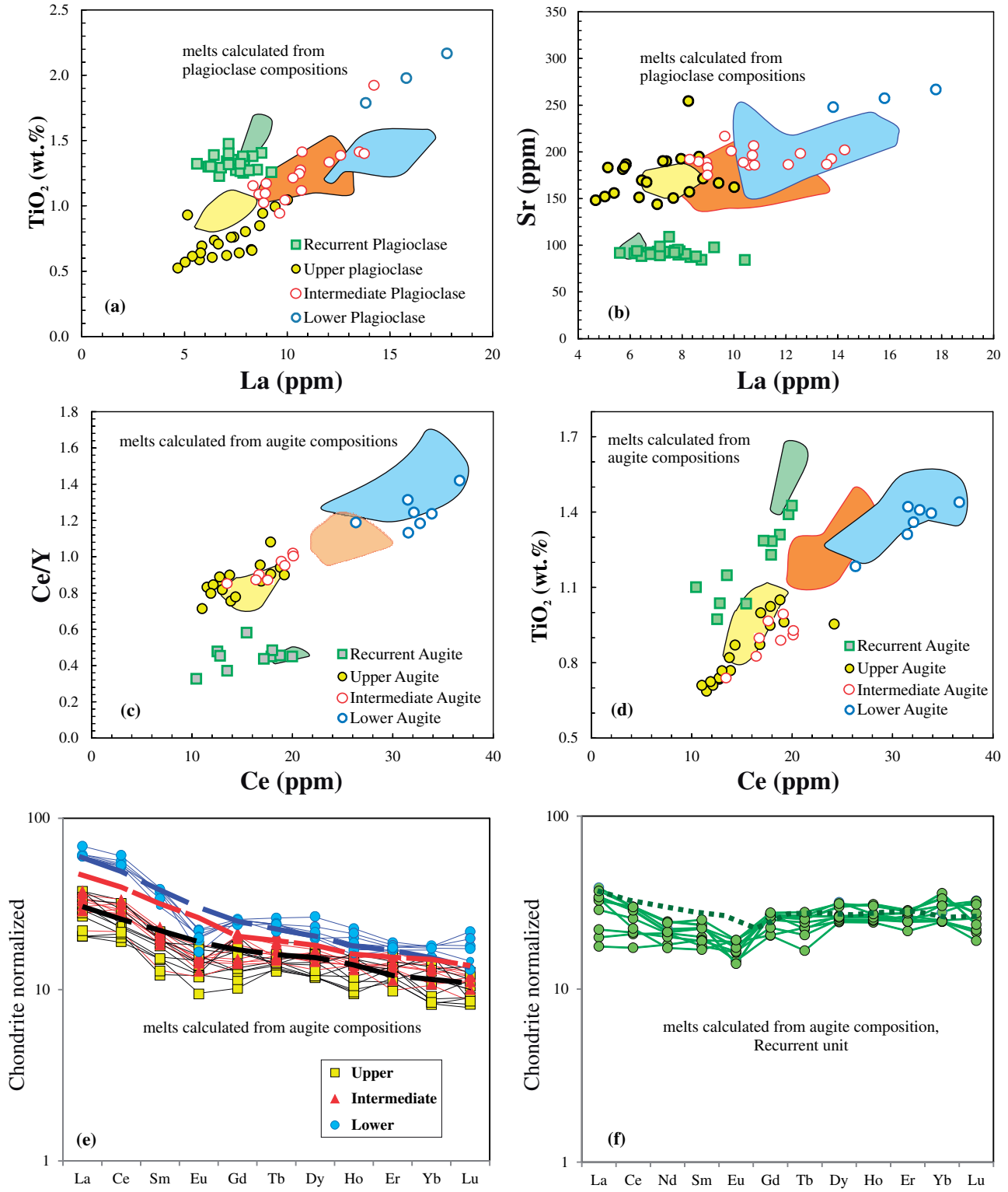

Fig. 20. Large symbols show melt compositions calculated from plagioclase (a, b) and augite (c–f) core compositions, LA-ICP-MS analyses. Blue circles, Lower sample data; red squares, Intermediate; yellow circles, Upper; green squares, Recurrent. Considered partition coefficients are reported in the Supplementary Data Table S9; supplementary data are available for downloading at http://www.petrology.oxfordjournals.org. Moroccan CAMP whole-rock compositions for each of the 4 lava units are shown by fields color-coded as in previous figures. (e, f) Chondrite normalized REE contents of melts calculated from augite compositions of Lower, Intermediate, Upper (e) and Recurrent augites (f). Chondrite values after McDonough & Sun (1995). Thick dashed lines in (e) and (f) represent average compositions for Lower (blue), Intermediate (red), Upper (black) and Recurrent (green) whole-rocks.

the highest La/Yb ratio, while this ratio is lowest in Recurrent basalt augites. Further systematic differences, consistent with whole-rock variations, are shown for example by Ba and Sr contents in plagioclase and by Ti and Zr in augite (see also Bertrand, 1991).

Compositions of equilibrium melts were calculated using the partition coefficients of Bédard (2014) and of Aigner-Torres *et al.* (2007) for augite and plagioclase, respectively (Fig. 20; Supplementary Data Table S9; supplementary data are available for downloading at http://www.petrology.oxfordjournals.org). Despite uncertainties related to the chosen partition coefficients, a quite good overlap of calculated melt and host whole-rock fields is obtained for REE data (LREE for plagioclase) or Ce/Y ratio, for example. The slightly more depleted calculated magma vs observed whole-rock compositions may be either due to the chosen partition coefficients or to the fact that the crystal cores analysed by LA-ICP-MS may have crystallized from slightly less evolved magmas compared to those represented by the whole-rocks. However, the trace element patterns and incompatible trace element ratios of the calculated melts generally overlap with the whole-rock compositions and display features typical of CAMP basalts. This is true, for example, for low TiO_2 contents and slightly enriched REE patterns (Fig. 20e).

In detail, however, some significant differences between the calculated melts and observed whole-rock compositions must be noted. First, REE patterns of melts calculated from augites of the Lower basaltic andesites and to a lesser extent those from Recurrent basalts and from a few Intermediate samples, exhibit Eu troughs (Fig. 20e and f). This suggests that plagioclase crystallized early in these magmas. Except for the Eu anomalies, REE patterns calculated from Recurrent unit augites are nearly flat (Fig. 20f), with chondrite normalized LREE/HREE ratios close to or below 1·0 (Ce/Yb_N = 0·7–1·2, mean 0·9), while the associated whole-rocks have slightly enriched LREE (Ce/Yb_N = 1·2–1·3).

A further notable difference between whole-rocks and melts calculated from augite compositions pertains to the Intermediate unit. Melts calculated from augite compositions from the Intermediate unit overlap with the compositions of Upper basalt whole-rocks, for example for REE contents and ratios (e.g. Ce/Yb and Ce contents) and for TiO_2 (Fig. 20), Sr and Zr contents (these latter elements are not shown in Fig. 20). In contrast, melts calculated from plagioclase from the same Intermediate rocks have enriched LREE and Sr compared to melts calculated from augites and overlap with Intermediate whole-rock compositions. This may suggest that the analysed augites of the Intermediate unit are in fact antecrysts or xenocrysts crystallized from magmas similar to the Upper basalts, pointing to an open-system evolution. On the contrary, the plagioclase crystallized as phenocrysts from the Intermediate unit-type melt.

Fractional crystallization at crustal depths

Whole-rock major and trace element variations within each group of lava flows, i.e. Lower, Intermediate, Upper and Recurrent basalts are relatively limited, hindering recognition of clear magma evolution trends. Recurrent basalts are slightly more evolved than Lower to Upper basalts, i.e. they have relatively low MgO contents. This is also confirmed by the negative anomalies of Sr and Ti, which argue for a significant plagioclase and oxide fractionation in the Recurrent basalts. Consistently, Recurrent basalts also yield lower crystallization temperatures based on augite, pigeonite and plagioclase geothermometers. Intrusive rocks display a slightly larger major element compositional range than the lava flows, but this may be related to mineral accumulation rather than to fractional crystallization.

Figure 11 shows liquid lines of descent calculated using MELTS (Ghiorso & Sack, 1995) from the same parental melt (Lower magma AN133) at distinct pressure conditions (0·1 and 0·9 GPa). Moreover, we also plotted the liquid line of descent at 1 GPa of a calculated primary liquid with a MgO content of about 15 wt %. The composition of this primary melt is calculated with the pMELTS software (Ghiorso *et al.*, 2002) for 8% partial melting of KLB1 peridotite (e.g. Hirose & Kushiro, 1993; Baker & Stolper, 1994) at 1·5 GPa. Redox conditions for the fractional crystallization models are set at the QFM buffer and initial water contents are 0·5 wt % for AN133 and 0·4 wt % for the calculated primary melt. Notably, water contents influence the temperature of saturation for plagioclase, while fO_2 influences the crystallization temperature of Fe–Ti-oxides. However, by varying these parameters in a reasonable manner, i.e. consistent with the mineral compositions, MELTS liquid lines of descent still do not reproduce the entire range of the Moroccan CAMP basalts and basaltic andesites, starting from a single parental magma (Fig. 11). In particular, the differences in SiO_2, TiO_2, CaO, Al_2O_3, P_2O_5 among the four units cannot be attributed to closed-system fractional crystallization processes, but require distinct parental magmas or open-system conditions, e.g. distinct crustal assimilation processes. Likewise, the systematic differences in incompatible element contents and ratios (e.g. La/Yb, Zr/Y; Fig. 12) among the four lava flow units cannot only be attributed to low-pressure, closed system differentiation involving crystallization of the observed mineral phases (clinopyroxene, plagioclase, olivine, Fe–Ti oxides). Notably, the distinct Sr, Nd and Pb isotope compositions of the four units formally exclude the possibility that they differentiated from the same parental magma under closed-system condititons.

Mass balance calculations have been performed to further constrain the fractionating mineral assemblage. The transition from a relatively little evolved (AN37) to a more evolved Lower basaltic andesite (AN66) would be consistent (sum of square residuals, $\sum R^2$ = 0·19) with

21 wt % fractionation of clinopyroxene (10 wt %), plagioclase (5 wt %), olivine (4 wt %) and magnetite (2 wt %). Likewise, an evolved Upper basalt (AN213) could be derived from a little evolved Upper basalt (AN725) by 45 wt % fractionation of clinopyroxene (31 wt %), plagioclase (10 wt %), olivine (2 wt %) and magnetite (2 wt %; $\sum R^2 = 0{\cdot}19$).

Open system differentiation

Interaction with the continental crust in the magmatic plumbing system is nearly inevitable in high magma flux systems and may significantly modify the compositions of evolving magmas, notably their isotopic ratios (e.g. Kerr *et al.*, 1995; Tegner *et al.*, 2005). Mineral and whole-rock data suggest differentiation of Moroccan CAMP magmas in mid to upper crustal magma chambers, as well as probably in deeper magma chambers where the primary mantle-derived magmas initially evolved. To develop a full understanding of the possible effects of assimilation of the local crust, we would need a complete geochemical data set representative of upper and lower crustal rocks. However, Pb and Os isotopic data are missing and Sr–Nd isotopic analyses are quite rare for the local lower crustal rocks.

The local basement was principally formed during three orogenic cycles, the Eburnean (*c.* 2·1 Ga), Pan-African (*c.* 0·6 Ga) and Hercynian events (*c.* 0·3 Ga). Pan-African granitic rocks from the Anti Atlas in southern Morocco (e.g. Toummite *et al.*, 2013) yield Sr and Nd isotopic ratios (calculated for 201 Ma) in the range 0·706–0·712 and 0·5122–0·5124, respectively, probably in the same range as most Hercynian rocks from the Meseta in central-northern Morocco (e.g. Chalot Prat, 1995). Eburnean felsic rocks cropping out in the Anti Atlas are both more evolved and older, yielding more extreme isotopic compositions ($^{87}Sr/^{86}Sr_{201Ma} > 0{\cdot}740$; $^{143}Nd/^{144}Nd_{201Ma}$ generally in the range 0·511–0·512; Ennih & Liégeois, 2008). Pb isotopic data for the local upper crust are not available, however Saharan dust has been analysed for Pb isotopes (Grousset & Biscaye (2005) and references therein) and such data will be used here as proxies for the upper crust (Table 5). Sr–Nd isotopic ratios of Middle Atlas granulitic xenoliths, entrained in Cenozoic–Quaternary alkali basalts, range from 0·705 to 0·718 and from 0·5121 to 0·5117, respectively (Moukadiri, 1999). These are the only available proxies for the composition of the lower crust. Since no Pb isotope data are available for these granulites and since world-wide granulites cover a very wide spectrum in Pb isotopic space (Meyzen *et al.*, 2005), we considered for the Moroccan granulites end-member compositions with either very low or very high Pb isotopic ratios ($^{206}Pb/^{204}Pb = 17$ or 19, respectively). Finally, Os isotopic values have been calculated considering estimated average upper and lower crustal values (Saal *et al.*, 1998; Peucker-Ehrenbrink & Jahn, 2001) and the distinct ages of the considered crustal contaminants. The considered crustal compositions are reported in Table 5.

EC-AFC modelling (Spera & Bohrson, 2001) starting from a composition similar to an Upper basalt, shows that crustal assimilation explains part but not all of the geochemical variations observed in the Moroccan CAMP basalts (Figs 12 and 16). In particular, variations within each unit, for example the Nd isotopic compositions of Lower and Intermediate basaltic andesites can be reproduced by quite small amounts of assimilation of upper crustal rocks (for example *c.*5–8% assimilation of the Eburnean granite). For such low degrees of assimilation of Eburnean granitic rocks, the shift of Sr, Nd and Pb isotopic ratios is moderate ($^{87}Sr/^{86}Sr$ from 0·7055 to 0·7065; $^{206}Pb/^{204}Pb$ from 18·20 to 18·51, $^{143}Nd/^{144}Nd$ from 0·5124 to 0·5122, respectively), consistent with the observed data. On the contrary, the Os isotopic ratio changes substantially (e.g. $^{187}Os/^{188}Os$ would change by about 0·03), though this range is speculative given that the Os composition of both the contaminant and the starting magma, as well as the Os partition coefficients, are poorly constrained. If the parental magma is assumed to have a $^{187}Os/^{188}Os$ ratio of 0·125, a highly plausible composition for a mantle-derived magma at 200 Ma, coupled with a $^{143}Nd/^{144}Nd$ ratio of 0·5124, calculated Os vs Nd isotopic variations due to assimilation of Eburnean granite are comparable to the observed variations displayed by the analysed Lower unit samples. Similar curves could be compatible with variations of most Upper and Intermediate samples, but only if a magma with very low $^{187}Os/^{188}Os$ ($\sim$0·110) is used as the starting composition (Fig. 17c), which seems extremely unlikely.

Assimilation of Pan-African granites would also be compatible with the observed Sr–Nd–Pb isotopic variations, but would require higher assimilation degrees (>15%). Assimilation of granulitic rocks with low $^{206}Pb/^{204}Pb$ (e.g. 17·5) does not reproduce the observed Pb isotopic variations, while assimilation of about 10% high $^{206}Pb/^{204}Pb$ (19.0) granulite could be consistent with the observed Sr–Nd–Pb isotopic data. In Nd–Os isotopic space, the calculated EC-AFC trends for granulite assimilation are not consistent with the observed data for variations within the Lower basaltic andesite group, but could explain the relatively high $^{187}Os/^{188}Os$ of one Intermediate and one Upper sample (Fig. 17c). It could perhaps also explain the relatively higher $^{187}Os/^{188}Os_{201Ma}$ of Lower vs two of the three Upper basalts. Nevertheless, caution should be used when interpreting the initial $^{187}Os/^{188}Os$ values of samples with highly radiogenic measured Os compositions as these require large age corrections. Such large corrections could be influenced by small perturbations in the measured $^{187}Re/^{188}Os$ ratios caused by minor geological alteration or non-recognized analytical factors. It is perhaps significant that the initial $^{187}Os/^{188}Os$ ratios of all samples with $^{187}Re/^{188}Os < 20$ are restricted to a fairly narrow range (0·1239 to 0·1307).

Table 5: Geochemical parameters used in EC-AFC modelling. La, Sm, Yb, Nb, Sr, Pb contents are given in ppm, Os in ppt

Crustal rock	La	Sm	Yb	Nb	Sr	$^{87}Sr/^{86}Sr$	Nd	$^{143}Nd/^{144}Nd$	Pb	$^{206}Pb/^{204}Pb$	$^{207}Pb/^{204}Pb$	Os	$^{187}Os/^{188}Os$
P.African granite	35 (0·05)	8·4 (0·06)	5 (0·25)	8 (0·01)	350 (1·5)	0·710	25 (0·25)	0·5120	5 (0·5)	18·8	15·7	30 (0·1)	0·8
Eburnean granite	50 (0·05)	9 (0·06)	4 (0·25)	9 (0·01)	170 (1·5)	0·740	40 (0·25)	0·5115	5 (0·5)	19·5	16·3	30 (0·1)	1·2
Granulite					250 (1·5)	0·717	10 (0·25)	0·5117	5 (0·5)	17·5/19		50 (0·1)	0·6
Initial Magma	6·5, *12* (0·06)	1·8, *2·6* (0·1)	1·83, *1·86* (0·28)	5 *10* (0·05)	200, *200* (1·5)	0·7055	10, *15* (0·25)	0·5124	2, *4* (0·5)	18·2	15·58	300, *300* (5)	0·110, *0·124*

Numbers in brackets refer to the considered partition coefficient. Data sources for Sr and Nd isotopic compositions of Pan-African and Eburnean granites and granulites: Toummite *et al.* (2013); Ennih & Liégeois (2008); Moukadiri (1999). Pb isotopic values for the upper crust were calculated from data reported in Grousset & Biscaye (2005). Os content and isotopic ratios of contaminants have been calculated following Saal *et al.* (1998) and Peucker-Ehrenbrink & Jahn (2001) for an age of 2 Ga and 0·6 Ga for Eburnean and Pan-African crust. The initial magma composition considered in EC-AFC modelling (last line of table) corresponds to an Upper basalt composition, except for trace element modelling (Fig. 12) and for Nd–Os isotopic modelling (Fig. 17), where the initial magma is similar to the Lower basalts (shown in italics in the Table). Magma partition coefficients in brackets (last line) have been calculated after Aigner-Torres *et al.* (2007) and Bédard (2014). For Os the same partition coefficients as those in previous studies on the CAMP (Callegaro *et al.*, 2013; Merle *et al.*, 2014) were used.

Variations of trace element contents and ratios are also partly reproduced by crustal assimilation models. This applies for example to La/Nb and La/Yb variations as shown in Fig. 12 g and h where it appears that part of the variability within the Lower unit and the variation from Upper to Intermediate samples can be attained by *c.*5–15% assimilation of Eburnean or Pan-African granite or *c.*10 % assimilation of granulite. Consistently, contamination of Upper basalts could lead to the slightly more evolved compositions (e.g. higher $^{87}Sr/^{86}Sr$ and $^{206}Pb/^{204}Pb$ and lower $^{143}Nd/^{144}Nd$) of the Intermediate basaltic andesites.

A common origin for the Upper and Intermediate magmas is also suggested by the similar trace element contents of equilibrium melt compositions calculated from clinopyroxenes from the two units, as opposed to the distinct compositions calculated from plagioclase crystals (Fig. 20). These mineral trace element data may constrain the timing of the crustal assimilation process, which possibly happened after crystallization of the clinopyroxene cores analysed by LA-ICP-MS and before crystallization of plagioclase crystals in the Intermediate magmas.

In further detail and considering the La/Nb variations (Fig. 12g), we suggest that distinct crustal contaminants may explain the slight difference between Central High Atlas (red circles, CHA samples) and Middle Atlas (red triangles, MM samples) Intermediate lavas. The latter yield in general higher La/Nb than the Central High Atlas samples and such a difference may suggest that the Middle Atlas Intermediate magmas were contaminated by a crustal rock with fairly high La/Nb, e.g. a rock similar to Eburnean granite (Ennih & Liégeois, 2008). On the contrary, the relatively low La/Nb of Central High Atlas Intermediate samples is indicative of contamination by a crustal rock with low La/Nb, like average lower crustal rocks (Rudnick & Gao, 2003) or Pan-African granite (Toummite *et al.*, 2013).

The ΔNb parameter (expressed as 1·74+log(Nb/Y) - 1·92 · log(Zr/Y); Fitton *et al.*, 1997) was originally proposed to distinguish between plume-related Icelandic and mid-ocean ridge basalts. In the case of continental LIPs, positive ΔNb values are typical of Nb undepleted mantle-derived basalts and have been related to mantle-plume activity, while negative ΔNb indicates either a Nb-depleted mantle source (e.g. DMM) or extensive crustal contamination. In Morocco, most Intermediate basaltic andesites yield negative ΔNb values, combined with relatively high La/Nb (Fig. 12i and j), the latter being a tracer for lithospheric input. On the contrary, most Lower and Upper basalts yield ΔNb values close to zero (Fig. 12j) combined with relatively low La/Nb, like those of basalts and picrites from the southern Karoo, which are considered as uncontaminated by the continental crust (e.g. Heinonen *et al.*, 2010, 2016; Ware *et al.*, 2018; Luttinen, 2018).

Recurrent basalts plot off any possible assimilation trend starting from a parental magma with Lower to Upper trace element and isotopic composition. Internal

variability within the Recurrent unit is negligible, in general, hampering any assimilation modelling. Nonetheless, some level of crustal contamination is still plausible for Recurrent basalts, as suggested in particular by the high $^{187}Os/^{188}Os_i$ of sample AN24, well above that of typical mantle-derived basalts. This sample yields a low Os (34 ppt) and strikingly high Re concentration (5502 ppt) and thus a quite large uncertainty on the Re/Os ratio, resulting in a very large uncertainty after error propagation on the calculated initial Os isotopic composition ($0{\cdot}453 \pm 0{\cdot}077$). Nevertheless, even taking the uncertainties into account, the initial Os isotopic composition of this sample is much more radiogenic than expected for any mantle-derived melt. Such a high Os isotopic ratio would suggest the assimilation of at least 22% of a granitic rock with $^{187}Os/^{188}Os = 1{\cdot}2$ and about 300 ppt Os content (an improbably high Os concentration for a granite), starting from a parental magma with $^{187}Os/^{188}Os_i$ of 0·130 and 300 ppt [Os]. Alternatively, and probably more realistically, the extremely high Re content of this sample may indicate assimilation of a sulfide phase, such as molybdenite, which would also be consistent with the high initial ratio. The other analysed Recurrent basalt, AN44, has a much lower $^{187}Os/^{188}Os_i$ ($0{\cdot}136 \pm 0{\cdot}017$), but due to its large uncertainty it is not possible to confirm or exclude a crustal contribution. The maximum $^{187}Os/^{188}Os_i$ of *c.*0·153 of this sample would require fairly low amounts of assimilation, i.e. about 8% assimilation of a highly-evolved granite ($^{187}Os/^{188}Os = 1{\cdot}2$) or 6% of a granulite (with $^{187}Os/^{188}Os = 0{\cdot}6$), starting from an initial magma with $^{187}Os/^{188}Os = 0{\cdot}124$. The apparent discrepancy in assimilation rate between the two Recurrent basalt samples are not compatible with their otherwise nearly indistinguishable major and trace element and Sr–Nd–Pb isotopic compositions. The most likely explanation is that radiogenic, Re-rich sulfide was added to AN24, either through assimilation or during a post-magmatic alteration event. Therefore, the sample with lower $^{187}Os/^{188}Os_i$ thus probably better constrains the upper limit of silicate rock assimilation of the Recurrent magmas.

Finally, we also attempted modelling the EC-AFC paths starting from a hypothetical primitive magma with fairly depleted, MORB-like characteristics (Fig. 16). The modelled magmas would reproduce the observed Sr–Nd–Pb isotopic compositions of the Moroccan CAMP basalts and basaltic andesites only through massive assimilation (>20%) of crustal rocks similar to the Pan-African granites (assimilation of Eburnean granites does not fit the data). However, such large amounts of assimilated granite combined with high amounts of fractional crystallization (the fractionated/assimilated mass would be in the range 0·6–0·9) would substantially modify the major and trace element compositions of the magmas, probably leading to the formation of quite high SiO_2 and MgO-poor magmas, unlike those observed. Moreover, the Os isotope compositions of heavily contaminated magmas are quite unlikely to be as low as those observed for our samples, even considering the large uncertainties related to the Re–Os systematics of the samples and of the crustal assimilates. Considering the same Os isotopic composition for the granitic assimilate as reported in Table 5, the $^{187}Os/^{188}Os$ ratio of 15–20% contaminated magmas would shift from 0·13 to over 0·20, i.e. to compositions higher than the measured (not age-corrected) $^{187}Os/^{188}Os$ of most Moroccan CAMP basalts.

To sum up, we suggest that low amounts of crustal assimilation (less than 10%) can explain the isotopic and trace element variations within single units. Even considering the uncertainties on the initial Os isotopic composition related to the high Re/Os of the analysed basalts and considering the lack of Re–Os data for the local crust, Os systematics rule out crustal assimilation significantly higher than 10% for most of the samples. This is consistent with detailed modelling of crustal assimilation for LIP basalts from other provinces (e.g. Karoo, Paranà; Heinonen *et al.*, 2010, 2016; De Min *et al.*, 2018). Such relatively low degrees of assimilation cannot account for most inter-unit chemical variations and exclude derivation of the Moroccan CAMP basalts from a single mantle source similar to those of Central Atlantic MORB. Nevertheless, EC-AFC modelling suggests that Intermediate magmas may be formed from contaminated parental Upper-like basalts.

Mantle source, major and trace element constraints

The data discussed so far indicate that subtle, but systematic differences exist among the four lava flow units and associated intrusive CAMP rocks from Morocco. As discussed before, these differences are in part explained by distinct amounts of fractional crystallization and crustal assimilation. In particular, crustal assimilation may partly explain the difference between the Upper and Intermediate rocks, the latter being more enriched and more contaminated, but nevertheless probably derived from a parental magma similar to that of the Upper basalts. On the contrary, the Lower and Recurrent basalts both have geochemical characteristics that are not compatible with their derivation from a parental magma equivalent to that of any other unit. Therefore, at least three distinct parental magma types (Lower, Upper, Recurrent) derived from somewhat distinct magma sources are required to explain the overall range of geochemical compositions.

None of the Moroccan CAMP samples can be considered as a primary mantle melt. Direct comparison with experimentally formed melts of possible mantle ultramafic or mafic source rocks is, therefore, not straightforward. In Fig. 11, we reported a liquid line of descent from a primary magma obtained from the peridotite KLB1 (Hirose & Kushiro, 1993; Baker & Stolper, 1994) at *c.*8% partial melting (primary melt composition calculated with pMELTS; Ghiorso *et al.*, 2002). This liquid line of descent reproduces the composition of the Upper

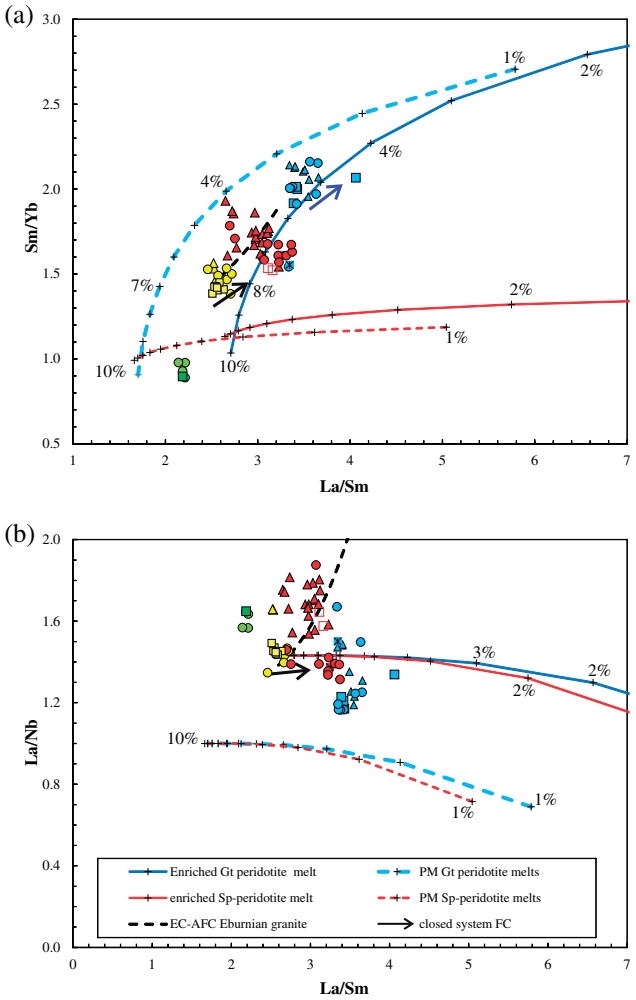

Fig. 21. Modelling of garnet and spinel peridotite non-modal equilibrium melting (from 1 to 10% shown by crosses) for (a) Sm/Yb vs La/Sm and (b) La/ Nb vs La/Sm. Considered parameters are as follows: modal mineral fractions in starting peridotite with primitive mantle or LREE-enriched relative REE abundances: olivine (ol) 0·58; orthopyroxene (opx) 0·24; clinopyroxene (cpx) 0·14 and spinel (sp) 0·04 in spinel peridotite; clinopyroxene 0·155 and garnet (grt) 0·025 in garnet peridotite. Melting coefficients: 0·05 (ol); 0·1 (opx); 0·5 (cpx); 0·35 (sp); 0·35 (grt). Starting REE contents (ppm): primitive peridotite (after McDonough & Sun, 1995): La = 0·65; Sm = 0·41; Yb = 0·44; Nb = 0·65 ppm; enriched peridotite is calculated by adding 2% of average upper crust (Rudnick & Gao, 2003) to the primitive mantle composition: La = 1·26; Sm = 0·5; Yb = 0·49; Nb = 0·88 ppm. Partition coefficients (McKenzie & O'Nions, 1991), La = 0·0004 (ol), 0·002 (opx), 0·05 (cpx), 0·01 (sp and grt); Sm = 0·001 (ol), 0·01 (opx), 0·26 (cpx), 0·01 (sp), 0·3 (grt); Yb = 0·005 (ol), 0·05 (opx), 0·28 (cpx), 0·01 (sp), 4 (grt); Nb = 0·005 (ol), 0·003 (opx), 0·004 (cpx), 0·001 (sp), 0·003 (grt). EC-AFC evolution black dashed line) starting from an Upper magma contaminated by a granite is shown as well (same parameters as in Fig. 12). The closed system FC (fractional crystallization) line represents 50% fractionation from a hypothetical parental Lower (blue arrow) or Upper (black arrow) magma and has been calculated assuming 40% augite and 10% plagioclase fractionation (partition coefficients from Aigner-Torres *et al.*, 2007; and Bédard, 2014).

basalts quite well. The relatively high Ca contents of the Upper basalts may reflect large melting degrees as suggested by experimental data for batch melting of spinel lherzolite (e.g. Hirose & Kushiro, 1993), which show that the highest Ca contents in peridotite melts are attained just before clinopyroxene exhaustion. By analogy, the high Al of the Upper basalts suggests that their melting occurred at temperatures lower than the complete melting (liquidus temperature) of the aluminiferous phase.

Lower basaltic andesites are relatively enriched in Si and depleted in Ca and Al compared to Upper basalts. These differences may reflect melting at lower degrees and a shallower depth of melting. However, a shallower melting depth for Lower vs Upper basalts is apparently not consistent with incompatible trace element modelling, which suggests a more significant garnet- vs spinel-peridotite signature for the Lower magmas (see below; Fig. 21). Alternatively, the Lower magmas may originate from hydrous peridotite, yielding melts richer in Si compared to anhydrous ones (e.g. Kushiro, 1996).

We calculated the REE and Nb contents of mantle melts generated by non-modal batch melting of spinel and garnet peridotites with a primitive-mantle or slightly enriched REE abundances, the latter being consistent with the enriched Sr–Nd isotopic compositions of the Moroccan CAMP (Fig. 21). The enriched peridotite composition is calculated by adding 2% of upper crust (average continental crust composition after Rudnick & Gao, 2003). Notably, the effects of closed-system fractional crystallization are quite small for the La/Sm and Sm/Yb ratios and in particular for La/Nb (fractional crystallization trends are shown by a solid black arrow in Fig. 21a). Therefore, measured values can be compared to calculated mantle melt compositions even if the samples are not primary (with the caveat that 'real' melting degrees are probably slightly higher than those apparent from direct comparison of calculated and measured trace element ratios in Fig. 21). However, crustal assimilation may induce a shift towards slightly higher La/Sm, and significantly higher Sm/Yb and La/Nb (dashed black curves in Fig. 21 are EC-AFC trends starting from an Upper basalt) as previously discussed (Fig. 12).

Taking into account open- or closed-system fractional crystallization, the trace element ratios of the basalts and basaltic andesites can be reproduced by various possible mantle melting models (see caption of Fig. 21 for details on the parameters used; the parameters are also reported in Supplementary Data Table S10; supplementary data are available for downloading at http://www.petrology.oxfordjournals.org). This modelling assumes a simple melting event occurring either in the presence of garnet or of spinel. We are aware that melting may occur over a relatively large depth range in a melting column, possibly starting within the garnet stability field and then achieving shallower depths where spinel is stable. The REE modelling we performed here is mainly intended to test if the CAMP magmas issued dominantly from the garnet or from the spinel stability depth. The relatively high LREE/HREE ratios of Lower to Upper basalts require the presence of residual garnet in their mantle source. Lower basaltic andesites would be consistent with about 3–4% melting of a garnet

peridotite with a primitive-mantle composition, or with 5–6% melting of a more fertile (enriched) garnet peridotite.

The Upper basalts yield generally lower La/Sm and Sm/Yb, pointing to a reduced garnet and more significant spinel signature. The Upper basalts could correspond to 8–9% melting of an enriched garnet peridotite or to *c.*7–8% melting of a primitive mantle peridotite. However, at such high melting degrees garnet would be entirely exhausted in the mantle source, not accounting for the high Al contents of the Upper basalts. This could suggest a significant contribution of a spinel peridotite source and the gap between observed and calculated compositions could be explained at least in part by fractional crystallization process (black arrow in Fig. 21a). This would suggest a shallower average melting region for the Upper basalts, possibly straddling the garnet-spinel transition. A progressively rising melting region would be consistent with CAMP magmatism occurring in an extensional tectonic regime leading to the observed progressive subsidence of the basins and probably to progressive thinning of the continental lithosphere (Labails *et al.*, 2010).

Recurrent basalts would require about 10% melting of a spinel peridotite source with primitive or even slightly depleted (not shown in the figure) REE abundances. We favour this latter hypothesis as it would be consistent with the slightly depleted Sr–Nd isotopic composition of the Recurrent basalts compared to the older magmas. We note also that melts calculated from augite compositions for the Recurrent basalts show REE patterns that resemble those of enriched MORB, highlighting the peculiar geochemical features of the Recurrent basalts within the CAMP.

Modelling of mantle melting also shows that the relatively low Nb and high La/Nb of the Moroccan CAMP basalts require a mantle source slightly enriched compared to the primitive mantle. As noted above, the enriched peridotite source shown in Fig. 21 was obtained by adding 2% upper continental crust (Rudnick & Gao, 2003) to a primitive mantle composition. Melts from such enriched peridotite fit the observed La/Nb compositions quite well. This suggests that the HFSE depletion characteristic of CAMP basalts (and of many LIP basalts, in general) can at least in part be explained by mantle source enrichment, i.e. by the presence of recycled crustal components within the mantle. Interestingly, the Moroccan CAMP basalts show ΔNb values close to zero (0·1 to -0·07; Fig. 12). Such values overlap those of MORB and of some virtually uncontaminated, primitive LIP basalts. In particular, picrites from the southern Karoo are interpreted as being derived from a subduction-influenced upper mantle (Luttinen, 2018) and plot quite close to the Moroccan basalts in terms of HFSE ratios (Fig. 12i and j). On the contrary, Atlantic OIB show significantly higher ΔNb compared to the Moroccan CAMP basalts, arguing against a common origin.

Mantle source, isotopic constraints

Moroccan CAMP samples have Sr-Nd-Pb isotopic compositions falling generally within the field of low-Ti basalts from throughout the huge aerial extent of the CAMP. The main characteristics of the CAMP rocks are relatively high $^{87}Sr/^{86}Sr$ and low $^{143}Nd/^{144}Nd$ values, combined with high $^{207}Pb/^{204}Pb$ and $^{208}Pb/^{204}Pb$ at only moderately high $^{206}Pb/^{204}Pb$ (i.e. they have high Δ7/4 and Δ8/4 as defined by Hart, 1984). These isotopic characteristics of the CAMP low-Ti basalts point to a common, enriched source which is different from those of central Atlantic MORB (local asthenosphere; e.g. Janney & Castillo, 2001) and from neighbouring OIB (e.g. Cabo Verde, Canary Islands; e.g. Holm *et al.*, 2006; Klügel *et al.*, 2017). Indeed, these oceanic basalts have compositions plotting along the NHRL (Northern Hemisphere Reference Line), whereas this is not the case for CAMP. Although, as previously discussed, some crustal assimilation en-route to the surface plausibly contributed to these enriched compositions, this process offers only a partial explanation. As shown for example in Fig. 16, EC-AFC trends starting from parental MORB compositions do indeed intersect the Sr–Nd–Pb isotopic values of the Moroccan CAMP basalts, but only for large degrees of assimilation (>20% assimilation of, e.g. Pan African granite). However, such high degrees of assimilation are not compatible with the unradiogenic Os isotopic compositions, with the relatively low incompatible trace element concentrations and with the basic composition of the CAMP samples. Therefore, the mantle source of CAMP magmas must have had an enriched signature.

The origin of this enriched component has been largely discussed in previous publications dealing with the North American and European regions of the CAMP (Puffer, 2001; Callegaro *et al.*, 2013, 2014a; Merle *et al.*, 2014; Whalen *et al.*, 2015; Shellnutt *et al.*, 2018) and the interpretation proposed therein probably applies to the Moroccan CAMP as well. Accordingly, involvement of lower and upper continental crustal materials subducted during the late Proterozoic or early Paleozoic (see Merle *et al.*, 2014) and stored below the Pangea mega-continent is modelled in Fig. 22. Unlike previous studies, we tried here to explore the possibility that the dominant mantle component is not represented by the DMM, but rather by a prevalent-mantle (PREMA-type mantle) similar to that defined in Jackson & Carlson (2011). This mantle source could be represented by the following isotopic compositions: $^{87}Sr/^{86}Sr = 0.7030$, $^{143}Nd/^{144}Nd = 0.5127$, $^{206}Pb/^{204}Pb = 18.0$ at 201 Ma (Zindler & Hart, 1986). As modelled in previous studies, only about 5% of recycled crustal materials with compositions similar to circum-Atlantic Late Proterozoic to Paleozoic crustal rocks are required to attain the enriched isotopic compositions of low-Ti CAMP basalts starting from the DMM (e.g. Callegaro *et al.*, 2013, 2014; Merle *et al.*, 2014). By contrast, because of its higher incompatible element abundances, the PREMA end-

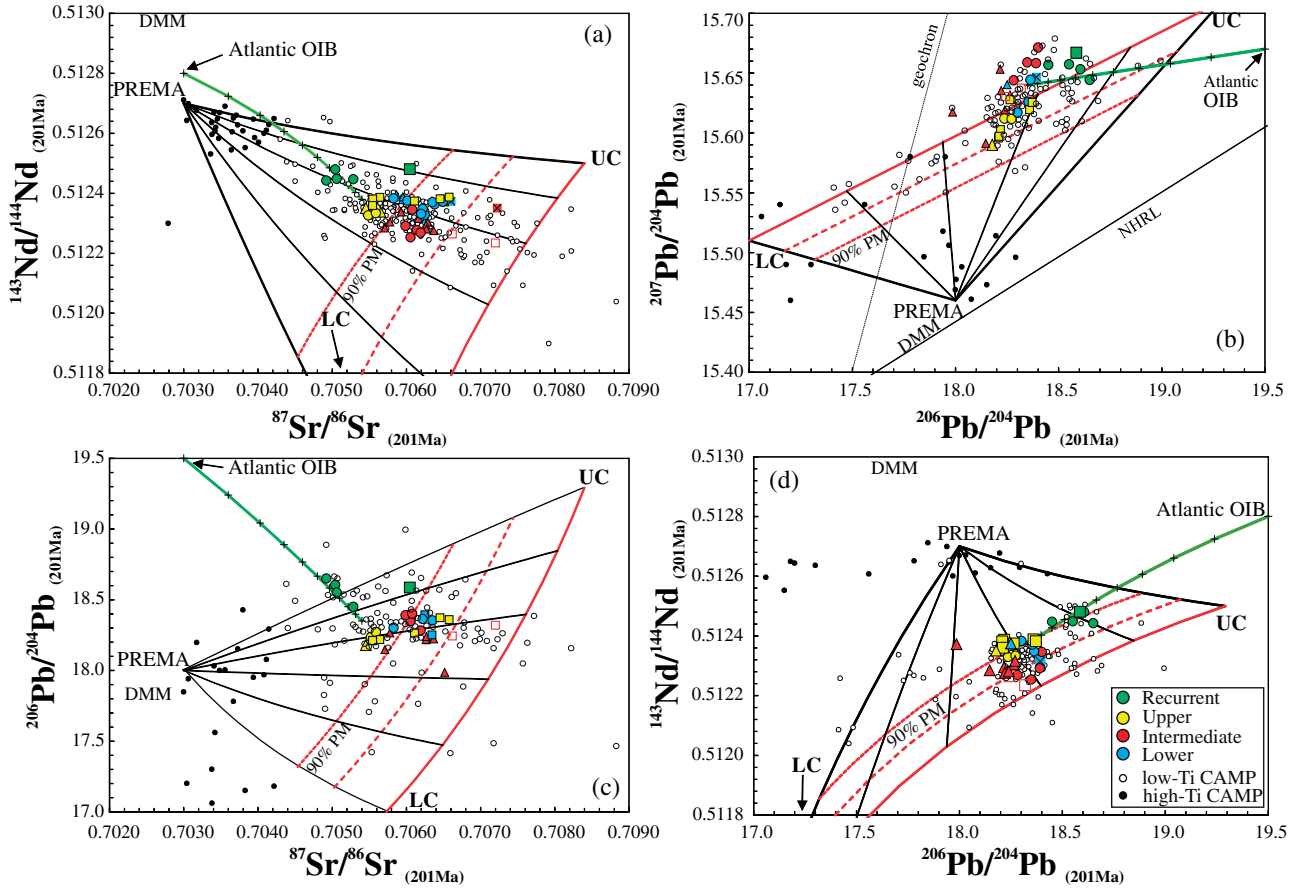

Fig. 22. Isotopic compositions of Moroccan CAMP basalts and basaltic andesites (same symbols as Fig. 16) compared to calculated compositions resulting from mixing of the PREMA (Prevalent Mantle; Zindler & Hart, 1986; Jackson & Carlson, 2011) with recycled upper and lower continental crust (UC and LC; Callegaro *et al.*, 2013). Red lines show 90% (dotted), 80% (dashed) and 0% (continuous) PREMA in the mixture; black lines show the UC/LC ratio (0, 20, 40, 60, 80, 100%) among crustal components. The green line is a mixing curve between the mantle source of the Upper basalts and an OIB mantle source similar to that of Atlantic OIB (e.g. Cape Verde, Canary Islands; Holm *et al.*, 2006; Klügel *et al.*, 2017). Tick marks (crosses) show 10% increments in the mixture. Compositions of the considered mantle components are reported in Supplementary Data Table S10; supplementary data are available for downloading at http://www.petrology.oxfordjournals.org.

member would require about 10% of such recycled crustal components to fit the observed composition of the Moroccan CAMP basalts. As shown for other LIPs (Jackson & Carlson, 2011), the PREMA end-member could represent 90% of the mantle source of the CAMP basalts (Fig. 22).

Isotopic compositions of Lower to Upper basalts are instead clearly different from any known OIB from the Central Atlantic (e.g. Cape Verde, Canary Islands; e.g. Holm *et al.*, 2006; Klügel *et al.*, 2017). Thus, any possible contribution from an Atlantic-type mantle-plume component is not supported by the very different and enriched geochemical composition of CAMP magmas. This is also consistent with trace element contents and ratios (e.g. Fig. 12i). Only the Recurrent basalts have relatively high $^{143}Nd/^{144}Nd$ (positive ε_{Nd}), relatively low $^{87}Sr/^{86}Sr$ and radiogenic Pb isotopes trending towards the composition of Atlantic OIB or of Moroccan alkaline and peridotitic rocks. In Fig. 22, we show a mixing curve between the possible mantle source of Moroccan Upper basalts (i.e. 93% PREMA plus 7% recycled crustal components) and a mantle similar to the source of Atlantic OIB, i.e. close to the C or FOZO component (Hanan & Graham, 1996). In this model, Recurrent basalts could issue from a source plotting along this mixing curve at about 20–30% of the Atlantic OIB (or C) component, while the remaining 70–80% would correspond to a mixture of PREMA (or DMM) plus recycled crustal rocks. However, it should be noted that Recurrent basalts are fairly evolved (MgO *c.*4 wt %) and possibly contaminated by the continental crust. This makes recognition of any mantle component quite problematic.

One peculiar characteristic of the Moroccan Lower to Upper magmas is their generally low Os isotopic composition (Fig. 17). In particular, some Upper and Intermediate samples yield among the lowest $^{187}Os/^{188}Os_{201Ma}$ of all CAMP rocks so far analysed and plot at lower values than the Primitive Upper Mantle (PUM; Meisel *et al.*, 2001), i.e. at lower values than most oceanic basalts or sub-lithospheric mantle components. As emphasized above, caution must be used when

interpreting these unradiogenic initial isotopic ratios because they are found only in samples for which a large correction for radiogenic ingrowth was necessary and other samples with similar corrections show surprisingly high initial $^{187}Os/^{188}Os$. Nevertheless, if taken at face value, the low $^{187}Os/^{188}Os_{201Ma}$ of several of the Moroccan CAMP basalts are comparable to those of Middle Atlas mantle xenoliths ($^{187}Os/^{188}Os_{201Ma}$ = 0·116–0·126; Wittig *et al.*, 2010a), of the nearby peridotite massifs of Beni Bousera and Ronda (*c.*0·11–0·125; Reisberg *et al.*, 1991, Reisberg & Lorand, 1995; Pearson & Nowell, 2004) and in general, of worldwide cratonic ($^{187}Os/^{188}Os$ about 0·105–0. ·125) and off-cratonic Subcontinental Lithospheric Mantle (SCLM) (about 0·115–0·135; Carlson, 2005). This might support a contribution from the local SCLM to the source of the Moroccan CAMP basalts. However, Moroccan mantle xenoliths as well as alkaline and ultra-alkaline rocks that possibly issued from this SCLM (e.g. carbonatites and lamproites; Wagner *et al.*, 2003; Bouabdellah *et al.*, 2010; Wittig *et al.*, 2010b; Bosch *et al.*, 2014) have Sr–Nd–Pb isotopic compositions distinct from CAMP and similar instead to compositions of OIB from the Cape Verde or the Canary Islands (Holm *et al.*, 2006; Klügel *et al.*, 2017). An apparent decoupling between lithophile element isotopes, yielding a signature distinct from the Moroccan lithospheric mantle xenoliths and Os isotopes, showing a significant SCLM signature is thus observed. This may be explained by the fact that, relative to abundances in typical mafic magmas, Os concentrations are high in the SCLM, while Sr, Nd and Pb concentrations are low, favouring perturbation of the Os isotope compositions of the magmas relative to those of the lithophile elements during passage of the asthenosphere-derived melts through the lithosphere. Alternatively, a selective assimilation process (Heinonen *et al.*, 2016) could be proposed. In this scenario, melts percolating through the relatively refractory and depleted SCLM are contaminated by Os-rich and low $^{187}Os/^{188}Os$ material, possibly sulfides stored within the cratonic SCLM (cf. Guex *et al.*, 2016). According to Guex *et al.* (2016) sulfides or sulphur-rich veins may remain stable at the base of the lithosphere during continental thinning, assuming that heat transfer from the asthenospheric mantle is low and the temperature within the SCLM does not exceed the sulfide solidus ($>$ 1200 °C at pressure $>$ 2 GPa for monosulfide solid solution; Bockrath *et al.*, 2004). Only enhanced thermal erosion and thinning of the SCLM may lead to melting and assimilation of the sulfides by the relatively hot, tholeiitic CAMP melts on their way to the surface. The contamination by old sulphides with low $^{187}Os/^{188}Os$ seems to increase from Lower to Upper basalts, possibly as a consequence of progressively increased heating, erosion and thinning of the SCLM, as the mantle upwelling rises. Moreover, it should be considered that the most refractory and isotopically depleted sulphides in the SCLM may be those entrained within silicate minerals, while interstitial sulfides may have less depleted Os isotopic signatures and can melt more readily (Harvey *et al.*, 2011).

A MODEL FOR THE GENESIS OF THE MOROCCAN CAMP

The main phase of CAMP magmatism occurred between 201·6 and 201·3 Ma. High volumes of Lower and Intermediate basaltic andesites erupted close to 201·5 Ma, while only minor volumes of Recurrent basalts erupted slightly later and were restricted to the Central High Atlas basins. CAMP basaltic or basaltic andesitic magmas of the main phase were emplaced throughout Morocco in a series of 4–5 main pulses. Such pulses were probably of short duration, with eruption rates exceeding that of any present-day volcanic district and in line instead with the eruption rates (10–100 km^3/yr) calculated from other continental flood basalt piles related to LIP activity. The pulsed eruption mechanism and high eruption rates reinforce the possibility that CAMP magmatism triggered end-Triassic climate change and mass extinction. The pulsed mechanism requires a rapid tapping of the magmatic plumbing system, which is likely to be associated with volatile fluxing from the magmatic plumbing system (Caricchi *et al.*, 2018) and may have caused widespread and intense seismicity. Notably, end-Triassic sedimentary strata with the abundant presence of seismites have been recently discovered in northern Europe and linked to CAMP volcanism and tectonism (Lindström *et al.*, 2015).

The magmatic activity was syn-extensional, with lava flows emplaced in progressively subsiding grabens (Fig. 23). Sills and feeder dykes crop out mainly in the Paleozoic basin of the Anti Atlas and yield geochemical compositions comparable to Intermediate, Upper and Recurrent flows, while only one sill and one dyke sample from central-western Morocco yielded compositions similar to Lower flows.

Volcanic sequences from throughout the country show similar time-related evolution, with generally abrupt compositional shifts among the four magmatic units (Lower to Recurrent). Some of the magmas were contaminated by the continental crust in shallow-level AFC processes, as suggested by the isotopic systematics and by augite trace element contents. According to this interpretation, Intermediate magmas were derived from parental melts similar to Upper basalts, but experienced more contamination, while Lower basaltic andesites evolved from a distinct, more enriched parental magma without significant amounts of crustal contamination. The highest rates of assimilation during the middle and main phase of volcanism (Intermediate unit for which distinct crustal contaminants are required in the Central High Atlas and in the Middle Atlas, respectively) may be related to a progressive heating of the crust intruded by the rising magmas. The lack of significant contamination for the Upper basalts may be due to a reduced magma flux, to a reduced fertility of

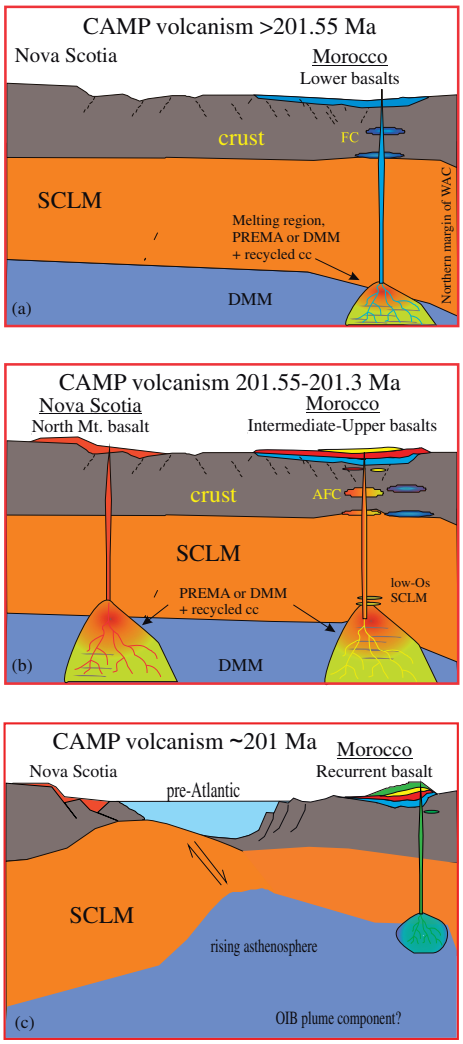

Fig. 23. Sketch of the formation of CAMP basalts from the latest Triassic (*c.*201·6 Ma) to earliest Jurassic (*c.*201 Ma). (a) Production of Lower basalts occurs dominantly at depths corresponding to the garnet stability field, i.e. >60 km. Such conditions may be attained at the northern margin of the West African Craton (WAC), where the SCLM may be relatively thick. The melting region is composed of enriched components possibly represented by recycled crustal material, while the depleted component may be of DMM or PREMA type. Shallow-level differentiation largely occurs as a closed-system fractional crystallization process (FC). During this earliest stage, CAMP magmatism seems to be confined to the African continent only, as suggested also by geochronologic data (Marzoli *et al.*, 2004; Blackburn *et al.*, 2013; Davies *et al.*, 2017). (b) At *c.*201·5 Ma, after eruption of the Lower basalts, CAMP magmatism affects the entire CAMP. In Morocco, erupted magmas belong to the Intermediate and Upper units fill the volcanosedimentary basins (grabens) formed during the extensional phase. The formation of subvolcanic bodies (sills and dykes) in the shallow crust is most active in this phase. Melting occurs at generally shallower depth, straddling the garnet–spinel stability field. Enriched components within the melting region are slightly more diluted than during generation of the Lower basalts. Contamination by low-$^{187}Os/^{186}Os$ components (sulphides?) may occur within the SCLM, while crustal assimilation (AFC) in shallow (mid-crustal) magma chambers affects Intermediate magmas in particular. (c) During the earliest Jurassic, Recurrent-type magmatism occurs in Morocco as well as in the U.S.A. Newark basins (not shown). These magmas issue from an even shallower depth and from a mantle source with slightly different geochemical composition.

the crustal rocks, or to armouring of the conduit systems.

The presence of at least three parental magma types is required, i.e. Lower, Upper and Recurrent. The melting mantle source of the Moroccan CAMP becomes progressively shallower from Lower to Recurrent basalts (Fig. 23). While a significant contribution from a garnet peridotite source is required to account for the geochemical features of the Lower magmas, Upper magmas likely issued from a mantle zone straddling the garnet-spinel transition and Recurrent basalts may result from melting of a prevailing spinel peridotite source. Such evolution is consistent with formation of the CAMP during progressive extension and consequent lithospheric thinning.

The four magmatic units share a common enriched isotopic and trace element signature similar to that of most other low-Ti CAMP basalts from throughout the province. This enriched signature might result from mixing between a dominant DMM- or PREMA-type mantle with subducted and recycled continental material, in accordance with many previous studies on the CAMP (see Callegaro *et al.*, 2013, 2014a; Merle *et al.*, 2014; Whalen *et al.*, 2015; Shellnutt *et al.*, 2018, for the most recent studies). However, each of the four Moroccan units also displays peculiar features. Lower unit magmas are slightly enriched compared to the Upper basalts in terms of their trace element contents and ratios as well as in Sr–Nd–Pb isotopic compositions. An enriched source is proposed for this magmatic unit. Notably, among all the CAMP relics, other rocks with geochemical compositions similar to those of the Moroccan Lower basaltic andesites (rocks forming the Tiourjdal group; Marzoli *et al.*, 2018) are only known from a relatively restricted area in northwestern Africa at the northern margin of the West African craton (Morocco, Algeria and Mali; Verati *et al.*, 2005; Chabou *et al.*, 2010; Marzoli *et al.*, 2018). Our hypothesis is that the Tiourjdal group magmas (including the Moroccan Lower unit) are probably the CAMP basalts with the strongest garnet-peridotite signature. They are produced by relatively low degree partial melting of a source in which the recycled component plays a more important role. This scenario would justify the enriched incompatible trace element contents and ratios of this magmatic group as well as their slightly more enriched Sr and Pb isotopic composition compared to the Upper basalts. The deeper melting region of the Tiourjdal group basalts may be possibly related to their location close to the West African Craton (Figs 1 and 23), where the lithosphere was thicker at least during the early stages of CAMP magmatism (cf. also Tegner *et al.*, in press).

Several Upper and Intermediate basalts, which probably derive from common parental magmas, are characterized by fairly low initial Os isotopic compositions. Despite the large corrections applied for radiogenic ingrowth, these data may point to the involvement of an old, possibly cratonic SCLM component. While

wholesale melting of such probably refractory and depleted mantle rocks is unlikely and not supported by the isotopic and trace element compositions of CAMP basalts, we envisage that only the Os isotopic system might fingerprint the cratonic SCLM signature, possibly due to assimilation of sulfides or sulfur-rich veins present locally along the margin of the West African craton.

Only the late and volumetrically minor Recurrent basalts yield compositions that might support involvement of a mantle component tapped also by Atlantic OIB. This is suggested by REE patterns and concentrations for Recurrent basalts and their augites, similar to those of enriched-MORB, as well as by Sr–Nd–Pb isotopic compositions distinct from those of other Moroccan CAMP rocks and trending towards a C or FOZO-type composition. A rapid decline of the magmatic activity after emplacement of the Upper and then of the Recurrent unit would be consistent with an exhaustion of the fertile components within the mantle-source, as suggested by Puffer (2003).

ACKNOWLEDGMENTS

D. Pasqual and R. Carampin (Padova) provided technical assistance during X-ray fluorescence and electron microprobe analyses, while C. Zimmermann aided with the Re-Os analyses. Valuable help during field-work was provided by C. Rapaille, K. Allenbach, R. Neuwrth, R. Martini, L. Zaninetti, S. Nomade, K. Knight, C. Verati, A.M Fioretti, H. Ibouh. K. Knight kindly provided TEL, OL and TJ samples, originally collected for magnetostratigraphy. John Puffer, Jussi Heinonen and Leo Melluso and the editor Simon Turner are thanked for detailed and constructive reviews.

SUPPLEMENTARY DATA

Supplementary data are available at *Journal of Petrology* online.

FUNDING

We acknowledge financial support from CARIPARO (Eccellenza-2008), PRIN (PRIN 20178LPCP), Padova University (CPDA132295/13) to A.M; CNRi (Italy)-CNRST (Morocco) to A.M and N.Y.; PICS CNRS (France)-CNRST (Morocco) to H.B. and N.Y.

REFERENCES

Abouchami, W., Boher, M., Michard, A. & Albarede, F. (1990). A major 2.1 Ga event of mafic magmatism in West Africa: An early stage of crustal accretion. *Journal of Geophysical Research* **95**, 17605–17629.

Aigner-Torres, M., Blundy, J., Ulmer, P. & Pettke, T. (2007). Laser Ablation ICPMS study of trace element partitioning between plagioclase and basaltic melts: An experimental approach. *Contributions to Mineralogy and Petrology* **153**, 647–667.

Alibert, C. (1985). A Sr-Nd isotope and REE study of Late Triassic dolerites from the Pyrenees (France) and the Messejana Dyke (Spain and Portugal). *Earth and Planetary Science Letters* **73**, 81–90.

Baker, M. B. & Stolper, E. M. (1994). Determining the composition of high-pressure mantle melts using diamond aggregates. *Geochimica et Cosmochimica Acta* **58**, 2811–2827.

Barrat, J. A., Keller, F., Amossé, J., Taylor, R. N., Nesbitt, R. W. & Hirata, T. (1996). Determination of rare earth elements in sixteen silicate reference samples by ICP-MS after TM addition and ion exchange separation. *Geostandards and Geoanalytical Research* **20**, 133–139.

Baudin, T., Chévremont, P., Razin, P., Youbi, N. Andries, D., Hoepffner, C., Thiéblemont, D., Chihani, E. & Tegyey, M. (2003). Carte géologique du Maroc au 1/50 000, feuille de Skhour des Rehamna. Mémoire explicatif. *Notes Mémoires Service Géolgique du Maroc* **435 bis**, 114.

Bédard, J. H. (2014). Parameterizations of calcic clinopyroxene-melt trace element partition coefficients. *Geochemistry, Geophysics, Geosystems* **15**, 303–336.

Béguelin, P., Chiaradia, M., Beate, B. & Spikings, R. (2015). The Yanaurcu volcano (Western Cordillera, Ecuador): A field, petrographic, geochemical, isotopic and geochronological study. *Lithos* **218–219**, 37–53.

Bensalah, M. K., Youbi, N., Mahmoudi, A., Bertrand, H., Mata, J., El Hachimi, H., Madeira, J., Martins, L., Marzoli, A., Bellon, H., Medina, F., Karroum, M., Karroum, L. A. & Ben Abbou, M. (2011). The Central Atlantic Magmatic Province (CAMP) volcanic sequences of Berrechid and Doukkala basins (Western Meseta, Morocco): Volcanology and geochemistry. *Comunicações Geológicas* **98**, 15–27.

Bensalah, M. K., Youbi, N., Mata, J., Madeira, J., Martins, L., El Hachimi, H., Bertrand, H., Marzoli, A., Bellieni, G., Doblas, M., Font, E., Medina, F., Mahmoudi, A., Beraâouz, E. H., Miranda, R., Verati, C., De Min, A., Ben Abbou, M. & Zayane, R. (2013). The Jurassic–Cretaceous basaltic magmatism of the Oued El-Abid syncline (High Atlas, Morocco): Physical volcanology, geochemistry and geodynamic implications. *Journal of African Earth Sciences* **81**, 60–81.

Berger, J., Liégeois, J. -P., Ennih, N. & Bonin, B. (2010). Flow of Canary mantle plume material through a subcontinental lithospheric corridor beneath Africa to the Mediterranean: Comment. *Geology* **38**, e202.

Berger, J., Ennih, N. & Liégeois, J. -P. (2014). Extreme trace elements fractionation in Cenozoic nephelinites and phonolites from the Moroccan Anti-Atlas (Eastern Saghro). *Lithos* **210–211**, 69–88.

Bertrand, H. (1991). The Mesozoic tholeiitic Province of Northwest Africa: A volcanotectonic record of the early opening of central Atlantic. In: Kampunzu, A. B. & Lulaba, R. T. (eds) *Magmatism in Extensional Settings: The Phanerozoic African Plate*. Berlin, Heidelberg: Springer, pp. 147–188.

Bertrand, H., Dostal, J. & Dupuy, C. (1982). Geochemistry of early Mesozoic tholeiites from Morocco. *Earth and Planetary Science Letters* **58**, 225–239.

Bertrand, H., Fornari, M., Marzoli, A., García-Duarte, R. & Sempere, T. (2014). The Central Atlantic Magmatic Province extends into Bolivia. *Lithos* **188**, 33–43.

Blackburn, T. J., Olsen, P. E., Bowring, S. A., Mclean, N. M., Kent, D. V., Puffer, J., McHone, G., Rasbury, E. T. & Et-Touhami, M. (2013). Zircon U–Pb geochronology links the end-triassic extinction with the central Atlantic Magmatic Province. *Science* **340**, 941–945.

Bockrath, C., Ballhaus, C. & Holzheid, A. (2004). Fractionation of the platinum-group elements during mantle melting. *Science* **305**, 1951–1953.

Boehnke, P., Watson, E. B., Trail, D., Harrison, T. M. & Schmitt, A. K. (2013). Zircon saturation re-revisited. *Chemical Geology* **351**, 324–334.

Bosch, D., Maury, R. C., El Azzouzi, M., Bollinger, C., Bellon, H. & Verdoux, P. (2014). Lithospheric origin for Neogene–Quaternary Middle Atlas lavas (Morocco): Clues from trace elements and Sr–Nd–Pb–Hf isotopes. *Lithos* **205**, 247–265.

Bouabdellah, M., Hoernle, K., Kchit, A., Duggen, S., Hauff, F., Klügel, A., Lowry, D. E. & Beaudoin, G. (2010). Petrogenesis of the Eocene Tamazert continental carbonatites (Central High Atlas, Morocco): Implications for a common source for the Tamazert and Canary and Cape Verde Island carbonatites. *Journal of Petrology* **51**, 1655–1686.

Bouiflane, M., Manar, A., Medina, F., Youbi, N. & Rimi, A. (2017). Mapping and characterization from aeromagnetic data of the Foum Zguid dolerite Dyke (Anti-Atlas, Morocco) a member of the Central Atlantic Magmatic Province (CAMP). *Tectonophysics* **708**, 15–27.

Brophy, J. G., Whittington, C. S. & Park, Y. R. (1999). Sector-zoned augite megacrysts in Aleutian high alumina basalts: Implications for the conditions of basalt crystallization and the generation of calc-alkaline series magmas. *Contributions to Mineralogy and Petrology* **135**, 277–290.

Burov, E. & Gerya, T. (2014). Asymmetric three–dimensional topography over mantle plumes. *Nature* **513**, 85–89.

Callegaro, S., Baker, D. R., De Min, A., Marzoli, A., Geraki, K., Bertrand, H., Viti, C. & Nestola, F. (2014b). Microanalyses link sulfur from large igneous provinces and Mesozoic mass extinctions. *Geology* **42**, 895–898.

Callegaro, S., Marzoli, A., Bertrand, H., Blichert-Toft, J., Reisberg, L., Cavazzini, G., Jourdan, F., Davies, J. F. H. L., Parisio, L., Bouchet, R., Paul, A., Schaltegger, U. & Chiaradia, M. (2017). Geochemical constraints provided by the Freetown Layered Complex (Sierra Leone) on the origin of high-ti tholeiitic CAMP magmas. *Journal of Petrology* **58**, 1811–1840.

Callegaro, S., Marzoli, A., Bertrand, H., Chiaradia, M., Reisberg, L., Meyzen, C., Bellieni, G., Weems, R. E. & Merle, R. (2013). Upper and lower crust recycling in the source of CAMP basaltic dykes from southeastern North America. *Earth and Planetary Science Letters* **376**, 186–199.

Callegaro, S., Rapaille, C., Marzoli, A., Bertrand, H., Chiaradia, M., Reisberg, L., Bellieni, G., Martins, L., Madeira, J., Mata, J., Youbi, N., De Min, A., Azevedo, M. R. & Bensalah, M. K. (2014a). Enriched mantle source for the Central Atlantic Magmatic Province: New supporting evidence from Southwestern Europe. *Lithos* **188**, 15–32.

Caricchi, L., Sheldrake, T. E. & Blundy, J. (2018). Modulation of magmatic processes by CO_2 flushing. *Earth and Planetary Science Letters* **491**, 160–171.

Carlson, R. W. (2005). Application of the Pt–Re–Os isotopic systems to mantle geochemistry and geochronology. *Lithos* **82**, 249–272.

Cebriá, J. M., López-Ruiz, J., Doblas, M., Martíns, L. T. & Munha, J. (2003). Geochemistry of the Early Jurassic Messejana-Plasencia dyke (Portugal-Spain); Implications on the origin of the Central Atlantic Magmatic Province. *Journal of Petrology* **44**, 547–568.

Chabou, M. C., Bertrand, H. & Sebaï, A. (2010). Geochemistry of the Central Atlantic Magmatic 774 Province (CAMP) in south-western Algeria. *Journal of African Earth Sciences* **58**, 211–219.

Chalokwu, C. I. (2001). Petrology of the Freetown layered complex, Sierra Leone: Part II. Magma evolution and crystallisation conditions. *Journal of African Earth Science* **32**, 519–540.

Chalot Prat, F. (1995). Genesis of rhyolitic ignimbrites and lavas from distinct sources at a deep crustal level: Field, petrographic, chemical and isotopic (Sr, Nd) constraints in the Tazekka volcanic complex (Eastern Morocco). *Lithos* **36**, 29–49.

Chiaradia, M., Müntener, O. & Beate, B. (2011). Enriched basaltic andesites from mid-crustal fractional crystallization, recharge and assimilation (Pilavo volcano, western Cordillera of Ecuador). *Journal of Petrology* **52**, 1107–1141.

Coltice, N., Phillips, B. R., Bertrand, H., Ricard, Y. & Rey, P. (2007). Global warming of the mantle at the origin of flood basalts over supercontinents. *Geology* **35**, 391–394.

Courtinat, B. & Algouti, A. (1985). Caractérisation probable du Sinémurien près de Telouet (Haut Atlas, Maroc). Datation palynologique. *Geobios* **18**, 857–864.

Cox, K. G. (1980). A model for flood basalt volcanism. *Journal of Petrology* **21**, 629–650.

Creaser, R. A., Papanastassiou, D. A. & Wasserburg, G. J. (1991). Negative thermal ionization mass-spectrometry of osmium, rhenium and iridium. *Geochimica et Cosmochimica Acta* **55**, 397–401.

Dal Corso, J., Marzoli, A., Tateo, F., Jenkyns, H. C., Bertrand, H., Youbi, N., Mahmoudi, A., Font, E., Buratti, N. & Cirilli, S. (2014). The dawn of CAMP volcanism and its bearing on the end-Triassic carbon cycle disruption. *Journal of the Geological Society of London* **171**, 153–164.

Davies, J., Marzoli, A., Bertrand, H., Youbi, N., Ernesto, M. & Schaltegger, U. (2017). End-Triassic mass extinction started by intrusive CAMP activity. *Nature Communications* DOI 10.1038/NCOMMS15596.

Deckart, K., Bertrand, H. & Liégeois, J.-P. (2005). Geochemistry and Sr, Nd, Pb isotopic composition of the Central Atlantic magmatic Province (CAMP) in Guyana and Guinea. *Lithos* **82**, 289–314.

Deenen, M. H. L., Ruhl, M., Bonis, N. R., Krijgsman, W., Kuerschner, W. N., Reitsma, M. & van Bergen, M. J. (2010). A new chronology for the end-Triassic mass extinction. *Earth and Planetary Science Letters* **291**, 113–125.

De Min, A., Callegaro, S., Marzoli, A., Nardy, A. J., Chiaradia, M., Marques, L. S. & Gabbarrini, I. (2018). Insights into the petrogenesis of low- and high-Ti basalts: Stratigraphy and geochemistry of four lava sequences from the central Paraná basin. *Journal of Volcanology and Geothermal Research* **355**, 232–252.

De Min, A., Piccirillo, E. M., Marzoli, A., Bellieni, G., Renne, P. R., Ernesto, M. & Marques, L. S. (2003). The Central Atlantic Magmatic Province (CAMP) in Brazil: Petrology, geochemistry, $^{40}Ar/^{39}Ar$ ages, paleomagnetism and geodynamic implications. In: Hames, W., McHone, G., Renne, P.R. & Ruppel, C. (eds) *AGU- Geophysical Monograph 136, The Central Atlantic Magmatic Province*. American Geophysical Union Monograph **136**, pp. 91–128.

Dinesen Petersen, K., Schiffer, C. & Nagel, T. (2018). LIP formation and protracted lower mantle upwelling induced by rifting and delamination. *Scientific Reports* **8**, 16578.

Dorais, M. J. & Tubrett, M. (2008). Identification of a subduction zone component in the Higganum dyke, Central Atlantic Magma Province: A LA-ICPMS study of clinopyroxene with implications for flood basalt petrogenesis. *Geochemistry, Geophysics, Geosystems* **9**, 1–13. http://dx.doi.org/10.1029/2008GC002079.

Dostal, J., Keppie, J. D., Hamilton, M. A., Aarab, E. M., Lefort, J. P. & Murphy, J. B. (2005). Crustal xenoliths in Triassic lamprophyre dykes in western Morocco: Tectonic implications for Rheic Ocean suture. *Geological Magazine* **142**, 159–172.

Duggen, S., Hoernle, K. A., Hauff, F., Klugel, A., Bouabdellah, M. & Thirlwall, M. F. (2009). Flow of Canary mantle plume material through a subcontinental lithospheric corridor beneath Africa to the Mediterranean. *Geology* **37**, 283–286.

Dupuy, C., Marsh, J., Dostal, J., Michard, A. & Testa, S. (1988). Asthenospheric sources for Mesozoic dolerites from Liberia (Africa): Trace element and isotopic evidence. *Earth and Planetary Science Letters* **87**, 100–110.

El Azzouzi, M., Maury, R. C., Bellon, H., Youbi, N., Cotten, J. & Kharbouch, F. (2010). Petrology and K–Ar chronology of the Neogene–Quaternary Middle Atlas basaltic province, Morocco. *Bulletin de la Societe Geologique de France* **181**, 243–257.

Elkins-Tanton, L. T. (2005). Continental magmatism caused by lithospheric delamination. *Geological Society of America Special Papers* **388**, 449–461.

Ennih, N. & Liégeois, J.-P. (2001). The Moroccan Anti-Atlas: The West African craton passive margin with limited Pan-African activity. *Implications for the Northern Limit of the Craton. Precambrian Research* **112**, 291–304.

Ennih, N. & Liégeois, J.-P. (2008). The Boundaries of the West African Craton, with special reference to the basement of the Moroccan Metacratonic anti-Atlas Belt. In: Ennih, N. & Liégeois, J.-P. (eds) *The Boundaries of the West African Craton. Geological Society, Vol.* **297**. London: Special Publication, pp. 1–17.

Fitton, J. G., Saunders, A. D., Norry, M. J., Hardarson, B. S. & Taylor, R. N. (1997). Thermal and chemical structure of the Iceland plume. *Earth and Planetary Science Letters* **153**, 197–208.

Font, E., Youbi, N., Fernandes, S., El Hachimi, H., Kratinova, Z. & Hamim, Y. (2011). Revisiting the magnetostratigraphy of the Central Atlantic Magmatic Province from Morocco. *Earth and Planetary Science Letters* **309**, 302–317.

Gasquet, D., Levresse, G., Cheilletz, A., Azizi-Samir, M. R. & Mouttaqi, A. (2005). Contribution to a geodynamic reconstruction of the Anti-Atlas (Morocco) during Pan-African times with the emphasis on inversion tectonics and metallogenic activity at the Precambrian–Cambrian transition. *Precambrian Research* **140**, 157–182.

Gasquet, D., Ennih, N., Liégeois, J. P., Soulaimani, A. & Michard, A. (2008). The Pan-African Belt. In: Michard, A., Saddiqi, O., Chalouan, A., Frizon de Lamotte, D. (eds.) *Continental Evolution: The Geology of Morocco. Lecture Notes in Earth Sciences*, Vol. 116. Berlin, Heidelberg: Springer, pp. 33–64.

Ghiorso, M. S., Hirschmann, M. M., Reiners, P. W. & Kress, V. C. (2002). The pMELTS: A revision of MELTS for improved calculation of phase relations and major element partitioning related to partial melting of the mantle to 3 GPa. *Geochemistry, Geophysics, Geosystems* **3**, 1–1029./2001GC 000217.

Ghiorso, M. S. & Sack, R. O. (1995). Chemical mass transfer in magmatic processes IV. A revised and internally consistent thermodynamic model for the interpolation and extrapolation of liquid-solid equilibria in magmatic systems at elevated temperatures and pressures. *Contributions to Mineralogy and Petrology* **119**, 197–212.

Grousset, F. E. & Biscaye, P. E. (2005). Tracing dust sources and transport patterns using Sr, Nd and Pb isotopes. *Chemical Geology* **222**, 149–167.

Guex, J., Pilet, S., Müntener, O., Bartolini, A., Spangenberg, J., Schoene, B., Sell, B. & Schaltegger, U. (2016). Thermal erosion of cratonic lithosphere as a potential trigger for mass-extinction. *Scientific Reports* **6**, 23168.http://dx.doi.org/10.1038/srep23168.

Hanan, B. B. & Graham, D. W. (1996). Lead and helium isotope evidence from oceanic basalts for a common deep source of mantle plumes. *Science (New York, N.Y.)* **272**, 991–995.

Harvey, J., Dale, C. W., Gannoun, A. & Burton, K. W. (2011). Osmium mass balance in peridotite and the effects of mantle-derived sulphides on basalt petrogenesis. *Geochimica et Cosmochimica Acta* **75**, 5574–5596.

Hart, S. R. (1984). A large-scale isotope anomaly in the Southern Hemisphere mantle. *Nature* **309**, 753–757.

Heatherington, A. L. & Mueller, P. A. (1999). Lithospheric sources of North Florida, USA tholeiites and implications for the origin of the Suwannee terrain. *Lithos* **46**, 215–233.

Heinonen, J. S., Carlson, R. W. & Luttinen, A. V. (2010). Isotopic (Sr, Nd, Pb, and Os) composition of highly magnesian dikes of Vestfjella, western Dronning Maud Land, Antarctica: a key to the origins of the Jurassic Karoo large igneous province? *Chemical Geology* **277**, 227–244.

Heinonen, J. S., Luttinen, A. V. & Bohrson, W. A. (2016). Enriched continental flood basalts from depleted mantle melts: Modeling the lithospheric contamination of Karoo lavas from Antarctica. *Contributions to Mineralogy and Petrology* **171**, 1–22.

Herzberg, C. & Gazel, E. (2009). Petrological evidence for secular cooling in mantle plumes. *Nature* **458**, 619–622.

Hesselbo, S. P., Robinson, S. A., Surlyk, F. & Piasecki, S. (2002). Terrestrial and marine mass extinction at the Triassic-Jurassic boundary synchronized with initiation of massive volcanism. *Geology* **30**, 251–254.

Hill, R. I. (1991). Starting plumes and continental break-up. *Earth and Planetary Science Letters* **104**, 398–416.

Hirose, K. & Kushiro, I. (1993). Partial melting of dry peridotites at high pressures: Determination of compositions of melts segregated from peridotite using aggregates of diamond. *Earth and Planetary Science Letters* **114**, 477–489.

Hofmann, C., Courtillot, V., Féraud, G., Rochette, P., Yirgu, G., Ketefo, E. & Pik, R. (1997). Timing of the Ethiopian flood basalt event and implications for plume birth and global change. *Nature* **389**, 838–841.

Hole, M. J. (2018). Mineralogical and geochemical evidence for polybaric fractional crystallization of continental flood basalts and implications for identification of peridotite and pyroxenite source lithologies. *Earth Science Reviews* **176**, 51–67.

Holm, P. M., Wilson, J. R., Christensen, B. P., Hansen, L., Hansen, S. L., Hein, K. M., Mortensen, A. K., Pedersen, R., Plesner, S. & Runge, M. K. (2006). Sampling the Cape Verde Mantle Plume: Evolution of melt compositions on Santo Antão, Cape Verde Islands. *Journal of Petrology* **47**, 145–189.

Huvelin, J. P. (1971). Faisceau de filons de microdiorite et tectogenèse hercynienne dans les Jbilest (Maroc.). *Comptes Rendus Académie des Sciences* **272**, 28–31.

Ishii, T. (1975). The relations between temperature and composition of pigeonite in some lavas and their application to geothermometry. *Mineralogical Journal* **8**, 48–57.

Jackson, M. G. & Carlson, R. W. (2011). An ancient recipe for flood-basalt genesis. *Nature* **476**, 316–319.

Janney, P. E. & Castillo, P. R. (2001). Geochemistry of the oldest Atlantic crust suggests mantle plume involvement in the early history of the Central Atlantic Ocean. *Earth and Planetary Sciences Letters* **192**, 291–302.

Jerram, D. A., Svensen, H. H., Planke, S., Polozov, A. G. & Torsvik, T. H. (2016). The onset of flood volcanism in the north-western part of the Siberian Traps: Explosive volcanism versus effusive lava flows. *Palaeogeography, Palaeoclimatology, Palaeoecology* **441**, 38–50.

Jourdan, F., Marzoli, A., Bertrand, H., Cosca, M. & Fontignie, D. (2003). The Northernmost CAMP: $^{40}Ar/^{39}Ar$ age, petrology and Sr-Nd-Pb isotope geochemistry of the Kerforne Dike, Brittany, France. In: Hames W. E., McHone, J. G., Renne, P. R. & Ruppel, C. (eds) *The Central Atlantic Magmatic Province: Insights from Fragments of Pangaea*. Washington, DC, U.S.A: American Geophysical Union Monograph **136**, 209–226.

Jourdan, F., Bertrand, H., Schärer, U., Blichert-Toft, J., Féraud, G. & Kampunzu, A. B. (2007). Major and trace element and Sr, Nd, Hf and Pb isotope compositions of the Karoo Large Igneous Province, Botswana-Zimbabwe: Lithosphere vs mantle plume contribution. *Journal of Petrology* **48**, 1043–1077.

Jourdan, F., Marzoli, A., Bertrand, H., Cirilli, S., Tanner, L. H., Kontak, D. J., McHone, G., Renne, P. R. & Bellieni, G. (2009). $^{40}Ar/^{39}Ar$ ages of CAMP in North America: Implications for the Triassic-Jurassic boundary and the ^{40}K decay constant bias. *Lithos* **110**, 167–180.

Jourdan, F., Sharp, W. D. & Renne, P. R. (2012). $^{40}Ar/^{39}Ar$ ages for deep ($\sim$3.3 km) samples from the Hawaii Scientific Drilling Project, Mauna Kea volcano, Hawaii. *Geochemistry, Geophysics, Geosystems* **13**, Q05004.

Kerr, A. C., Kempton, P. D. & Thompson, R. N. (1995). Crustal assimilation during turbulent magma ascent (ATA); new isotopic evidence from the Mull Tertiary lava succession, N. W. Scotland. *Contributions to Mineralogy and Petrology* **119**, 142–154.

Klein, E. L., Angélica, R. S., Harris, C., Jourdan, F. & Babinski, M. (2013). Mafic dykes intrusive into Pre-Cambrian rocks of the São Luís cratonic fragment and Gurupi Belt (Parnaíba Province), north–northeastern Brazil: Geochemistry, Sr–Nd–Pb–O isotopes, $^{40}Ar/^{39}Ar$ geochronology and relationships to CAMP magmatism. *Lithos* **172–173**, 222–242.

Klügel, A., Galipp, K., Hoernle, K., Hauff, F. & Groom, S. (2017). Geochemical and volcanological evolution of La Palma, Canary Islands. *Journal of Petrology* **58**, 1227–1248.

Knight, K. B., Nomade, S., Renne, P. R., Marzoli, A., Bertrand, H. & Youbi, N. (2004). The Central Atlantic Magmatic Province at the Triassic–Jurassic boundary: Paleomagnetic and $^{40}Ar/^{39}Ar$ evidence from Morocco for brief, episodic volcanism. *Earth and Planetary Science Letters* **228**, 143–160.

Kontak, D. J. (2008). On the edge of CAMP: Geology and volcanology of the Jurassic North Mountain Basalt, Nova Scotia. *Lithos* **101**, 74–101.

Kushiro, I. (1996). Partial melting of a fertile mantle peridotite at high pressures: An experimental study using aggregates of diamond. In: Basu, A. & Hart, S. (eds) *Earth Processes: Reading the Isotopic Code*. Washington, DC, USA: American Geophysical Union Monograph **95**, 109–122.

Labails, C., Olivet, J. L., Aslanian, D. & Roest, W. R. (2010). An alternative early opening scenario for the Central Atlantic Ocean. *Earth and Planetary Science Letters* **297**, 355–368.

Le Bas, M. J., Le Maitre, R. W., Streckeisen, A. & Zanettin, B. (1986). A chemical classification of volcanic rocks based on the total alkali-silica diagram. *Journal of Petrology* **27**, 745–750.

Lindström, S., Pedersen, G. K., van de Schootbrugge, B., Hansen, K. H., Kuhlmann, N., Thein, J., Johansson, L., Petersen, H. I., Alwmark, C., Dybkjær, K., Weibel, R., Erlström, M., Nielsen, L. H., Oschmann, W. & Tegner, C. (2015). Intense and widespread seismicity during the end-Triassic mass extinction due to emplacement of a large igneous province. *Geology* **43**, 387–390.

Lindström, S., van de Schootbrugge, B., Hansen, K. H., Pedersen, G. K., Alsen, P., Thibault, N., Dybkjær, K., Bjerrum, C. J. & Nielsen, L. H. (2017). A new correlation of Triassic–Jurassic boundary successions in NW Europe, Nevada and Peru and the Central Atlantic Magmatic Province: A time-line for the end-Triassic mass extinction. *Palaeogeography, Palaeoclimatology, Palaeoecology* **478**, 80–102.

Lipman, P. W., Sisson, T. W., Coombs, M. L., Calvert, A. & Kimura, J.-I. (2006). Piggyback tectonics: Long-term growth of Kilauea on the south flank of Mauna Loa. *Journal of Volcanology and Geothermal Research* **151**, 73–108.

Ludwig, K. R. (2003). *User's Manual for Isoplot 3.00*. Berkeley, USA: Berkeley Geochronology Center Special Publication, p. 74.

Luttinen, A. V. (2018). Bilateral geochemical asymmetry in the Karoo large igneous province. *Scientific Reports* **8**:5223, 1–11.

Mahmoudi, A. & Bertrand, H. (2007). Identification géochimique de la province magmatique de l'Atlantique central en domaine plissé: Exemple du Moyen Atlas marocain. *Comptes Rendus Geoscience* **339**, 545–552.

Manspeizer, W., Puffer, J. H. & Cousminer, H. L. (1978). Separation of Morocco and eastern North America: A Triassic-Liassic stratigraphic record. *Geological Society of America Bulletin* **89**, 901–920.

Martins, L. T., Madeira, J., Youbi, N., Munhá, J., Mata, J. & Kerrich, R. (2008). Rift-related magmatism of the Central Atlantic magmatic province in Algarve, Southern Portugal. *Lithos* **101**, 102–124.

Marzoli, A., Bertrand, H., Knight, K. B., Cirilli, S., Buratti, N., Vérati, C., Nomade, S., Renne, P. R., Youbi, N., Martini, R., Allenbach, K., Neuwerth, R., Rapaille, C., Zaninetti, L. & Bellieni, G. (2004). Synchrony of the Central Atlantic magmatic province and the Triassic-Jurassic boundary climatic and biotic crisis. *Geology* **32**, 973–976.

Marzoli, A., Bertrand, H., Knight, K., Cirilli, S., Nomade, S., Renne, P., Vérati, C., Youbi, N., Martini, R. & Bellieni, G. (2008). Comments on "Synchrony between the Central Atlantic magmatic province and the Triassic–Jurassic mass-extinction event?" by Whiteside et al. (2007). *Palaeogeography, Palaeoclimatology, Palaeoecology* **262**, 189–193.

Marzoli, A., Callegaro, S., Dal Corso, J., Davies, J. H. F. L., Chiaradia, M., Youbi, N., Bertrand, H., Reisberg, L., Merle, R. & Jourdan, F. (2018). The Central Atlantic Magmatic Province (CAMP): A review. In: Tanner, L. H. (ed.) *The Late Triassic World. Topics in Geobiology* **46**. Heidelberg: Springer, pp. 91–125.

Marzoli, A., Davies, J. H. F. L., Youbi, N., Merle, R., Dal Corso, J., Dunkley, D. J., Fioretti, A. M., Bellieni, G., Medina, F., Wotzlaw, J. F., McHone, G., Font, E. & Bensalah, M. K. (2017). Proterozoic to Mesozoic evolution of North-West Africa and Peri-Gondwana microplates: Detrital zircon ages from Morocco and Canada. *Lithos* **278–281**, 229–239.

Marzoli, A., Jourdan, F., Bussy, F., Chiaradia, M. & Costa, F. (2014). Petrogenesis of tholeiitic basalts from the Central Atlantic magmatic province as revealed by mineral major and trace elements and Sr isotopes. *Lithos* **188**, 44–59.

Marzoli, A., Jourdan, F., Puffer, J. H., Cuppone, T., Tanner, L. H., Weems, R. E., Bertrand, H., Cirilli, S., Bellieni, G. & De Min, A. (2011). Timing and duration of the Central Atlantic magmatic province in the Newark and Culpeper basins, eastern USA. *Lithos* **122**, 175–188.

Marzoli, A., Renne, P. R., Picirillo, E. M., Ernesto, M. & De Min, A. (1999). Extensive 200-million-year-old continental flood basalts of the Central Atlantic Magmatic Province. *Science* **284**, 616–618.

May, P. R. (1971). Pattern of Triassic-Jurassic diabase dikes around the North Atlantic in the context of pre-drift position

of the continents. *Geological Society of America Bulletin* **82**, 1285–1129.

McDonough, W. F. & Sun, S. S. (1995). The composition of the Earth. *Chemical Geology* **120**, 223–253.

McHone, J. G. (2000). Non-plume magmatism and rifting during the opening of the central Atlantic Ocean. *Tectonophysics* **316**, 287–296.

McKenzie, D. & O'Nions, R. K. (1991). Partial melt distribution from inversion of rare earth element concentrations. *Journal of Petrology* **32**, 1021–1091.

Meddah, A., Bertrand, H., Seddiki, A. & Tabeliouna, M. (2017). The Triassic-Liassic volcanic sequence and rift evolution in the Saharan Atlas basins (Algeria.). *Eastward Vanishing of the Central Atlantic Magmatic Province. Geologica Acta* **15**, 11–23.

Medina, F. (1991). Superimposed extensional tectonics in the Argana Triassic formations (Morocco), related to the early rifting of the Central Atlantic. *Geological Magazine* **128**, 525–536.

Meisel, T., Walker, R. J., Irving, A. J. & Lorand, J.-P. (2001). Osmium isotopic compositions of mantle xenoliths: A global perspective. *Geochimica et Cosmochimica Acta* **65**, 1311–1323.

Melluso, L., Beccaluva, L., Brotzu, P., Gregnanin, A., Gupta, A. K., Morbidelli, L. & Traversa, G. (1995). Constraints on the mantle sources of the Deccan Traps from the petrology and geochemistry of the basalts of Gujarat State (Western India). *Journal of Petrology* **36**, 1393–1432.

Melluso, L., Mahoney, J. J. & Dallai, L. (2006). Mantle sources and crustal input as recorded in high-Mg Deccan Traps basalts of Gujarat (India). *Lithos* **89**, 259–274.

Merle, R., Marzoli, A., Bertrand, H., Reisberg, L., Verati, C., Zimmermann, C., Chiaradia, M., Bellieni, G. & Ernesto, M. (2011). $^{40}Ar/^{39}Ar$ ages and Sr–Nd–Pb–Osgeochemistry of CAMP tholeiites from the western Maranhão basin (NE-Brazil). *Lithos* **122**, 137–151.

Merle, R., Marzoli, A., Reisberg, L., Bertrand, H., Nemchin, A., Chiaradia, M., Callegaro, S., Jourdan, F., Bellieni, G., Kontak, D., Puffer, J. H. & McHone, J. G. (2014). Sr, Nd, Pb and Os isotope systematics of CAMP tholeiites from Eastern North America (ENA): Evidence of a subduction-enriched mantle source. *Journal of Petrology* **55**, 133–180.

Meyzen, C. M., Ludden, J. N., Humler, E., Luais, B., Toplis, M. J., Mével, C. & Storey, M. (2005). New insights into the origin and distribution of the DUPAL isotope anomaly in the Indian Ocean mantle from MORB of the Southwest Indian Ridge. *Geochemistry Geophysics Geosystems* **Q11K11**, 36.

Michard, A., Hoepffner, C., Soulaimani, A. & Baidder, L. (2008). The Variscan Belt. In: Michard, A., Saddiqi, O., Chalouan, A. & Frizon de Lamotte, D. (eds) *Continental Evolution: The Geology of Morocco. Lecture Notes in Earth Sciences 116*. Berlin, Heidelberg: Springer Verlag, pp. 65–132.

Miller, C., Zanetti, A., Thöni, M., Konzett, J. & Klötzli, U. (2012). Mafic and silica-rich glasses in mantle xenoliths from Wau-en-Namus, Libya: Textural and geochemical evidence for peridotite–melt reactions. *Lithos* **128–131**, 11–26.

Morimoto, N., Fabries, J., Ferguson, A. K., Ginzburg, I. V., Ross, M., Seifert, F. A. & Zussman, J. (1988). Nomenclature of pyroxenes. *Mineralogical Magazine* **52**, 535–550.

Moukadiri, A. (1999). Essai de caractérisation de la lithosphère sous le Moyen Atlas (Maroc) par l'étude des xénolites basi-crustaux et mantelliques dans les basaltes alcalins quaternaires. PhD Thesis, Cadi Ayyad University, Faculty of Sciences-Semlalia, Marrakech, p. 181.

Neave, D. A. & Putirka, K. (2017). Clinopyroxene-liquid barometry revisited: Magma storage pressures under Icelandic rift zones. *American Mineralogist* **102**, 777–794.

Nomade, S., Knight, K. B., Beutel, E., Renne, P. R., Vérati, C., Féraud, G., Marzoli, A., Youbi, N. & Bertrand, H. (2007). Chronology of the Central Atlantic Magmatic Province: Implications for the Central Atlantic rifting processes and the Triassic–Jurassic biotic crisis. *Palaeogeography, Palaeoclimatology, Palaeoecology* **246**, 326–344.

Oyarzun, R., Doblas, M., López-Ruiz, J. & María Cebrá, J. (1997). Opening of the Central Atlantic and asymmetric mantle upwelling phenomena: Implications for long-lived magmatism in western North Africa and Europe. *Geology* **25**, 727–730.

Palencia Ortas, A., Ruiz-Martínez, V. C., Villalaín, J. J., Osete, M. L., Vegas, R., Touil, A., Hafid, A., McIntosh, G., van Hinsbergen, D. J. J. & Torsvik, T. H. (2011). A new 200 Ma paleomagnetic pole for Africa and paleo-secular variation scatter from Central Atlantic Magmatic Province (CAMP) intrusives in Morocco (Ighrem and Foum Zguid dykes). *Geophysical Journal International* **185**, 1220–1234.

Panfili, G., Cirilli, S., Dal Corso, J., Bertrand, H., Medina, F., Youbi, N. & Marzoli, A. (2019). New palynological constraints show rapid emplacement of the Central Atlantic magmatic province during the end-Triassic mass extinction interval. *Global and Planetary Change* **172**, 60–68.

Papike, J. J., Cameron, K. L. & Baldwin, K. (1974). Amphiboles and pyroxenes: Characterization of other than quadrilateral components and estimates of ferric iron from microprobe data. *Geological Society of America, Abstracts with Progrrams* **6**, 1053–1054.

Parisio, L., Jourdan, F., Marzoli, A., Melluso, L., Sethna, S. & Bellieni, G. (2016). $^{40}Ar/^{39}Ar$ ages of alkaline and tholeiitic rocks from the northern Deccan traps: Implications for magmatic processes and the K–Pg boundary. *Journal of the Geological Society of London* **173**, 679–688.

Peate, D. W. (1997). The Paraná-Etendeka Province. In: Mahoney, J. J. & Coffin, M. F. (eds) *Large Igneous Provinces: Continental, Oceanic and Planetary Flood Volcanism*. Washington, DC, USA: American Geophysical Union Monograph **100**, pp. 217–246

Pearson, D. G. & Nowell, G. M. (2004). Re-Os and Lu-Hf isotope constraints on the origin and age of pyroxenites from the Beni Bousera Peridotite Massif: Implications for mixed peridotite-pyroxenite mantle sources. *Journal of Petrology* **45**, 439–455.

Pegram, W. J. (1990). Development of continental lithospheric mantle as reflected in the chemistry of the Mesozoic Appalachian tholeiites, USA. *Earth and Planetary Science Letters* **97**, 316–331.

Pereira, M. F., El Houicha, M., Chichorro, M., Armstrong, R., Jouhari, A., El Attari, A., Ennih, N. & Silva, J. B. (2015). Evidence of a Paleoproterozoic basement in the Moroccan Variscan Belt (Rehamna Massif, Western Meseta). *Precambrian Research* **268**, 61–73.

Peucker-Ehrenbrink, B. & Jahn, B.-M. (2001). Rhenium–osmium isotope systematics and platinum group element concentrations: Loess and the upper continental crust. *Geochemistry, Geophysics, Geosystems* 2001GC000172, pp. 1–22.

Puffer, J. H. (1992). Eastern North American flood basalts in the context of the incipient breakup of Pangaea. In: Puffer, J. H. & Ragland, P. C. (eds) *Eastern North American Mesozoic Magmatism*. Boulder, USA: Geological Society of America Special Paper **268**, 95–119.

Puffer, J. H. (2001). Contrasting high field strength element contents of continental flood basalts from plume versus reactivated-arc sources. *Geology* **29**, 675–678.

Puffer, J. H. (2003). A reactivated back-arc source for CAMP magma. In: Hames, W. E., McHone, J. G., Renne, P. R. & Ruppel, C. (eds) *The Central Atlantic Magmatic Province: Insights from Fragments of Pangea*. Geophysical

Monograph, Washington, DC, USA: American Geophysical Union **136**, 151–162.

Puffer, J. H., Block, K. A. & Steiner, J. C. (2009). Transmission of flood basalts through a shallow crustal sill and the correlations of the sill layers with extrusive flows: The Palisades intrusive system and the basalts of the Newark Basin, New Jersey, USA. *Journal of Geology* **117**, 139–155.

Putirka, K. (2005). Igneous thermometers and barometers based on plagioclase + liquid equilibria: Tests of some existing models and new calibrations. *American Mineralogist* **90**, 336–346.

Putirka, K. (2008). Thermometers and barometers for volcanic systems. In: Putirka, K. & Tepley, F. J. (eds) *Minerals, Inclusions and Volcanic Processes. Mineralogical Society of America*. Chantilly, USA: Reviews in Mineralogy and Geochemistry **69**, pp. 61–120.

Putirka, K., Johnson, M., Kinzler, R., Longhi, J. & Walker, D. (1996). Thermobarometry of mafic igneous rocks based on clinopyroxene-liquid equilibria, 0-30 kbar. *Contributions to Mineralogy and Petrology* **123**, 92–108.

Putirka, K., Kuntz, M. A., Unruh, D. M. & Vaid, N. (2009). Magma evolution and ascent at the craters of the moon and neighboring volcanic fields, Southern Idaho, USA: Implications for the evolution of polygenetic and monogenetic volcanic fields. *Journal of Petrology* **50**, 1639–1665.

Reisberg, L., Allegre, C. J. & Luck, J. M. (1991). The Re-0s systematics of the Ronda Ultramafic Complex of southern Spain. *Earth and Planetary Science Letters* **105**, 196–213.

Reisberg, L. & Lorand, J.-P. (1995). Longevity of sub-continental mantle lithosphere from osmium isotope systematics in orogenic peridotite massifs. *Nature* **376**, 159–162.

Renne, P. R., Balco, G., Ludwig, K. R., Mundil, R. & Min, K. (2011). Response to the comment by W.H. Schwarz et al. on "Joint determination of K-40 decay constants and ^{40}*Ar/^{40}K for the Fish Canyon sanidine standard and improved accuracy for ^{40}Ar/^{39}Ar geochronology" by P.R. Renne et al. (2010). *Geochimica et Cosmochimica Acta* **75**, 5097–5100.

Renne, P. R., Swisher, C. C., Deino, A. L., Karner, D. B., Owens, T. & DePaolo, D. J. (1998). Intercalibration of standards, absolute ages and uncertainties in ^{40}Ar/^{39}Ar dating. *Chemical Geology (Isotope Geoscience Section)* **145**, 117–152.

Rudnick, R. L. & Gao, S. (2003). Composition of the continental crust. *Treatise on Geochemistry* **3**, 1–64.

Ruhl, M., Hesselbo, S. P., Hinnov, L., Jenkyns, H. C., Xu, W., Riding, J. B., Storm, M., Minisini, D., Ullmann, C. V. & Leng, M. J. (2016). Astronomical constraints on the duration of the Early Jurassic Pliensbachian Stage and global climatic fluctuations. *Earth and Planetary Science Letters* **455**, 149–165.

Ruiz-Martínez, V. C., Torsvik, T., Hinsbergen, D. J. J. & Gaina, C. (2012). Earth at 200 Ma: Global palaeogeography refined from CAMP palaeomagnetic data. *Earth and Planetary Science Letters* **331–332**, 67–79.

Saal, A. E., Rudnick, R. L., Ravizza, G. E. & Hart, S. R. (1998). Re-Os isotope evidence for the composition, formation and age of the lower continental crust. *Nature* **393**, 58–61.

Sahabi, M., Aslanian, D. & Olivet, J. L. (2004). A new starting point for the history of the central Atlantic. *Comptes Rendus Geosciences* **336**, 1041–1052.

Schnepp, E., Pucher, R., Goedicke, C., Manzano, A., Muller, U. & Lanos, P. (2003). Paleomagnetic directions and thermoluminescence dating from a bread oven-floor sequence in Lqbeck (Germany): A record of 450 years of geomagnetic secular variation. *Journal of Geophysical Research* **108**, 1–14.

Schoene, B., Guex, J., Bartolini, A., Schaltegger, U. & Blackburn, T. J. (2010). Correlating the end-Triassic mass extinction and flood basalt volcanism at the 100 ka level. *Geology* **38**, 387–390.

Sebai, A., Féraud, G., Bertrand, H. & Hanes, J. (1991). ^{40}Ar/^{39}Ar dating and geochemistry of tholeiitic magmatism related to the early opening of the Central Atlantic rift. *Earth and Planetary Science Letters* **104**, 455–472.

Shellnutt, J., Dostal, J. & Yeh, M. W. (2018). Mantle source heterogeneity of the early Jurassic basalt of eastern North America. *International Journal of Earth Sciences* **107**, 1033–1058.

Silva, P. F., Henry, B., Marques, F. O., Madureira, P. & Miranda, J. M. (2006). Paleomagnetic study of the great Foum Zguid Dyke (southern Morocco); a positive contact test related to metasomatic processes. *Geophysical Research Letters* **33**, L21301.

Smoliar, M. I., Walker, R. J. & Morgan, J. W. (1996). Re–Os isotope constraints on the age of Group IIA, IIIA, IVA and IVB iron meteorites. *Science* **271**, 1099–1102.

Spera, F. J. & Bohrson, W. A. (2001). Energy-constrained open-system magmatic processes I: General model and energy-constrained assimilation and fractional crystallization (EC-AFC) formulation. *Journal of Petrology* **42**, 999–1018.

Sun, S-S. & McDonough, W. F. (1989). Chemical and isotopic systematics of oceanic basalts: Implications for mantle composition and processes. In: Saunders, A. D. & Norry, M. J. (eds) *Magmatism in the Ocean Basins*. London, UK: Geological Society, London, UK: Special Publications **42**, 313–345.

Tegner, C., Duncan, R. A., Bernstein, S., Brooks, C. K., Bird, D. K. & Storey, M. (1998). ^{40}Ar/^{39}Ar geochronology of Tertiary mafic intrusions along the East Greenland rifted margin: Relation to flood basalts and the Iceland hotspot track. *Earth and Planetary Science Letters* **156**, 75–88.

Tegner, C., Michelis, S. A. T., McDonald, I., Youbi, N., Callegaro, S., Lindström, S. & Marzoli, A. (in press). Mantle Dynamics of the Central Atlantic Magmatic Province (CAMP): Constraints from platinum group, gold and lithophile elements in flood basalts of Morocco. *Journal of Petrology*

Tegner, C., Wilson, J. R. & Robins, B. (2005). Crustal contamination in basalt and jotunite: Constraints from layered intrusions. *Lithos* **83**, 299–316.

Thomas, R. J., Chevallier, L. P., Gresse, P. G., Harmer, R. E., Eglington, B. M., Armstrong, R. A., de Beer, C. H., Martini, J. E. J., de Kock, G. S., Macey, P. H. & Ingram, B. A. (2002). Precambrian evolution of the Sirwa Window, Anti-Atlas Orogen, Morocco. *Precambrian Research* **118**, 1–57.

Thordarson, T. & Self, S. (1993). The Laki, (Skaftár Fires), Grímsvötn eruptions in 1783–1785. *Bullettin of Volcanology*, **55**, 2–2.

Thy, P., Lesher, C. E. & Tegner, C. (2013). Further work on experimental plagioclase equilibria and the Skaergaard liquidus temperature. *American Mineralogist* **98**, 1360–1367.

Tollo, R. P. & Gottfried, D. (1992). Petrochemistry of Jurassic Basalt from Eight Cores, Newark Basin, New Jersey: Implications for the volcanic petrogenesis of the Newark supergroup. In: Puffer, J. H. & Ragland, P. C. (eds) *Eastern North American Mesozoic Magmatism*. Boulder, USA: Geological Society of America, Special Paper **268**, pp. 233–259.

Toummite, A., Liegeois, J. P., Gasquet, D., Bruguier, O., Beraaouz, E. H. & Ikenne, M. (2013). Field, geochemistry and Sr-Nd isotopes of the Pan-African granitoids from the Tifnoute Valley (Sirwa, Anti-Atlas, Morocco): A post-collisional event in a metacratonic setting. *Mineralogy and Petrology* **107**, 739–763.

Verati, C., Bertrand, H. & Féraud, G. (2005). The farthest record of the Central Atlantic Magmatic Province into West Africa craton: Precise $^{40}Ar/^{39}Ar$ dating and geochemistry of Taoudenni basin intrusives (northern Mali). *Earth and Planetary Science Letters* **235**, 391–407.

Verati, C., Rapaille, C., Féraud, G., Marzoli, A., Bertrand, H. & Youbi, N. (2007). $^{40}Ar/^{39}Ar$ ages and duration of the Central Atlantic Magmatic Province volcanism in Morocco and Portugal and its relation to the Triassic-Jurassic boundary. *Palaeogeography Palaeoclimatology Palaeoecology* **244**, 308–325.

Villiger, S., Ulmer, P., Muntener, O. & Thmpson, A. B. (2004). The liquid line of descent of anhydrous, mantle-derived, tholeiitic liquids by fractional and equilibrium crystallization—An experimental study at 1·0 GPa. *Journal of Petrology* **45**, 2369–2388.

Volkening, J., Walczyk, T. & Heumann, K. G. (1991). Osmium isotope determinations by negative thermal ionization mass spectrometry. *International Journal of Mass Spectrometry Ion Physics* **105**, 147–159.

Wagner, C., Mokhtari, A., Deloule, E. & Chabaux, F. (2003). Carbonatite and alkaline magmatism in Taourirt (Morocco): Petrological, geochemical and Sr–Nd isotope characteristics. *Journal of Petrology* **44**, 937–965.

Ware, B., Jourdan, F., Tohver, E., Fernandes, K. G. & Chiaradia, M. (2018). Primary hydrous minerals from the Karoo LIP magmas: Evidence for a hydrated source component. *Earth and Planetary Science Letters* **503**, 181–193.

Weems, R. E., Tanner, L. H. & Lucas, S. G. (2016). Synthesis and revision of the lithostratigraphic groups and formations in the Upper Permian?–Lower Jurassic Newark supergroup of eastern North America. *Stratigraphy* **13**, 111–153.

Whalen, L., Gazel, E., Vidito, C., Puffer, J., Bizimis, M., Henika, W. & Caddick, M. J. (2015). Supercontinental inheritance and its influence on supercontinental breakup: The Central Atlantic Magmatic Province and the breakup of Pangea. *Geochemistry, Geophysics, Geosystems* **16**, 3532–3554.

Whiteside, J. H., Olsen, P. E., Kent, D. V., Fowell, S. J. & Et-Touhami, M. (2007). Synchrony between the Central Atlantic Magmatic Province and the Triassic–Jurassic mass-extinction event? *Palaeogeography, Palaeoclimatology, Palaeoecology* **244**, 345–367.

Whiteside, J. H., Olsen, P. E., Kent, D. V., Fowell, S. J. & Et-Touhami, M. (2008). Synchrony between the Central Atlantic Magmatic Province and the Triassic–Jurassic mass-extinction event? Reply to comment of Marzoli et al., 2008. *Palaeogeography, Palaeoclimatology, Palaeoecology* **262**, 194–198.

Wittig, N., Pearson, D. G., Baker, J. A., Duggen, S. & Hoernle, K. (2010a). A major element, PGE and Re–Os isotope study of Middle Atlas (Morocco) peridotite xenoliths: Evidence for coupled introduction of metasomatic sulphides and clinopyroxene. *Lithos* **115**, 15–26.

Wittig, N., Pearson, D. G., Duggen, S., Baker, J. A. & Hoernle, K. (2010b). Tracing the metasomatic and magmatic evolution of continental mantle roots with Sr, Nd, Hf and Pb isotopes: A case study of Middle Atlas (Morocco) peridotite xenoliths. *Geochimica et Cosmochimica Acta* **74**, 1417–1435.

Wotzlaw, J. F., Guex, J., Bartolini, A., Gallet, Y., Krystyn, L., McRoberts, C. A., Taylor, D., Schoene, B. & Schaltegger, U. (2014). Towards accurate numerical calibration of the Late Triassic: High-precision U–Pb geochronology constraints on the duration of the Rhaetian. *Geology* **42**, 571–574.

Youbi, N., Kouyaté, D., Söderlund, U., Ernst, R. E., Soulaimani, A., Hafid, A., Ikenne, M., El Bahat, A., Bertrand, H., Rkha Chaham, K., Ben Abbou, M., Mortaji, A., El Ghorfi, M., Zouhair, M. & El Janati, M. (2013). The 1750 Ma magmatic event of the West African Craton (Anti-Atlas, Morocco). *Precambrian Research* **236**, 106–123.

Youbi, N., Martins, L., Munhá, J. M., Ibouh, H., Madeira, J., Aït Chayeb, E. H. & El Boukhari, A. (2003). The Late Triassic–Early Jurassic volcanism of Morocco and Portugal in the framework of the Central Atlantic Magmatic Province. In: Hames, W. E., McHone, J. M., Renne, P. R. & Ruppel, C. (eds) *The Central Atlantic Magmatic Province: Insights from Fragments of Pangea*. Washington, DC, USA: American Geophysical Union Monograph **136**, 179–207.

Zindler, A. E. & Hart, S. R. (1986). Chemical geodynamics. *Annual Review of Earth and Planetary Sciences* **14**, 493–571.